

Phenomenological comparison of models with extended Higgs sectors

Master's Thesis
of

Jonas Wittbrodt

At the faculty of Physics
Institute for Theoretical Physics (ITP)

Reviewer: Prof. Dr. M. M. Mühlleitner
Second reviewer: P.D. Dr. M. Spira

19. October 2015 — 29. September 2016

Hiermit versichere ich, dass ich die vorliegende Arbeit selbständig verfasst und keine anderen als die angegebenen Hilfsmittel benutzt, die wörtlich oder inhaltlich übernommenen Stellen als solche kenntlich gemacht und die Satzung des Karlsruher Instituts für Technologie (KIT) zur Sicherung guter wissenschaftlicher Praxis in der aktuell gültigen Fassung beachtet habe.

Karlsruhe, den 29.9.2016

.....
(Jonas Wittbrodt)

Als Masterarbeit akzeptiert

Contents

1. Introduction	1
2. Overview of the studied Higgs sector extensions	5
2.1. The Complex singlet-extension of the Standard Model	5
2.2. The Two-Higgs-Doublet Model	7
2.2.1. Couplings of the C2HDM	8
2.3. The Next-to-Minimal Supersymmetric Model	9
3. The Next-to-Two-Higgs-Doublet Model	13
3.1. The N2HDM scalar potential	13
3.1.1. Diagonalization of the charged and pseudoscalar sectors	14
3.1.2. Diagonalization of the scalar sector	15
3.1.3. Parametrizations of the Potential	15
3.2. Higgs couplings to SM particles	16
3.2.1. Yukawa couplings and \mathbb{Z}_2 -symmetric fermion sectors	16
3.2.2. Higgs-gauge couplings	17
3.3. Vacuum stability constraints	17
3.3.1. Conditions for the potential to be bounded from below	18
3.3.2. Vacuum decay and global minimum condition	18
3.4. Tree-level perturbative unitarity	20
4. Scans of the parameter space	23
4.1. The CxSM parameter scan	24
4.2. The C2HDM parameter scan	25
4.2.1. Scan ranges in the type II C2HDM	26
4.3. The N2HDM parameter scan	27
4.3.1. Scan ranges in the type II N2HDM	27
4.4. The NMSSM parameter scan	28
4.5. Mass distributions of the neutral scalars	28
4.6. The effect of new constraints on the C2HDM parameter space	30
5. Phenomenological results	33
5.1. Properties of the h_{125}	33
5.1.1. Phenomenology of the h_{125} singlet admixture	34
5.1.2. Pseudoscalar admixture in the C2HDM	38
5.2. Distinguishing Higgs sector extensions through the properties of two Higgs bosons	40
5.2.1. Decays into SM particles	40
5.2.2. Yukawa and gauge boson sum-rules	44
6. Conclusions	51

A. Explicit parameter transformations and triple-Higgs couplings	55
A.1. Explicit parameter transformation	55
A.2. Triple-Higgs couplings	56
B. N2HDM parameter points with global charge and CP-breaking minima	59
C. Global minimum conditions	61
C.1. 2HDM-like stationary points	62
C.1.1. Case I	62
C.1.2. Case II	63
C.1.3. Case III	63
C.2. Stationary points with a singlet VEV	64
C.2.1. Case sI	64
C.2.2. Case sII	64
C.2.3. Case sIII	65
C.2.4. Case sIV	65
C.3. Special case $\lambda_4 = \lambda_5$	65
D. The code N2HDECAY	67
Acknowledgement / Danksagung	69
Bibliography	71

CHAPTER 1

Introduction

The discovery of a Higgs boson by the ATLAS [1] and CMS [2] experiments provided the last missing piece of the Standard Model (SM) of particle physics [3–7]. Establishing whether the discovered particle is the SM Higgs boson is one of the big goals of current particle physics. Any deviation from the SM expectation can reveal a lot about the physics Beyond-the-SM (BSM) at work.

The mass of the Higgs boson is already known very precisely [8] and fits into the SM. Measurements of the Higgs couplings are also in agreement with the SM [9]. The precision of these measurements, however, still allows considerable room for BSM theories.

In this thesis, we study and compare what kind of phenomenology different BSM theories with extended Higgs sectors might entail. For this comparison, we choose four models with very different theoretical structure. We only consider models that respect custodial symmetry and produce the correct value of the ρ -parameter at tree-level. This is naturally ensured by all models which add only Higgs-singlet and doublet fields to the SM Higgs sector.

Among the simplest possible extensions of the SM Higgs-sector is the Complex singlet-extension of the SM (CxSM) [10, 11]. The CxSM adds a complex singlet field to the SM Higgs sector, resulting in a total of three CP-even neutral Higgs bosons. In the CxSM all couplings of a Higgs boson to SM particles are rescaled by a common factor. This results in a very simple phenomenology, where Higgs-to-Higgs decays can still lead to interesting differences from the SM [11]. The CxSM could furthermore provide inert singlet dark matter [12–26]. We choose to study the CxSM phase without a DM candidate (also called the broken phase [10, 11]). In this phase, all three CP-even Higgs fields of the theory mix thus offering an interesting phenomenology as a toy model.

Supersymmetric models always require a second Higgs-doublet. It is, therefore, interesting to study the non-supersymmetric Two-Higgs-Doublet Model (2HDM) [27–29] which has the same Higgs sector as the Minimal Supersymmetric Standard Model (MSSM). The phenomenology of the CP-conserving Real 2HDM (R2HDM) is very well studied. We, instead, focus on the Complex 2HDM (C2HDM) [30–39] which incorporates sources of CP-violation in the Higgs-sector. The C2HDM is the simplest model with a CP-violating Higgs sector. We include it in our analysis to study the phenomenological similarities and differences induced

by CP-violating pseudoscalar admixture compared to CP-conserving singlet admixture. The C2HDM contains three neutral Higgs bosons of mixed CP as well as a charged Higgs boson.

The Next-to-Two-Higgs-Doublet Model (N2HDM) [40–42] extends the SM by a Higgs-doublet and a real Higgs-singlet field. The N2HDM has been previously studied with an inert dark matter singlet [41] and could also provide inert doublet dark matter in analogy to the inert 2HDM [43–49]. We study the fully mixing N2HDM, which does not address the dark matter problem. This model has eleven free parameters in the Higgs sector which allow for an extremely rich phenomenology in agreement with current constraints. It contains three CP-even and one CP-odd neutral Higgs boson as well as a charged Higgs boson. We treat it as a toy model with natural flavor and CP-conservation to understand what kind of phenomenological consequences BSM theories with large extended Higgs sectors might entail. We are the first to study the N2HDM without any approximation. We especially study the possibility of singlet admixture to the 125 GeV Higgs boson, which has been neglected in previous studies [40, 42].

The Next-to-minimal Supersymmetric Standard Model (NMSSM) [50–66] is the final model of our study. Supersymmetric models address the issues of the SM by solving the naturalness problem of the SM Higgs boson mass and providing dark matter candidates in the form of neutralinos. We choose the NMSSM as opposed to the simpler Minimal Supersymmetric Standard Model (MSSM) as it requires considerably less fine-tuning to reach a Higgs mass of 125 GeV. The singlet field introduced in the NMSSM can furthermore solve the μ -problem of the MSSM [67]. The NMSSM has more free parameters compared to the MSSM and can produce a richer phenomenology in the Higgs sector, which is composed of three CP-even and two CP-odd neutral Higgs bosons and one charged Higgs boson. However, supersymmetry puts strong constraints on the phenomenology of the NMSSM making it more strongly constrained than the non-supersymmetric models even though it contains the most free parameters.

All of our models contain two additional neutral Higgs bosons which mix with the 125 GeV state. The CxSM contains no further Higgs particles, while there is an additional charged Higgs boson in the C2HDM and the neutral Higgs bosons are no eigenstates of the CP operator. The N2HDM contains a charged and a pseudoscalar Higgs in addition to the three mixing CP-even scalars. The NMSSM extends the N2HDM Higgs sector by another pseudoscalar and also contains the superpartners of all the SM particles and Higgs bosons.

A prerequisite for the phenomenological studies is the generation of parameter point samples that fulfill all applicable constraints. In the CxSM we use the published implementation in the `ScannerS` [10, 68] framework to perform the parameter scan. In the NMSSM the parameter scan is performed using the `NMSSMtools` package [64, 69–74] as described in [11, 66].

We have created an implementation of the C2HDM as a `ScannerS` model class. This implementation is the first C2HDM parameter scan that includes the constraint of the CP-violating electric dipole moment of the electron [75]. We further use an in-house extension of `HDECAY` [76, 77] to the C2HDM. This allows us to be the first to check exclusion bounds from collider Higgs searches in the C2HDM using the `HiggsBounds` [78] code. Theoretical, electroweak, and flavor constraints as well as the measurements of the 125 GeV Higgs bosons properties have also been assembled and included. We discuss the influence of the new constraints on our parameter scan and compare our results to a previous work in the literature [39].

The N2HDM parameter scan is also performed with a `ScannerS` implementation. We diagonalize the N2HDM Lagrangian and derive all three particle couplings required for the parameter scan without any approximation. Theoretical constraints from the stability of the electroweak vacuum in the N2HDM potential are for the first time derived and implemented

in this thesis. The constraints from tree-level perturbative unitarity have been rederived and numerically verified. We have created the `N2HDECAY` code which extends `HDECAY` to the N2HDM and calculates the decay properties of all Higgs bosons. The decay properties are used with the `HiggsBounds` code to check exclusion bounds from collider searches and to verify agreement with the observed properties of the 125 GeV Higgs boson. Constraints from electroweak precision and flavor observables are also included in our parameter scan.

We use these samples of physical parameter points to study the properties of the 125 GeV Higgs boson. We compare the phenomenological possibilities our models predict and discuss how these deviations from the SM remain in agreement with the observations. We especially study the possibility of singlet or pseudoscalar admixture to the 125 GeV Higgs boson. We point out differences between the amounts of admixture allowed in our models and show which measurements put the strongest constraints on the admixtures.

Afterward, we discuss the phenomenology of the lightest non-125 GeV neutral (CP-even in the CxSM, N2HDM, and NMSSM) Higgs boson at the LHC. We study inclusive signal rates and explain in what regions our models can enhance these rates above the SM reference. We further point out possible observations that could allow us to distinguish between our models. We finally present an analysis of coupling sums of the lightest two neutral (CP-even in the CxSM, N2HDM, and NMSSM) Higgs bosons of our models. We show how the model predictions for these partial coupling sums differ. We point out several observations that could make the exclusion of a model feasible provided the couplings of two Higgs bosons are known with sufficient precision. Such an analysis will be challenging with LHC data only and could be considerably improved by measurements at a possible future linear collider [79–81].

The work is structured as follows. In chapter 2 we introduce the CxSM, the real and complex 2HDM, and the NMSSM. Chapter 3 is entirely devoted to the N2HDM. We present the diagonalization of the scalar potential in section 3.1 and derive the effective couplings of the scalars to the SM particles in section 3.2. In sections 3.3 and 3.4 we establish the theoretical constraints from tree-level vacuum stability and perturbative unitarity. Chapter 4 describes the parameter scans performed in the four models. We detail the constraints applied to the models as well as the parameter ranges used in the scans. We furthermore comment on the mass distributions of the neutral Higgs bosons and compare our results in the C2HDM to [39]. Chapter 5 finally contains the phenomenological analysis described in the previous paragraphs. We study the differences between our models in their predictions for the properties of the 125 GeV Higgs boson in section 5.1. Section 5.2 presents ways to distinguish the models provided a second Higgs boson is observed. We study the phenomenology of this second boson in section 5.2.1 and the possibilities offered by a sum-rule analysis of both Higgs bosons in section 5.2.2. We conclude in chapter 6.

In appendix A we present explicit formulas for the parameter transformations and triple-Higgs couplings in the N2HDM. Appendix B contains examples of N2HDM parameter points with a vacuum structure impossible in the 2HDM. The complete results of the global minimum analysis in the N2HDM are shown in appendix C. In appendix D we finally give a short overview on how to use the `N2HDECAY` code.

Overview of the studied Higgs sector extensions

In this chapter, we introduce the models studied in this thesis. We order them by their number of free parameters and start with a short review of the CxSM. Afterward, we give an introduction to the 2HDM. We focus on the C2HDM, while also establishing the R2HDM as a starting point for the extension to the N2HDM in chapter 3. We finally give a short overview of the NMSSM Higgs sector.

2.1. The Complex singlet-extension of the Standard Model

In the CxSM the SM Higgs sector is extended by a complex scalar singlet of hypercharge zero. The resulting scalar potential is

$$\begin{aligned}
 V = & \frac{m^2}{2} \Phi^\dagger \Phi + \frac{\lambda}{4} (\Phi^\dagger \Phi)^2 + \frac{\delta_2}{2} \Phi^\dagger \Phi |S|^2 + \frac{b_2}{2} |S|^2 + \frac{d_2}{4} |S|^4 \\
 & + \left(\frac{b_1}{4} S^2 + a_1 S + \text{c.c.} \right) .
 \end{aligned}
 \tag{2.1}$$

The field Φ is the SM Higgs-doublet field, and S is the complex singlet. The potential obeys a global $U(1)$ symmetry which is softly broken by the second line of eq. (2.1) to prevent the appearance of a Goldstone boson after electroweak symmetry breaking. We study the version of the model with a \mathbb{Z}_2 symmetry of $\text{Im}(S)$ imposed. This forces b_1 and a_1 to be real. All other parameters are required to be real by hermiticity. Hence, the CxSM has seven real parameters

$$m^2, \quad \lambda, \quad \delta_2, \quad b_2, \quad d_2, \quad b_1 \quad \text{and} \quad a_1 .
 \tag{2.2}$$

The scalar fields are expanded as

$$\Phi = \frac{1}{\sqrt{2}} \begin{pmatrix} G^\pm \\ v + h + iG^0 \end{pmatrix},
 \tag{2.3}$$

$$S = \frac{1}{\sqrt{2}} [v_s + s + i(v_a + a)]
 \tag{2.4}$$

around their vacuum expectation values (VEVs) v , v_s and v_a . We only consider the broken singlet phase [10, 11], where the three VEVs are non-zero and set $v \approx 246$ GeV. The fields G^\pm and G^0 are the charged and neutral would-be Goldstone bosons, respectively.

The three neutral fields $\rho_1 := h$, $\rho_2 := s$ and $\rho_3 := a$ mix. Their 3×3 mass matrix is

$$(\mathcal{M}^2)_{ij} = - \left\langle \frac{\partial^2 V}{\partial \rho_i \partial \rho_j} \right\rangle , \quad (2.5)$$

where the angle braces denote the vacuum expectation value. It is diagonalized by a mixing matrix R , defined through

$$\begin{pmatrix} H_1 \\ H_2 \\ H_3 \end{pmatrix} = R \begin{pmatrix} \rho_1 \\ \rho_2 \\ \rho_3 \end{pmatrix} . \quad (2.6)$$

The gauge eigenstates ρ_i are rotated into the mass eigenstates $H_{1,2,3}$ ordered by ascending mass as

$$m_{H_1}^2 < m_{H_2}^2 < m_{H_3}^2 . \quad (2.7)$$

We introduce the shorthands

$$s_x := \sin x , \quad c_x := \cos x , \quad t_x := \tan x \quad (2.8)$$

and parametrize R as

$$R = \begin{pmatrix} c_{\alpha_1} c_{\alpha_2} & c_{\alpha_2} s_{\alpha_1} & s_{\alpha_2} \\ -c_{\alpha_3} s_{\alpha_1} - c_{\alpha_1} s_{\alpha_2} s_{\alpha_3} & c_{\alpha_1} c_{\alpha_3} - s_{\alpha_1} s_{\alpha_2} s_{\alpha_3} & c_{\alpha_2} s_{\alpha_3} \\ -c_{\alpha_1} c_{\alpha_3} s_{\alpha_2} + s_{\alpha_1} s_{\alpha_3} & -c_{\alpha_3} s_{\alpha_1} s_{\alpha_2} - c_{\alpha_1} s_{\alpha_3} & c_{\alpha_2} c_{\alpha_3} \end{pmatrix} \quad (2.9)$$

where the mixing angles $\alpha_{1,2,3}$ take values in

$$-\frac{\pi}{2} \leq \alpha_{1,2,3} < \frac{\pi}{2} . \quad (2.10)$$

The seven independent parameters of the CxSM scalar potential can be conveniently expressed through the parameter set

$$\alpha_1 , \quad \alpha_2 , \quad \alpha_3 , \quad v \approx 246 \text{ GeV} , \quad v_s , \quad m_{H_i} \quad \text{and} \quad m_{H_j} , \quad (2.11)$$

where v_a and the third Higgs mass are functions of the other parameters [11].

One feature common to all extensions of the Higgs sector that only introduce singlet fields is the particularly simple way in which couplings are modified. The couplings of a Higgs boson H_i to a set of SM particles (p) are given by

$$\lambda_i^{(p)} = R_{i1} \lambda_{\text{SM}}^{(p)} . \quad (2.12)$$

The triple and quartic Higgs couplings of the CxSM can be found in the appendix of [11].

2.2. The Two-Higgs-Doublet Model

For a detailed introduction to the 2HDM we recommend the review by Branco et al. [29]. In the following we use the conventions from [37] for the C2HDM.

The 2HDM Higgs sector contains two scalar $SU(2)_L$ doublet fields with hypercharge $Y = 1$. The scalar potential is given by

$$V = m_{11}^2 \Phi_1^\dagger \Phi_1 + m_{22}^2 \Phi_2^\dagger \Phi_2 - \left(m_{12}^2 \Phi_1^\dagger \Phi_2 + \text{h.c.} \right) + \frac{\lambda_1}{2} \left(\Phi_1^\dagger \Phi_1 \right) + \frac{\lambda_2}{2} \left(\Phi_2^\dagger \Phi_2 \right) + \lambda_3 \Phi_1^\dagger \Phi_1 \Phi_2^\dagger \Phi_2 + \lambda_4 \Phi_1^\dagger \Phi_2 \Phi_2^\dagger \Phi_1 + \left(\frac{\lambda_5}{2} \left(\Phi_1^\dagger \Phi_2 \right)^2 + \text{h.c.} \right). \quad (2.13)$$

The potential (2.13) obeys a \mathbb{Z}_2 symmetry imposed on each doublet, which is softly broken by the m_{12}^2 term.

Requiring hermiticity forces all parameters except m_{12}^2 and λ_5 to be real. If $\arg(m_{12}^2) = \arg(\lambda_5)$ these complex phases can be absorbed by a basis transformation. If such a rotation, making λ_5 and m_{12}^2 real, exists we call the remaining eight-parameter model the real 2HDM (R2HDM). When this is not possible the Higgs sector entails sources of CP violation and we call the model the C2HDM. The C2HDM has ten real parameters.

In the 2HDM both doublet fields are expanded as ($i = 1, 2$)

$$\Phi_i = \begin{pmatrix} \phi_i^\pm \\ \frac{1}{\sqrt{2}} (v_i + \rho_i + i\eta_i) \end{pmatrix}, \quad (2.14)$$

where v_i denotes the VEV of the respective doublet. In principle, there could be a complex phase between the VEVs of the two doublets. This phase can, however, always be removed by a change of basis [30] which is why we omit it. The requirement that the vacuum

$$\langle \Phi_i \rangle = \begin{pmatrix} 0 \\ \frac{v_i}{\sqrt{2}} \end{pmatrix} \quad (2.15)$$

is a minimum of the scalar potential leads to the minimum conditions

$$m_{11}^2 v_1 + \frac{\lambda_1}{2} v_1^3 + \frac{\lambda_{345}}{2} v_1 v_2^2 = m_{12}^2 v_2, \quad (2.16a)$$

$$m_{22}^2 v_2 + \frac{\lambda_2}{2} v_2^3 + \frac{\lambda_{345}}{2} v_1^2 v_2 = m_{12}^2 v_1, \quad (2.16b)$$

$$2 \text{Im}(m_{12}^2) = v_1 v_2 \text{Im}(\lambda_5), \quad (2.16c)$$

where $\lambda_{345} = \lambda_3 + \lambda_4 + \text{Re}(\lambda_5)$. Using eqs. (2.16a) and (2.16b) we can trade the parameters m_{11}^2 and m_{22}^2 for v_1 and v_2 . Equation (2.16c) yields a relation between the two sources of CP violation in the scalar potential. This fixes one of the ten parameters of the C2HDM.

The scalar particle spectrum of the 2HDM contains three neutral scalars and a charged scalar. This can be easily seen by rotating the doublets into the Higgs basis [82, 83]

$$\begin{pmatrix} \mathcal{H}_1 \\ \mathcal{H}_2 \end{pmatrix} = \begin{pmatrix} \cos \beta & \sin \beta \\ -\sin \beta & \cos \beta \end{pmatrix} \begin{pmatrix} \Phi_1 \\ \Phi_2 \end{pmatrix} \quad (2.17)$$

with $\tan \beta = v_2/v_1$. In this basis, the doublets are given by

$$\mathcal{H}_1 = \begin{pmatrix} G^\pm \\ \frac{1}{\sqrt{2}} (v + H^0 + iG^0) \end{pmatrix}, \quad \mathcal{H}_2 = \begin{pmatrix} H^\pm \\ \frac{1}{\sqrt{2}} (R_2 + iI_2) \end{pmatrix}. \quad (2.18)$$

The complete VEV $v = \sqrt{v_1^2 + v_2^2}$ is now in doublet one, along with the massless would-be Goldstone bosons G^\pm and G^0 . The charged Higgs state H^\pm is already a mass eigenstate with mass

$$m_{H^\pm} = \frac{m_{12}^2}{s_\beta c_\beta} - v^2 (\lambda_4 + \text{Re}(\lambda_5)) . \quad (2.19)$$

We calculate the 3×3 mass matrix of the neutral Higgs bosons

$$(\mathcal{M}^2)_{ij} = - \left\langle \frac{\partial^2 \mathcal{V}}{\partial \rho_i \partial \rho_j} \right\rangle , \quad (2.20)$$

in the basis ρ_1, ρ_2 (from eq. (2.14)), and $\rho_3 := I_2$ (from eq. (2.18)). The mass matrix \mathcal{M}^2 is diagonalized by the mixing matrix R (same parametrization as in eq. (2.9)). The mass eigenstates $H_{1,2,3}$ are given as a function of the $\rho_{1,2,3}$ through

$$\begin{pmatrix} H_1 \\ H_2 \\ H_3 \end{pmatrix} = R \begin{pmatrix} \rho_1 \\ \rho_2 \\ \rho_3 \end{pmatrix} . \quad (2.21)$$

In the C2HDM the nine independent input parameters can be chosen as [33]

$$v \approx 246 \text{ GeV} , \quad \tan \beta , \quad \alpha_{1,2,3} , \quad m_{H_i} , \quad m_{H_j} , \quad m_{H^\pm} \quad \text{and} \quad m_{12}^2 , \quad (2.22)$$

where m_{H_i} and m_{H_j} denote any two of the three neutral Higgs masses. It is straightforward to work out formulas for calculating the third Higgs mass analytically (see e.g. [33]). Analytic relations between this set of parameters and the λ parameters of the Lagrangian can be found e.g. in [37]. We do not use either of these relations and instead perform these tasks numerically.

Note that in the CP-conserving case the mass matrix (2.20) is block diagonal and $\rho_3 = I_2$ is a pseudoscalar mass eigenstate A with

$$m_A = \frac{m_{12}^2}{s_\beta c_\beta} - 2v^2 \lambda_5 . \quad (2.23)$$

The remaining 2×2 block for the CP-even scalars is conventionally chosen to be diagonalized through

$$\begin{pmatrix} H \\ h \end{pmatrix} = \begin{pmatrix} c_\alpha & s_\alpha \\ -s_\alpha & c_\alpha \end{pmatrix} \begin{pmatrix} \rho_1 \\ \rho_2 \end{pmatrix} , \quad (2.24)$$

where α lies in the same range as $\alpha_{1,2,3}$ from eq. (2.10). The eight independent parameters of the R2HDM can be expressed through

$$v \approx 246 \text{ GeV} , \quad \tan \beta , \quad \alpha , \quad m_H , \quad m_h , \quad m_A , \quad m_{H^\pm} \quad \text{and} \quad m_{12}^2 . \quad (2.25)$$

2.2.1. Couplings of the C2HDM

Here we will give formulas for the effective couplings of the Higgs bosons to gauge bosons and fermions. We define the effective coupling c of a Higgs boson H_i to a set of SM particles (p) as

$$c(H_i(p)) := \frac{\lambda_i^{(p)}}{\lambda_{\text{SM}}^{(p)}} , \quad (2.26)$$

Table 2.1.: The four Yukawa types in the \mathbb{Z}_2 -symmetric 2HDM. It is shown which Higgs-doublet each kind of fermions couples to.

	u -type	d -type	leptons
type I	Φ_2	Φ_2	Φ_2
type II	Φ_2	Φ_1	Φ_1
lepton-specific	Φ_2	Φ_2	Φ_1
flipped	Φ_2	Φ_1	Φ_2

Table 2.2.: Yukawa coupling coefficients of the Higgs boson H_i in the 2HDM. The expressions given here correspond to $a + ib\gamma_5$ from eq. (2.28).

	u -type	d -type	leptons
type I	$\frac{R_{i2}}{s_\beta} - i\frac{R_{i3}}{t_\beta}\gamma_5$	$\frac{R_{i2}}{s_\beta} + i\frac{R_{i3}}{t_\beta}\gamma_5$	$\frac{R_{i2}}{s_\beta} + i\frac{R_{i3}}{t_\beta}\gamma_5$
type II	$\frac{R_{i2}}{s_\beta} - i\frac{R_{i3}}{t_\beta}\gamma_5$	$\frac{R_{i1}}{c_\beta} - it_\beta R_{i3}\gamma_5$	$\frac{R_{i1}}{c_\beta} - it_\beta R_{i3}\gamma_5$
lepton-specific	$\frac{R_{i2}}{s_\beta} - i\frac{R_{i3}}{t_\beta}\gamma_5$	$\frac{R_{i2}}{s_\beta} + i\frac{R_{i3}}{t_\beta}\gamma_5$	$\frac{R_{i1}}{c_\beta} - it_\beta R_{i3}\gamma_5$
flipped	$\frac{R_{i2}}{s_\beta} - i\frac{R_{i3}}{t_\beta}\gamma_5$	$\frac{R_{i1}}{c_\beta} - it_\beta R_{i3}\gamma_5$	$\frac{R_{i2}}{s_\beta} + i\frac{R_{i3}}{t_\beta}\gamma_5$

where λ denotes the Feynman rule of the corresponding vertex and the division is understood to cancel equal tensor structure. The Feynman rule can be extracted from the effective coupling by multiplying with the corresponding SM Feynman rule which can be found e.g. in [28]. Further Feynman rules of the C2HDM can be found in the appendix of [37].

The effective coupling of a Higgs boson H_i to a pair of gauge bosons $VV \in \{W^+W^-, ZZ\}$ is given by

$$c(H_iVV) = c_\beta R_{i1} + s_\beta R_{i2} . \quad (2.27)$$

In the presence of two scalar doublets, Higgs-mediated tree-level flavor changing neutral currents can appear. In order to agree with the experimental observations, these need to be strongly suppressed [84]. The \mathbb{Z}_2 symmetries of the scalar potential can be extended to the Yukawa sector in a way that completely eliminates Higgs-mediated flavor changing neutral currents. This behavior is called natural flavor conservation [85, 86]. It is achieved by allowing any type of fermion to couple to only one Higgs doublet. The u -type quarks conventionally couple to Φ_2 resulting in the four phenomenologically different types of 2HDMs shown in table 2.1.

Expanding the Yukawa Lagrangian and transforming all fields into the mass basis yields

$$\mathcal{L}_Y = - \sum_{i=1}^3 \frac{m_f}{v} \bar{\psi}_f (a + ib\gamma_5) \psi_f H_i \quad (2.28)$$

for every fermion ψ_f with mass m_f and neutral Higgs boson H_i . The coefficients a and b can be found in table 2.2.

In the R2HDM the expressions given above reduce to the known couplings given e.g. in [29].

2.3. The Next-to-Minimal Supersymmetric Model

Supersymmetry requires the introduction of at least two Higgs-doublet superfields \hat{H}_u and \hat{H}_d . The superfield \hat{H}_u couples to u -type quarks, while \hat{H}_d couples to d -type quarks and

leptons. All superfields are denoted by hats. In the NMSSM an additional complex singlet superfield \hat{S} is added to this minimal Higgs sector. We will now review the NMSSM Higgs particle spectrum and clarify how the parameters used in the scan are defined. A complete review of the NMSSM can be found in [64, 65].

The NMSSM Higgs potential receives contributions from the superpotential

$$W = \lambda \hat{S} \hat{H}_u \hat{H}_d + \frac{\kappa}{3} \hat{S}^3 + h_t \hat{Q}_3 \hat{H}_u \hat{t}_R^c + h_b \hat{Q}_3 \hat{H}_d \hat{b}_R^c - h_\tau \hat{L}_3 \hat{H}_d \hat{\tau}_R^c. \quad (2.29)$$

For simplicity we only write terms including the third generation fermion superfields. These are the left handed doublet quark (\hat{Q}_3) and lepton (\hat{L}_3) superfields as well as the right handed singlet quark (\hat{t}_R^c, \hat{b}_R^c) and lepton ($\hat{\tau}_R^c$) superfields. The superpotential is parametrized by the parameters λ, κ , and the three Yukawa couplings $h_{t,b,\tau}$.

The soft SUSY breaking Lagrangian contains the mass terms for the scalar components of the complex superfields. This part of the Lagrangian reads

$$-\mathcal{L}_{\text{mass}} = m_{H_u}^2 |H_u|^2 + m_{H_d}^2 |H_d|^2 + m_S^2 |S|^2 + m_{\tilde{Q}_3}^2 |\tilde{Q}_3|^2 + m_{\tilde{t}_R}^2 |\tilde{t}_R|^2 + m_{\tilde{b}_R}^2 |\tilde{b}_R|^2 + m_{\tilde{L}_3}^2 |\tilde{L}_3|^2 + m_{\tilde{\tau}_R}^2 |\tilde{\tau}_R|^2. \quad (2.30)$$

The m^2 are the scalar mass parameters for the Higgs (H_u, H_d and S), squark (the doublet \tilde{Q}_3 and the singlets \tilde{t}_R and \tilde{b}_R), and slepton (doublet \tilde{L}_3 and singlet $\tilde{\tau}_R$) fields.

The part of the soft SUSY breaking Lagrangian containing the trilinear terms is

$$-\mathcal{L}_{\text{tril}} = \lambda A_\lambda H_u H_d S + \frac{1}{3} \kappa A_\kappa S^2 + h_t A_t \tilde{Q}_3 H_u \tilde{t}_R^c - h_b A_b \tilde{Q}_3 H_d \tilde{b}_R^c - h_\tau A_\tau \tilde{L}_3 H_d \tilde{\tau}_R^c + \text{h.c.} \quad (2.31)$$

and the part with the gaugino mass terms is

$$-\mathcal{L}_{\text{gaugino}} = \frac{1}{2} \left(M_1 \tilde{B} \tilde{B} + M_2 \sum_{a=1}^3 \tilde{W}_a \tilde{W}^a + M_3 \sum_{b=1}^8 \tilde{G}_b \tilde{G}^b \right). \quad (2.32)$$

The parameters A in eq. (2.31) are the soft SUSY breaking parameters for the Higgs self couplings (A_λ and A_κ) and the Yukawa couplings (A_t, A_b and A_τ), respectively. The gaugino sector contains the soft SUSY breaking bino \tilde{B} , wino \tilde{W} and gluino \tilde{G} mass terms with their corresponding mass parameters M_i .

After electroweak symmetry breaking the Higgs fields are expanded around their VEVs v_d, v_u and v_s as

$$H_d = \begin{pmatrix} \frac{v_d + h_d + ia_d}{\sqrt{2}} \\ h_d^- \end{pmatrix}, \quad H_u = \begin{pmatrix} h_u^+ \\ \frac{v_u + h_u + ia_u}{\sqrt{2}} \end{pmatrix}, \quad S = \frac{v_s + h_s + ia_s}{\sqrt{2}}. \quad (2.33)$$

The 2×2 mass matrix of the charged sector can be diagonalized in a straightforward way yielding the charged Goldstone bosons G^\pm and the charged Higgs bosons H^\pm . In the pseudoscalar sector, a first rotation of the 3×3 mass matrix separates the massless Goldstone boson G^0 . Diagonalizing the remaining 2×2 matrix yields the mass eigenstates A_1 and A_2 with the masses $m_{A_1} < m_{A_2}$. The CP-even neutral sector yields a 3×3 mass matrix with mass eigenstates H_1, H_2 , and H_3 after rotating to the mass basis. The corresponding masses are ordered as $m_{H_1} < m_{H_2} < m_{H_3}$.

The NMSSM Higgs sector contains seven parameters at tree level

$$\lambda, \quad A_\lambda, \quad \kappa, \quad A_\kappa, \quad v \approx 246 \text{ GeV}, \quad \tan \beta = v_u/v_d \quad \text{and} \quad \mu_{\text{eff}} = \lambda v_s. \quad (2.34)$$

The parameter μ_{eff} replaces the μ parameter of the MSSM. The MSSM faces the so called μ -problem meaning that the parameter μ , which would naturally be of the order of the SUSY breaking scale, has to be of the order of v to allow for a proper electroweak symmetry breaking. The value of μ_{eff} in the NMSSM is generated by the singlet VEV v_s which is naturally of order v and thus dynamically solves the μ -problem [67].

The parameter relations induced by supersymmetry differentiate the NMSSM from the non-supersymmetric models. A further difference is that the Higgs masses are not independent input parameters in the NMSSM. They have to be calculated including higher order corrections to obtain a precise prediction and in particular to reproduce the measured mass value of the 125 GeV Higgs boson. Through this calculation the other parameters from eqs. (2.30) to (2.32) enter the Higgs sector. This makes the NMSSM our model with the largest number of free parameters.

The Next-to-Two-Higgs-Doublet Model

The scalar Lagrangian of the N2HDM is given by

$$\mathcal{L}_{\text{scalar}}^{\text{N2HDM}} = (D^\mu \Phi_1)^\dagger (D^\mu \Phi_1) + (D^\mu \Phi_2)^\dagger (D^\mu \Phi_2) + (\partial^\mu \Phi_S)^2 - V_{\text{scalar}} , \quad (3.1)$$

with the electroweak covariant derivative

$$D^\mu = \partial^\mu + i\frac{g}{2}\vec{\sigma}\vec{W}^\mu + i\frac{g'}{2}B^\mu . \quad (3.2)$$

This includes the vector of the three $SU(2)_L$ gauge fields W^μ and $U(1)_Y$ gauge field B^μ as well as the corresponding coupling constants g and g' . The vector $\vec{\sigma}$ contains the three Pauli matrices.

As can be inferred from the kinetic terms, we added a real, hypercharge zero, $SU(2)_L$ singlet field Φ_S to the 2HDM. The first section of this chapter is dedicated to the N2HDM scalar potential V_{scalar} and provides details on the diagonalization procedure.

The second section contains formulas for various Higgs couplings to SM particles and information on the sum-rules those fulfill. The formulas for the triple Higgs couplings can be found in appendix A. The last section addresses theoretical constraints from vacuum stability and tree-level perturbative unitarity.

3.1. The N2HDM scalar potential

The N2HDM is based on the CP-conserving 2HDM with a softly broken \mathbb{Z}_2 symmetry, the R2HDM of section 2.2. The N2HDM was first studied by Chen, Freid, and Sher [40]. It has so far been used as a model that provides a dark matter candidate, which appears if the singlet VEV vanishes [41]. It has also been considered as a possible explanation for the 750 GeV diphoton excess [87, 88] through a sub-GeV scalar state [42]. This excess has since disappeared [89, 90].

In all of these studies, some level of approximation was applied. In particular, the possibility of a singlet admixture to the 125 GeV Higgs boson was neglected. In the following, we will diagonalize the N2HDM Lagrangian without any such assumptions.

The scalar potential of the N2HDM reads

$$\begin{aligned}
V = & m_{11}^2 \Phi_1^\dagger \Phi_1 + m_{22}^2 \Phi_2^\dagger \Phi_2 - m_{12}^2 (\Phi_1^\dagger \Phi_2 + \text{h.c.}) + \frac{\lambda_1}{2} (\Phi_1^\dagger \Phi_1)^2 + \frac{\lambda_2}{2} (\Phi_2^\dagger \Phi_2)^2 \\
& + \lambda_3 \Phi_1^\dagger \Phi_1 \Phi_2^\dagger \Phi_2 + \lambda_4 \Phi_1^\dagger \Phi_2 \Phi_2^\dagger \Phi_1 + \frac{\lambda_5}{2} \left((\Phi_1^\dagger \Phi_2)^2 + \text{h.c.} \right) \\
& + \frac{1}{2} u_s^2 \Phi_S^2 + \frac{\lambda_6}{8} \Phi_S^4 + \frac{\lambda_7}{2} (\Phi_1^\dagger \Phi_1) \Phi_S^2 + \frac{\lambda_8}{2} (\Phi_2^\dagger \Phi_2) \Phi_S^2 .
\end{aligned} \tag{3.3}$$

The last line is the difference to the R2HDM potential eq. (2.13) and describes the contribution of the singlet field Φ_S .

One can see that this introduces no new sources of \mathbb{Z}_2 breaking for the doublet fields. The singlet field has an exact \mathbb{Z}_2 symmetry. Furthermore, we work in the CP-conserving version of the model, where all parameters and all VEVs are required to be real. The above potential contains all possible renormalizable terms that respect these symmetries. It contains a total of twelve real parameters.

The doublet fields are defined as in eq. (2.14) and the singlet field acquires a real VEV v_s . We expand the fields in the broken phase as

$$\Phi_1 = \begin{pmatrix} H_1^+ \\ \frac{1}{\sqrt{2}}(v_1 + \rho_1 + i\eta_1) \end{pmatrix}, \quad \Phi_2 = \begin{pmatrix} H_2^+ \\ \frac{1}{\sqrt{2}}(v_2 + \rho_2 + i\eta_2) \end{pmatrix}, \tag{3.4}$$

$$\Phi_S = v_s + \rho_s . \tag{3.5}$$

By requiring the potential to have a stationary point at the VEV we obtain the three minimum conditions

$$\left\langle \frac{dV}{dv_1} \right\rangle = 0 \quad \Rightarrow \quad \frac{v_2}{v_1} m_{12}^2 - m_{11}^2 = \frac{1}{2} (v_1^2 \lambda_1 + v_2^2 \lambda_{345} + v_s^2 \lambda_7) , \tag{3.6a}$$

$$\left\langle \frac{dV}{dv_2} \right\rangle = 0 \quad \Rightarrow \quad \frac{v_1}{v_2} m_{12}^2 - m_{22}^2 = \frac{1}{2} (v_1^2 \lambda_{345} + v_2^2 \lambda_2 + v_s^2 \lambda_8) , \tag{3.6b}$$

$$\left\langle \frac{dV}{dv_s} \right\rangle = 0 \quad \Rightarrow \quad -m_s^2 = \frac{1}{2} (v_1^2 \lambda_7 + v_2^2 \lambda_8 + v_s^2 \lambda_6) . \tag{3.6c}$$

The shorthand

$$\lambda_{345} = \lambda_3 + \lambda_4 + \lambda_5 \tag{3.7}$$

has been introduced here. These relations will be used to simplify the mass matrices below.

3.1.1. Diagonalization of the charged and pseudoscalar sectors

Since we only introduce a real singlet with a real VEV, the charged and pseudoscalar sectors of the model remain unchanged with respect to the R2HDM. This means that the charged and pseudoscalar mass matrices can still be diagonalized by the rotation matrix

$$R_\beta = \begin{pmatrix} \cos \beta & \sin \beta \\ -\sin \beta & \cos \beta \end{pmatrix}, \tag{3.8}$$

with β defined through

$$\tan \beta = \frac{v_2}{v_1} . \tag{3.9}$$

This yields the charged and neutral Goldstone modes as well as the physical charged Higgs boson H^\pm with mass (2.19) and the physical pseudoscalar Higgs boson A with mass (2.23).

3.1.2. Diagonalization of the scalar sector

The CP-even neutral mass matrix is modified with respect to the R2HDM. In the basis

$$(\rho_1 \quad \rho_2 \quad \rho_s) \quad (3.10)$$

it is now a 3×3 matrix given by

$$M_{\text{scalar}}^2 = \begin{pmatrix} v^2 \lambda_1 c_\beta^2 + m_{12}^2 t_\beta & v^2 \lambda_{345} c_\beta s_\beta - m_{12}^2 & v v_s \lambda_7 c_\beta \\ v^2 \lambda_{345} c_\beta s_\beta - m_{12}^2 & v^2 \lambda_2 s_\beta^2 + m_{12}^2 / t_\beta & v v_s \lambda_8 s_\beta \\ v v_s \lambda_7 c_\beta & v v_s \lambda_8 s_\beta & v_s^2 \lambda_6 \end{pmatrix}, \quad (3.11)$$

where eqs. (3.6) and (3.9) have been used to trade the parameters m_{11}^2 , m_{22}^2 , and m_s^2 for v , $\tan \beta$, and v_s .

The orthogonal matrix R that diagonalizes M_{scalar}^2 is again parametrized by

$$R = \begin{pmatrix} c_{\alpha_1} c_{\alpha_2} & c_{\alpha_2} s_{\alpha_1} & s_{\alpha_2} \\ -c_{\alpha_3} s_{\alpha_1} - c_{\alpha_1} s_{\alpha_2} s_{\alpha_3} & c_{\alpha_1} c_{\alpha_3} - s_{\alpha_1} s_{\alpha_2} s_{\alpha_3} & c_{\alpha_2} s_{\alpha_3} \\ -c_{\alpha_1} c_{\alpha_3} s_{\alpha_2} + s_{\alpha_1} s_{\alpha_3} & -c_{\alpha_3} s_{\alpha_1} s_{\alpha_2} - c_{\alpha_1} s_{\alpha_3} & c_{\alpha_2} c_{\alpha_3} \end{pmatrix}. \quad (3.12)$$

This is the same parametrization as eq. (2.9) in the previous chapter. Since the sign of the mass eigenstates has no physical relevance, the angles α can without loss of generality be taken in the range

$$-\frac{\pi}{2} \leq \alpha_{1,2,3} < \frac{\pi}{2}. \quad (3.13)$$

We call the physical states H_1 to H_3 with masses m_{H_1} to m_{H_3} and impose the mass ordering

$$m_{H_1} < m_{H_2} < m_{H_3}. \quad (3.14)$$

The mass eigenstates are given as linear combinations of the gauge eigenstates through

$$\begin{pmatrix} H_1 \\ H_2 \\ H_3 \end{pmatrix} = R \begin{pmatrix} \rho_1 \\ \rho_2 \\ \rho_s \end{pmatrix}. \quad (3.15)$$

A value that is useful for understanding the phenomenology is the singlet admixture Σ_i . In the N2HDM we define

$$\Sigma_i = (R_{i3})^2, \quad (3.16)$$

which specifies the fraction of the singlet field in the physical CP-even neutral scalar H_i .

3.1.3. Parametrizations of the Potential

In the original notation the scalar potential eq. (3.3) contains twelve real independent parameters. We call this the Lagrangian parametrization and the parametrization by masses and mixing angles the physical one. The parameters in each basis are:

$$\text{Lagrangian:} \quad m_{11}^2, m_{22}^2, m_s^2, \quad \lambda_{1-8}, \quad m_{12}^2, \quad (3.17)$$

$$\text{physical:} \quad v, \tan \beta, v_s, \quad m_{H_{1,2,3}}, m_A, m_{H^\pm}, \alpha_{1,2,3}, \quad m_{12}^2. \quad (3.18)$$

Table 3.1.: Explicit formulas for the effective Yukawa couplings of the neutral CP-even Higgs states in the type I and type II models, normalized to the SM values.

(a) Type I			
$c(H_i f f)$	u	d	l
H_1	$(c_{\alpha_2} s_{\alpha_1})/s_\beta$	$(c_{\alpha_2} s_{\alpha_1})/s_\beta$	$(c_{\alpha_2} s_{\alpha_1})/s_\beta$
H_2	$(c_{\alpha_1} c_{\alpha_3} - s_{\alpha_1} s_{\alpha_2} s_{\alpha_3})/s_\beta$	$(c_{\alpha_1} c_{\alpha_3} - s_{\alpha_1} s_{\alpha_2} s_{\alpha_3})/s_\beta$	$(c_{\alpha_1} c_{\alpha_3} - s_{\alpha_1} s_{\alpha_2} s_{\alpha_3})/s_\beta$
H_3	$-(c_{\alpha_1} s_{\alpha_3} + c_{\alpha_3} s_{\alpha_1} s_{\alpha_2})/s_\beta$	$-(c_{\alpha_1} s_{\alpha_3} + c_{\alpha_3} s_{\alpha_1} s_{\alpha_2})/s_\beta$	$-(c_{\alpha_1} s_{\alpha_3} + c_{\alpha_3} s_{\alpha_1} s_{\alpha_2})/s_\beta$
(b) Type II			
$c(H_i f f)$	u	d	l
H_1	$(c_{\alpha_2} s_{\alpha_1})/s_\beta$	$(c_{\alpha_1} c_{\alpha_2})/c_\beta$	$(c_{\alpha_1} c_{\alpha_2})/c_\beta$
H_2	$(c_{\alpha_1} c_{\alpha_3} - s_{\alpha_1} s_{\alpha_2} s_{\alpha_3})/s_\beta$	$-(c_{\alpha_3} s_{\alpha_1} + c_{\alpha_1} s_{\alpha_2} s_{\alpha_3})/c_\beta$	$-(c_{\alpha_3} s_{\alpha_1} + c_{\alpha_1} s_{\alpha_2} s_{\alpha_3})/c_\beta$
H_3	$-(c_{\alpha_1} s_{\alpha_3} + c_{\alpha_3} s_{\alpha_1} s_{\alpha_2})/s_\beta$	$(s_{\alpha_1} s_{\alpha_3} - c_{\alpha_1} c_{\alpha_3} s_{\alpha_2})/c_\beta$	$(s_{\alpha_1} s_{\alpha_3} - c_{\alpha_1} c_{\alpha_3} s_{\alpha_2})/c_\beta$

The minimum conditions eqs. (3.6a) to (3.6c) in combination with eq. (3.9) allow to trade m_{11}^2 , m_{22}^2 , and m_s^2 for $v \approx 246$ GeV, $\tan \beta$, and v_s . Furthermore, the soft \mathbb{Z}_2 breaking parameter m_{12}^2 is an independent parameter in both parametrizations.

This leaves the eight λ_i in the parametrization of the Lagrangian and the five particle masses and three α_i in the physical parametrization. By requiring that the mass matrices are diagonalized by the corresponding rotation matrices a system of equations linear in the λ_i can be found. Solving this system yields analytic expressions that allow expressing all parameters of the Lagrangian through the physical ones. These are mainly useful for simplifying the triple-Higgs couplings. They are, therefore, given along with the triple-Higgs couplings in appendix A. Since the system is not linear in the mixing angles α_i it is not possible to obtain the inverse transformation analytically.

3.2. Higgs couplings to SM particles

The singlet field ρ_s has no direct couplings to SM particles. This means that all changes in the tree-level Higgs couplings compared to the R2HDM come from the 3×3 scalar mixing matrix (3.12). Furthermore, any couplings not involving the CP-even neutral Higgs bosons remain unchanged from the R2HDM and can be found e.g. in [29]. We give effective couplings normalized to the SM coupling wherever a corresponding SM coupling exists.

3.2.1. Yukawa couplings and \mathbb{Z}_2 -symmetric fermion sectors

There are four possible ways of extending the \mathbb{Z}_2 symmetry to the Yukawa sector, exactly as in the 2HDM (see table 2.1). These four types again all prevent the appearance of tree-level flavor changing neutral currents. The effective couplings of the Higgs boson H_i to fermions are given by the mixing matrix element R_{ij} where j is the index of the doublet in table 2.1 divided by c_β for $j = 1$ and s_β for $j = 2$. Explicit formulas for the type I and type II N2HDM are given in table 3.1.

The fermion couplings allow the construction of a sum-rule in the type II model:

$$\frac{1}{\sum_{i=1}^3 c^2(H_i uu)} + \frac{1}{\sum_{i=1}^3 c^2(H_i dd)} = 1. \quad (3.19)$$

Since the couplings of the type I model do not contain c_β it is impossible to construct a sum-rule independent of β for that type.

$c(H_i VV)$	
H_1	$c_{\alpha_2} c_{\beta-\alpha_1}$
H_2	$-c_{\beta-\alpha_1} s_{\alpha_2} s_{\alpha_3} + c_{\alpha_3} s_{\beta-\alpha_1}$
H_3	$-c_{\alpha_3} c_{\beta-\alpha_1} s_{\alpha_2} - s_{\alpha_3} s_{\beta-\alpha_1}$

Table 3.3: Effective couplings of the neutral CP-even Higgs bosons to gauge bosons normalized to the SM values. The couplings to W^+W^- and ZZ differ only in their SM value leading to a common effective coupling denoted by VV .

$\tilde{c}(H_i V H)$	
H_1	$-c_{\alpha_2} s_{\beta-\alpha_1}$
H_2	$c_{\alpha_3} c_{\beta-\alpha_1} + s_{\beta-\alpha_1} s_{\alpha_2} s_{\alpha_3}$
H_3	$-c_{\beta-\alpha_1} s_{\alpha_3} + c_{\alpha_3} s_{\beta-\alpha_1} s_{\alpha_2}$

Table 3.4: Mixing angle dependency of the Higgs-gauge couplings involving a CP-even neutral scalar and either AZ or $H^\pm W^\mp$. The corresponding prefactors are given in eq. (3.21).

3.2.2. Higgs-gauge couplings

The interactions between Higgs and gauge bosons stem from the covariant derivatives in the kinetic terms in eq. (3.1). As the singlet does not transform under electroweak gauge transformations it has no direct couplings to gauge bosons. All couplings are therefore results of the mixing matrix (2.9). In the following, we only present three-particle couplings which are relevant for decays.

The effective couplings to a pair of gauge bosons are given in table 3.3. Since the N2HDM respects custodial symmetry the effective couplings to W^+W^- and ZZ are equal. They fulfill an even simpler sum-rule than the Yukawa couplings:

$$\sum_{i=1}^3 c^2(H_i VV) = 1. \quad (3.20)$$

The two other kinds of gauge couplings that are modified from their R2HDM values are $H_i AZ$ and $H_i H^\pm W^\mp$. They do not have an SM equivalent to normalize to and depend on the momenta of the scalars. We, therefore, adopt the convention that the momentum p_i of the H_i is always incoming and the momentum p_{A/H^\pm} of the A or H^\pm is outgoing. This is the convention used in the Higgs Hunter's guide [28].

The Feynman rules for the vertices are given by

$$\lambda^\mu(H_i AZ) = \frac{\sqrt{g^2 + g'^2}}{2} (p_A + p_i)^\mu \times \tilde{c}(H_i V H), \quad (3.21a)$$

$$\lambda^\mu(H_i H^\pm W^\pm) = \mp \frac{ig}{2} (p_{H^\pm} + p_i)^\mu \times \tilde{c}(H_i V H), \quad (3.21b)$$

with the coupling factors $\tilde{c}(H_i V H)$ in terms of the mixing angles given in table 3.4.

The three particle Higgs-gauge couplings involving only the pseudoscalar A and the charged Higgs bosons H^\pm are not modified with respect to their R2HDM values. These can be found e.g. in [29].

3.3. Vacuum stability constraints

In this section, we describe the criteria used to verify that the vacuum of electroweak symmetry breaking is the global minimum of the N2HDM scalar potential. We first present the conditions for the N2HDM scalar potential to be bounded from below. Afterward, we analyze all stationary points of the potential and show how to assure the electroweak vacuum is the global minimum.

3.3.1. Conditions for the potential to be bounded from below

A global minimum of the scalar potential exists if the potential is bounded from below. We consider the potential to be bounded from below in the strong sense, which is defined as the potential being strictly positive as the fields approach infinity. The necessary and sufficient conditions for this are given in [91]. They depend on the discriminant

$$D = \begin{cases} \lambda_4 - \lambda_5, & \text{for } \lambda_4 > \lambda_5 \\ 0, & \text{for } \lambda_4 \leq \lambda_5 \end{cases}. \quad (3.22)$$

The allowed region is

$$\Omega_1 \cup \Omega_2 \quad (3.23)$$

with

$$\Omega_1 = \left\{ \lambda_1, \lambda_2, \lambda_6 > 0; \sqrt{\lambda_1 \lambda_6} + \lambda_7 > 0; \sqrt{\lambda_2 \lambda_6} + \lambda_8 > 0; \right. \\ \left. \sqrt{\lambda_1 \lambda_2} + \lambda_3 + D > 0; \lambda_7 + \sqrt{\frac{\lambda_1}{\lambda_2}} \lambda_8 \geq 0 \right\}, \quad (3.24)$$

$$\Omega_2 = \left\{ \lambda_1, \lambda_2, \lambda_6 > 0; \sqrt{\lambda_2 \lambda_6} \geq \lambda_8 > -\sqrt{\lambda_2 \lambda_6}; \right. \\ \left. \sqrt{\lambda_1 \lambda_6} > -\lambda_7 \geq \sqrt{\frac{\lambda_1}{\lambda_2}} \lambda_8; \right. \\ \left. \sqrt{(\lambda_7^2 - \lambda_1 \lambda_6)(\lambda_8^2 - \lambda_2 \lambda_6)} > \lambda_7 \lambda_8 - (D + \lambda_3) \lambda_6 \right\}. \quad (3.25)$$

While obvious from the formulas we emphasize that this forces λ_1, λ_2 and λ_6 to be strictly positive, which is useful for optimizations of the parameter scan.

3.3.2. Vacuum decay and global minimum condition

If the physical vacuum of the scalar potential is not the global minimum it is possible for the vacuum to tunnel into the global minimum [92, 93]. Since the catastrophic consequences of such a tunneling have obviously not been observed, the physical vacuum either has to be the global minimum of the theory (called a stable vacuum) or the tunneling time has to be large compared to the age of the universe (called a metastable vacuum). The calculation of tunneling times is beyond the scope of this work. We, therefore, do not consider metastable vacua and require the physical vacuum to be the global minimum of the N2HDM scalar potential. In the following, we present conditions that check this requirement. A discussion of vacuum stability in the R2HDM including an approximate calculation of tunneling times can be found in [94].

In the 2HDM it has been proven [95] that the existence of a normal minimum of the form eq. (2.15) ensures there is no deeper minimum that breaks electromagnetic charge or CP. This proof does not generalize to the N2HDM as can be seen from the counterexamples given in appendix B. We, therefore, have to include the possibility of CP and charge breaking minima in our analysis. We consider the most general static field configuration

$$\langle \Phi_1 \rangle = \begin{pmatrix} 0 \\ v_1 \end{pmatrix}, \quad \langle \Phi_2 \rangle = \begin{pmatrix} v_{\text{cb}} \\ v_2 + i v_{\text{cp}} \end{pmatrix}, \quad \langle \Phi_S \rangle = v_s. \quad (3.26)$$

We have used the four degrees of freedom of the $SU(2)_L \times U(1)_Y$ gauge group to remove four degrees of freedom in the static field configuration. Equation (3.26), therefore, parametrizes a

gauge slice onto which all possible static field configurations of the N2HDM can be projected via a gauge transformation.

We will in the following refer to the static fields v_1 , v_2 , and v_s as well as to the CP-violating v_{cp} and the charge breaking v_{cb} as VEVs even though this is technically only correct if the configuration describes a minimum of the scalar potential. The \mathbb{Z}_2 symmetries of the potential manifest in this parametrization as a \mathbb{Z}_2 symmetry for v_s , v_{cb} , and v_{cp} as well as a simultaneous \mathbb{Z}_2 symmetry of v_1 and v_2 . This allows us to choose all VEVs except v_2 to be positive without loss of generality.

In order to classify all possible minima we look at the stationarity conditions for all five VEVs

$$\left\langle \frac{dV}{dv_1} \right\rangle = 0 \Leftrightarrow v_2 m_{12}^2 - v_1 m_{11}^2 = \frac{1}{2} v_1 (v_1^2 \lambda_1 + v_2^2 \lambda_{345} + v_{\text{cb}}^2 \lambda_3 + v_{\text{cp}}^2 \lambda_{34-5} + v_s^2 \lambda_7) , \quad (3.27)$$

$$\left\langle \frac{dV}{dv_2} \right\rangle = 0 \Leftrightarrow v_1 m_{12}^2 - v_2 m_{22}^2 = \frac{1}{2} v_2 (v_1^2 \lambda_{345} + v_2^2 \lambda_2 + v_{\text{cb}}^2 \lambda_2 + v_{\text{cp}}^2 \lambda_2 + v_s^2 \lambda_8) , \quad (3.28)$$

$$\left\langle \frac{dV}{dv_{\text{cb}}} \right\rangle = 0 \Leftrightarrow -v_{\text{cb}} m_{22}^2 = \frac{1}{2} v_{\text{cb}} (v_1^2 \lambda_3 + v_2^2 \lambda_2 + v_{\text{cb}}^2 \lambda_2 + v_{\text{cp}}^2 \lambda_2 + v_s^2 \lambda_8) , \quad (3.29)$$

$$\left\langle \frac{dV}{dv_{\text{cp}}} \right\rangle = 0 \Leftrightarrow -v_{\text{cp}} m_{22}^2 = \frac{1}{2} v_{\text{cp}} (v_1^2 \lambda_{34-5} + v_2^2 \lambda_2 + v_{\text{cb}}^2 \lambda_2 + v_{\text{cp}}^2 \lambda_2 + v_s^2 \lambda_8) , \quad (3.30)$$

$$\left\langle \frac{dV}{dv_s} \right\rangle = 0 \Leftrightarrow -v_s m_s^2 = \frac{1}{2} v_s (v_1^2 \lambda_7 + v_2^2 \lambda_8 + v_{\text{cb}}^2 \lambda_8 + v_{\text{cp}}^2 \lambda_8 + v_s^2 \lambda_6) . \quad (3.31)$$

Here the shorthands

$$\lambda_{345} = \lambda_3 + \lambda_4 + \lambda_5 \quad \text{and} \quad \lambda_{34-5} = \lambda_3 + \lambda_4 - \lambda_5 \quad (3.32)$$

have been used.

Note that we have not made assumptions on any of the VEVs being non-zero. Looking at eqs. (3.29) and (3.30) we notice, that they are almost equal. If we assume both v_{cb} and v_{cp} to be non-zero we obtain

$$\lambda_4 - \lambda_5 = 0 . \quad (3.33)$$

With the exception of this special case v_{cb} and v_{cp} cannot be simultaneously non-zero. We obtain a similar condition by setting $v_1 = 0$ in eq. (3.27) or equivalently $v_2 = 0$ in eq. (3.28). This leads to

$$(v_1 = 0 \Leftrightarrow v_2 = 0) \vee m_{12}^2 = 0 . \quad (3.34)$$

In the following we will only consider the case $|m_{12}^2| > 0$, implying that v_1 and v_2 are either both zero or both non-zero. All possible combinations of VEVs being zero or non-zero are listed in table 3.5.

The simplest cases are (s)III and sIV. In these, the equations reduce to a linear system of equations for the squares of the non-zero VEVs. The solutions of these systems can be inserted directly into the scalar potential and yield only three distinct values of the scalar potential. Along with these stationary values, we obtain positivity conditions for the squared VEVs, which have to be fulfilled in order for the solution to exist. The stationary values and corresponding conditions are given in appendix C.

In the cases (s)II the minimum conditions eqs. (3.29) and (3.30) allow a great simplification of the v_2 minimum condition eq. (3.28). This leads to a solution that is unique up to the sign

Table 3.5.: All possible cases of VEVs being zero (0) or non-zero (1). Cases which are only allowed when certain parameter conditions are satisfied are not shown.

Case	I	IIa	IIb	IIIa	IIIb	IIIc	sI	sIIa	sIIb	sIIIa	sIIIb	sIIIc	sIV
v_1	1	1	1	0	0	0	1	1	1	0	0	0	0
v_2	1	1	1	0	0	0	1	1	1	0	0	0	0
v_{cp}	0	1	0	1	1	0	0	1	0	1	1	0	0
v_{cb}	0	0	1	1	0	1	0	0	1	1	0	1	0
v_s	0	0	0	0	0	0	1	1	1	1	1	1	1

of v_2 . The value of the scalar potential at the stationary point, however, does not depend on this sign. The cases (s)II each yield a unique stationary value given in appendix C along with the related positivity conditions.

The cases I and sI, where the minimum has the form of a normal R2HDM or N2HDM minimum, respectively, are the most complicated ones. The form of the system of equations can in both cases easily be brought to a system of coupled cubic equations for v_1 and v_2 . By parametrizing them as

$$v_1 = v \cos(\delta) , \quad v_2 = v \sin(\delta) \quad (3.35)$$

they can be reduced to a single quartic equation of $\sin^2(\delta)$. This leads to up to four valid solutions for $\sin^2(\delta)$ (real and in the open interval $(0, 1)$). The additional freedom in the sign of $\sin(\delta)$ and v_2 leads to a maximum of 16 solutions for each of the case I configurations. These solutions still have to satisfy positivity constraints of the squared VEVs. The full procedure is again detailed in appendix C.

We do not try to discern which of these stationary points are minima, maxima, or saddle points. To check if our minimum is the global one, we simply compare the value of the scalar potential at our minimum with the ones at all other stationary points. This involves four comparisons with an analytically known value, which cover the cases II, III and IV and the comparisons with the numeric solutions for the case I configurations.

3.4. Tree-level perturbative unitarity

Tree-level perturbative unitarity is a requirement following directly from S-matrix unitarity [96]. It is usually considered by requiring that the $2 \rightarrow 2$ scalar scattering matrix has no eigenvalue with an absolute value larger than 8π . This is the strict upper limit above which unitarity is violated. It can be useful to require a limit lower than 8π at tree level to account for possible large enhancements of the scalar couplings through higher order corrections.

We follow [96] in both procedure and naming. We calculate the full $2 \rightarrow 2$ scattering matrix of the gauge basis fields (see eq. (3.5))

$$H_1^\pm, H_2^\pm, \rho_1, \rho_2, \rho_s, \eta_1, \eta_2 \quad (3.36)$$

in `Mathematica`. This scattering matrix is block diagonal.

The block matrices that do not contain ρ_s have the unique eigenvalues

$$f_1 := \lambda_3 + \lambda_4 , \quad p_1 := \lambda_3 - \lambda_4 , \quad (3.37a)$$

$$f_- := \lambda_3 + \lambda_5 , \quad e_2 := \lambda_3 - \lambda_5 , \quad (3.37b)$$

$$f_+ := \lambda_3 + 2\lambda_4 + 3\lambda_5 , \quad e_1 := \lambda_3 + 2\lambda_4 - 3\lambda_5 , \quad (3.37c)$$

and

$$c_{\pm} := \frac{1}{2} \left(\lambda_1 + \lambda_2 \pm \sqrt{(\lambda_1 - \lambda_2)^2 + 4\lambda_4^2} \right) , \quad (3.37d)$$

$$b_{\pm} := \frac{1}{2} \left(\lambda_1 + \lambda_2 \pm \sqrt{(\lambda_1 - \lambda_2)^2 + 4\lambda_5^2} \right) . \quad (3.37e)$$

These same eigenvalues are also found in the R2HDM. The blocks involving the singlet field ρ_s contribute the eigenvalues

$$s_1 = \lambda_7 , \quad (3.37f)$$

$$s_2 = \lambda_8 \quad (3.37g)$$

and the eigenvalues $a_{1,2,3}$ which are the real roots of the cubic polynomial

$$\begin{aligned} & 4(-27\lambda_1\lambda_2\lambda_6 + 12\lambda_3^2\lambda_6 + 12\lambda_3\lambda_4\lambda_6 + 3\lambda_4^2\lambda_6 + 6\lambda_2\lambda_7^2 - 8\lambda_3\lambda_7\lambda_8 - 4\lambda_4\lambda_7\lambda_8 + 6\lambda_1\lambda_8^2) \\ & + x(36\lambda_1\lambda_2 - 16\lambda_3^2 - 16\lambda_3\lambda_4 - 4\lambda_4^2 + 18\lambda_1\lambda_6 + 18\lambda_2\lambda_6 - 4\lambda_7^2 - 4\lambda_8^2) \\ & + x^2(-6(\lambda_1 + \lambda_2 + \lambda_6)) + x^3 . \end{aligned} \quad (3.38)$$

The obtained eigenvalues are not all independent. As noted in [96]

$$3f_1 = p_1 + e_1 + f_+ , \quad (3.39)$$

$$3e_2 = 2p_1 + e_1 , \quad (3.40)$$

$$3f_- = 2p_1 + f_+ . \quad (3.41)$$

We can, therefore, drop the conditions on f_1 , e_2 and f_- as they are implied by taking p_1 , e_1 and f_+ into account. Since $\lambda_1, \lambda_2 > 0$ is necessary for the potential to be bounded from below (see section 3.3.1) we obtain

$$|c_+| > |c_-| , \quad (3.42)$$

$$|b_+| > |b_-| . \quad (3.43)$$

The resulting conditions for tree-level perturbative unitarity are thus

$$|\lambda_3 - \lambda_4| < 8\pi , \quad (3.44a)$$

$$|\lambda_3 + 2\lambda_4 \pm 3\lambda_5| < 8\pi \quad (3.44b)$$

$$\left| \frac{1}{2} \left(\lambda_1 + \lambda_2 + \sqrt{(\lambda_1 - \lambda_2)^2 + 4\lambda_4^2} \right) \right| < 8\pi , \quad (3.44c)$$

$$\left| \frac{1}{2} \left(\lambda_1 + \lambda_2 + \sqrt{(\lambda_1 - \lambda_2)^2 + 4\lambda_5^2} \right) \right| < 8\pi , \quad (3.44d)$$

$$|a_{1,2,3}| < 8\pi \quad (3.44e)$$

where $a_{1,2,3}$ are the real roots of eq. (3.38).

CHAPTER 4

Scans of the parameter space

In this chapter we describe the **ScannerS** [10, 68] framework used to perform parameter scans in the CxSM, C2HDM and N2HDM. We describe in some detail the theoretical and experimental constraints used to decide whether an N2HDM or C2HDM point with given fixed parameters is physical (i.e. in agreement with theoretical requirements and current experimental data) or not. We also review the constraints applied on the CxSM and NMSSM in [11]. Afterward, we discuss the mass distribution of the neutral scalars in the obtained parameter samples and compare the C2HDM sample to an earlier work [39].

ScannerS is a code that performs parameter scans in models with extended Higgs sectors. The program first generates a uniform VEV configuration according to the symmetry-breaking pattern of the model. It also generates a tree-level Higgs sector mixing matrix uniformly with respect to the Haar measure [97]. Afterward, it solves the linear system of constraints which define the local minimum. This linear system relates the physical particle masses to the parameters of the Lagrangian given a fixed mixing matrix and fixed VEVs. It finally finds which parameters of the model are independent, generates uniform values for them, and calculates the dependent parameters. Every parameter point generated this way is checked by **ScannerS** for agreement with all constraints specified by the user. The program also includes a model independent check of tree-level perturbative unitarity and provides interfaces to various programs for particle phenomenology. A detailed description of the **ScannerS** scanning procedure can be found in [10].

In the following we denote the discovered Higgs boson by h_{125} with a mass of

$$m_{h_{125}} = 125.09 \text{ GeV} , \tag{4.1}$$

which is the central value of the current mass measurement [8]. Electroweak corrections are not included in both parameter scans and analysis as they are not available for all of our models.

4.1. The CxSM parameter scan

The `ScannerS` implementation of the CxSM is publicly available and has been described in detail in [10, 11]. We did not generate new CxSM points but instead reused the sample generated for [11]. The tree-level theoretical constraints have been checked as described in [10]. They include checks for tree-level perturbative unitarity, for the potential to be bounded from below, and for the `ScannerS` minimum to be the global one. There are no constraints from flavor physics that apply to the CxSM. In singlet models, all couplings of a given Higgs boson to SM particles are suppressed by the same mixing factor. This allows calculating the oblique parameters S , T and U [98], which parametrize constraints from electroweak precision measurements, directly from the SM values [10]. Compatibility of these parameters with the SM fit [99] was demanded at the 2σ level including correlations.

The public tool `SHDECAY` [11] was used to calculate the Higgs boson decay properties. Agreement with the Higgs searches was checked with `HiggsBounds v6.50` [78]. In the CxSM all QCD corrections to the production processes cancel upon normalization to the SM. The production cross sections normalized to the SM which are required by `HiggsBounds` are therefore simply given by the corresponding effective coupling squared. The CxSM parameter scan is described in more detail in [11].

From this sample, we only consider those parameter points where only one Higgs boson h_{125} contributes to the 125 GeV Higgs signal. To this end we require a window of $m_{h_{125}} \pm 5$ GeV to be free of any Higgs bosons except for h_{125} . We impose this condition in all our models as we do not want to study the superposition and interference effects of a degenerate Higgs signal. A detailed discussion of the statistical treatment of such superimposed signals can be found in [100]. We check the properties of the h_{125} by requiring that the global signal strength μ is within 2σ of the experimental fit value [9]. The one parameter fit is a natural parametrization for the CxSM due to the simple coupling structure. The signal strength of h_{125} is given by [11]

$$\mu \approx (R_{h_{125}1})^2 \times \sum_{X_{\text{SM}}} \text{BR}(h_{125} \rightarrow X_{\text{SM}}) . \quad (4.2)$$

The mixing matrix R is defined in eq. (2.6) and h_{125} is one of the H_i from eq. (2.6). The sum includes all decay channels X_{SM} of h_{125} into SM particles. We do not include the effects of chain production studied in [11] for any of our models.

The sample was generated using eq. (2.11) as input parameters. One of the Higgs bosons is identified with h_{125} and the remaining are constrained to the mass range

$$30 \text{ GeV} \leq m_{H_i} < 1 \text{ TeV} . \quad (4.3)$$

The doublet VEV v is fixed to the SM value

$$v = \frac{1}{\sqrt{\sqrt{2}G_F}} , \quad (4.4)$$

while v_a and v_s are allowed to lie within

$$1 \text{ GeV} \leq v_s, v_a < 1.5 \text{ TeV} . \quad (4.5)$$

The mixing angles $\alpha_{1,2,3}$ range over their whole allowed region (2.10).

4.2. The C2HDM parameter scan

We have created an implementation of the C2HDM as a `ScannerS` model class. All constraints that apply in the C2HDM have been calculated and used before. We, however, provide the first simultaneous application of all of these constraints in a full parameter scan. We use the conditions for the potential to be bounded from below as well as the discriminant to prevent vacuum decay from [101]. The inequalities to ensure tree-level perturbative unitarity are given in [29] for the general (real and complex) 2HDM. They have been checked against the model-independent numeric default procedure of `ScannerS`.

The flavor constraints on R_b [102, 103] and $B \rightarrow X_s \gamma$ [103–106] generalize from the R2HDM to the C2HDM as they only depend on the charged Higgs boson. These constraints are checked as 2σ exclusion bounds in the m_{H^\pm} - $\tan\beta$ -plane. We note that the newest calculation [106] enforces

$$m_{H^\pm} > 480 \text{ GeV} \quad (4.6)$$

in the type II and lepton specific 2HDM. Agreement with electroweak precision measurements is again verified using the oblique parameters S , T and U . The formulas to calculate the oblique parameters are given in [29] for the general 2HDM. We calculate S , T and U and demand 2σ compatibility with the SM fit [99]. We take the full correlation among the three parameters into account.

Constraints on the Higgs sector from collider searches are checked using the `HiggsBounds` [78] code and the individual signal strength fit [9] for the h_{125} . In order to use these constraints, we need information on the Higgs boson production and decay properties. We use an in-house implementation of the C2HDM into `HDECAY v6.51` [76, 77] to calculate the Higgs boson decay widths and branching ratios. This includes state-of-the-art QCD corrections to the decay processes. Additionally, the Higgs boson production cross sections normalized to the SM are required. The production cross sections via gluon fusion (ggF) and b -quark fusion (bbF) are obtained through the `ScannerS` interface to `SusHi v1.6.0` [107] at NNLO QCD. We calculate the contributions to the cross sections from the CP-even and CP-odd Yukawa couplings separately and add them incoherently. The obtained cross section is normalized to the CP-even SM production cross section. We define

$$\mu_F = \frac{\sigma_{\text{C2HDM}}^{\text{even}}(\text{ggF}) + \sigma_{\text{C2HDM}}^{\text{even}}(\text{bbF}) + \sigma_{\text{C2HDM}}^{\text{odd}}(\text{ggF}) + \sigma_{\text{C2HDM}}^{\text{odd}}(\text{bbF})}{\sigma_{\text{SM}}^{\text{even}}(\text{ggF})} \quad (4.7)$$

where we neglect the SM bbF cross section compared to the ggF one. All QCD corrections to production cross sections mediated by gauge bosons cancel upon normalization to the SM. The Vector Boson Fusion (VBF) and Vector boson associated (VH) production channels thus yield

$$\mu_V = \frac{\sigma_{\text{C2HDM}}(\text{VBF})}{\sigma_{\text{SM}}(\text{VBF})} = \frac{\sigma_{\text{C2HDM}}(\text{VH})}{\sigma_{\text{SM}}(\text{VH})} = c^2(H_i VV) . \quad (4.8)$$

There is no CP-odd contribution to these channels and the effective couplings $c(H_i VV)$ are given in eq. (2.27). Finally, `HiggsBounds` requires the cross sections through t -quark and b -quark associated production. The QCD corrections to these processes do not cancel upon normalization due to the incoherent addition of CP-even and CP-odd contributions. These cross section ratios are therefore used at leading order where they are given by the effective coupling $a^2 + b^2$ with a and b from table 2.2. This information is passed to `HiggsBounds` via the `ScannerS` interface and `HiggsBounds v4.3.1` is used to check agreement with all 2σ exclusion limits from LEP, Tevatron and LHC Higgs searches. As in the CxSM, we require a window of $m_{h_{125}} \pm 5 \text{ GeV}$ to be free of additional Higgs bosons in order to avoid degenerate

Higgs signals. The properties of the h_{125} are checked using the six-parameter signal strength fit from [9]. The six fit parameters are

$$\frac{\mu_F}{\mu_V}, \mu_F^{\gamma\gamma}, \mu_F^{ZZ}, \mu_F^{WW}, \mu_F^{\tau\tau}, \mu_F^{bb}, \quad (4.9)$$

with

$$\mu_F^{xx} = \mu_F \frac{\text{BR}_{\text{C2HDM}}(H_i \rightarrow xx)}{\text{BR}_{\text{SM}}(H_i \rightarrow xx)}. \quad (4.10)$$

We require agreement with the fit results [9] at the $2 \times 1\sigma$ level.

Due to the presence of CP-violation in the C2HDM, constraints on CP-violating quantities are important. The strongest one is the constraint on the electric dipole moment of the electron [108] using the experimental limit by the ACME collaboration [75]. We have implemented the calculation from [109] and impose that the results are compatible with the 90% c.l. bound given in [75].

4.2.1. Scan ranges in the type II C2HDM

We use the input parameters from eq. (2.22). We fix v to its SM value (4.4) and vary $\tan\beta$ within

$$0.25 \leq \tan\beta < 35. \quad (4.11)$$

The lower bound on $\tan\beta$ from the R_b measurement is stronger than the lower bound in eq. (4.11). Therefore, the lower bound of eq. (4.11) has no influence on the physical parameter points. We transform the mixing matrix generated by `ScannerS` such that it is parametrized as eq. (2.9) with

$$-\frac{\pi}{2} \leq \alpha_{1,2,3} < \frac{\pi}{2}. \quad (4.12)$$

We further identify one of the neutral Higgs bosons H_i with h_{125} and choose the charged Higgs mass in the range

$$480 \text{ GeV} \leq m_{H^\pm} < 1 \text{ TeV}. \quad (4.13)$$

We observe that the electroweak precision constraints force the mass of at least one of the neutral Higgs bosons to be close to m_{H^\pm} . We use this information to increase the efficiency of the parameter scan by generating a second neutral Higgs mass m_H in the interval

$$m_{H^\pm} - 100 \text{ GeV} \leq m_H < m_{H^\pm} + 250 \text{ GeV}. \quad (4.14)$$

We have performed a scan without this parametrization and only the electroweak precision constraints enabled. The interval (4.14) was then chosen such that all points that fulfill the electroweak precision constraints lie within. In the final sample with all constraints turned on we found no physical parameter point within 30 GeV of the interval borders. This verifies that this parametrization does not influence the phenomenology.

The third neutral Higgs mass is not an independent parameter and is automatically calculated by `ScannerS`. We require the two non- h_{125} Higgs masses to be within

$$30 \text{ GeV} \leq m_{H \neq h_{125}} < 1 \text{ TeV}. \quad (4.15)$$

Finally we generate $\text{Re}(m_{12}^2)$ in the interval

$$0 \text{ GeV}^2 \leq \text{Re}(m_{12}^2) < 500\,000 \text{ GeV}^2. \quad (4.16)$$

In the C2HDM there exist physical parameter points with $\text{Re}(m_{12}^2) < 0 \text{ GeV}^2$. They are, however, extremely rare and we do not include them in our study.

4.3. The N2HDM parameter scan

We have implemented the theoretical constraints on the N2HDM at tree-level as described in sections 3.3 and 3.4. The requirement that the potential is bounded from below is verified using eqs. (3.24) and (3.25). We require the vacuum state found by `ScannerS` to be the global minimum of the scalar potential. To ensure that, we verify that the value of the scalar potential at the `ScannerS` vacuum is deeper than at all of the stationary points described in section 3.3.2 and appendix C. We check tree-level unitarity using eq. (3.44). `ScannerS` includes a model independent numeric check of tree-level perturbative unitarity. We verified that both methods yield the same results and use eq. (3.44) because of its lower run-time.

Most of the experimental constraints applied on the C2HDM in section 4.2 also apply to the N2HDM. We first apply the constraints on R_b and $B \rightarrow X_s \gamma$ from flavor physics. Since these are only sensitive to the charged Higgs boson, the 2HDM calculation and the resulting 2σ limits in the m_{H^\pm} - $\tan\beta$ -plane can be taken over to the N2HDM. The oblique parameters S , T , and U are calculated with the general formulas in [110, 111]. We again demand 2σ compatibility with the SM fit including the full correlation.

We calculate the branching ratios and total widths of the Higgs bosons with `N2HDECAY` (see appendix D). The code is an implementation of the N2HDM in `HDECAY` based on `HDECAY v6.51` [76, 77] including all QCD corrections available in `HDECAY`. All required Higgs production cross sections need to be normalized to the SM. The cross sections through ggF and bbF are treated as in the C2HDM (see section 4.2) without the CP-odd contributions. In all other production cross sections, the QCD corrections cancel upon normalization to the SM. This means that each normalized cross section is simply the corresponding effective coupling squared. The effective couplings can be found in section 3.2. This information is passed to `HiggsBounds v4.3.1` which checks for agreement with all 2σ exclusion bounds from Higgs searches. We use the same signal strength parametrization as in section 4.2 to check the properties of h_{125} . We also require the same $m_{h_{125}} \pm 5$ GeV window to be free of additional Higgs particles.

4.3.1. Scan ranges in the type II N2HDM

We use the parameter set (3.18) as input parameters. We fix v to its SM value from eq. (4.4) and allow for

$$0.25 \leq \tan\beta < 35, \quad (4.17)$$

with the same reasoning as in the C2HDM. We further identify one of the H_i with h_{125} and transform the mixing matrix generated by `ScannerS` to match eq. (3.12), with

$$-\frac{\pi}{2} \leq \alpha_{1,2,3} < \frac{\pi}{2}. \quad (4.18)$$

We allow the remaining neutral Higgs bosons to have masses within

$$30 \text{ GeV} \leq m_{H \neq h_{125}}, m_A < 1 \text{ TeV}, \quad (4.19)$$

while forcing

$$480 \text{ GeV} \leq m_{H^\pm} < 1 \text{ TeV} \quad (4.20)$$

to comply with eq. (4.6). Finally, we generate the singlet VEV v_s in the interval

$$1 \text{ GeV} \leq v_s < 1.5 \text{ TeV} \quad (4.21)$$

and the soft Z_2 breaking parameter m_{12}^2 in

$$0 \text{ GeV}^2 < m_{12}^2 < 500\,000 \text{ GeV}^2. \quad (4.22)$$

The condition $m_{12}^2 > 0$ is found to be necessary for our minimum to be the global minimum of the scalar potential. The same behavior is observed in the R2HDM.

Table 4.1.: Input parameter ranges of the NMSSM parameter scan. All parameters have been varied independently between the given minimum and maximum values.

	$\tan\beta$	λ	κ	M_1	M_2	M_3	A_t	A_b	A_τ	$m_{\tilde{Q}_3}$	$m_{\tilde{L}_3}$	A_λ	A_κ	μ_{eff}
	in TeV													
min	1	0	-0.7	0.1	0.2	1.3	-2	-2	-2	0.6	0.6	-2	-2	-1
max	30	0.7	0.7	1	1	3	2	2	2	3	3	2	2	1

4.4. The NMSSM parameter scan

We performed a parameter scan in the NMSSM following the procedure described in [11, 66]. In the following, we will give an overview of the scanning procedure. For a more detailed description, we refer to [66].

We use the `NMSSMtools` package [64, 69–74] for most of the analysis. `NMSSMtools` calculates the spectrum of the Higgs and SUSY particles including higher order corrections. The branching ratios are calculated with the tool `NMHDECAY` [73] for the Higgs bosons and `NMSDECAY` [70, 74] for the SUSY particles. Additionally, the package checks for vacuum stability verifies LEP and Tevatron exclusion bounds from searches for SUSY particles and tests low-energy observables. More information can be found on the website [112].

The resulting points are checked for compatibility with the searches for SUSY particles at LHC [113–126]. The `NMSSMtools` interface with `micrOMEGAS` [69, 127] is used to calculate the relic density. We require that the relic density does not exceed the value measured by the PLANCK collaboration [128]. Exclusion bounds from Higgs searches are verified using a link to `HiggsBounds` in the effective coupling approximation. We require a neutral CP-even Higgs boson between 124 GeV and 126 GeV. We also impose that the window $m_{h_{125}} \pm 5$ GeV is free of further Higgs bosons, as for the other models. Agreement with the observed h_{125} is again verified using the signal strength fit described in section 4.2 at the $2 \times 1\sigma$ level. The required signal strengths are computed by `NMSSMtools`.

The parameter ranges used to generate our sample are given in table 4.1. The parameters $\tan\beta$ and λ are conventionally chosen to be positive, while κ and the soft SUSY breaking A parameters can have both signs. To ensure perturbativity and unitarity up to the GUT scale we require [64]

$$\lambda^2 + \kappa^2 < 0.7^2 . \quad (4.23)$$

The mass parameters for the third generation sfermions, which are missing in table 4.1, are

$$m_{\tilde{t}_R} = m_{\tilde{Q}_3} , \quad m_{\tilde{\tau}_R} = m_{\tilde{L}_3} , \quad \text{and} \quad m_{\tilde{b}_R} = 3 \text{ TeV} . \quad (4.24)$$

All first and second generation sfermion mass parameters are set to 3 TeV. In addition we only keep points with all Higgs masses between 30 GeV and 1 TeV for consistency with the other models.

4.5. Mass distributions of the neutral scalars

In this section and the following we discuss some properties of the samples of physical parameter points obtained using the procedure described in sections 4.1 to 4.4. Each of our models contains a set of three mixing neutral Higgs bosons $H_{1,2,3}$ one of which is identified with the h_{125} state. In the CP-conserving models, these are the three CP-even neutral Higgs bosons of the theory. In the C2HDM they are the neutral states of mixed CP quantum numbers. In

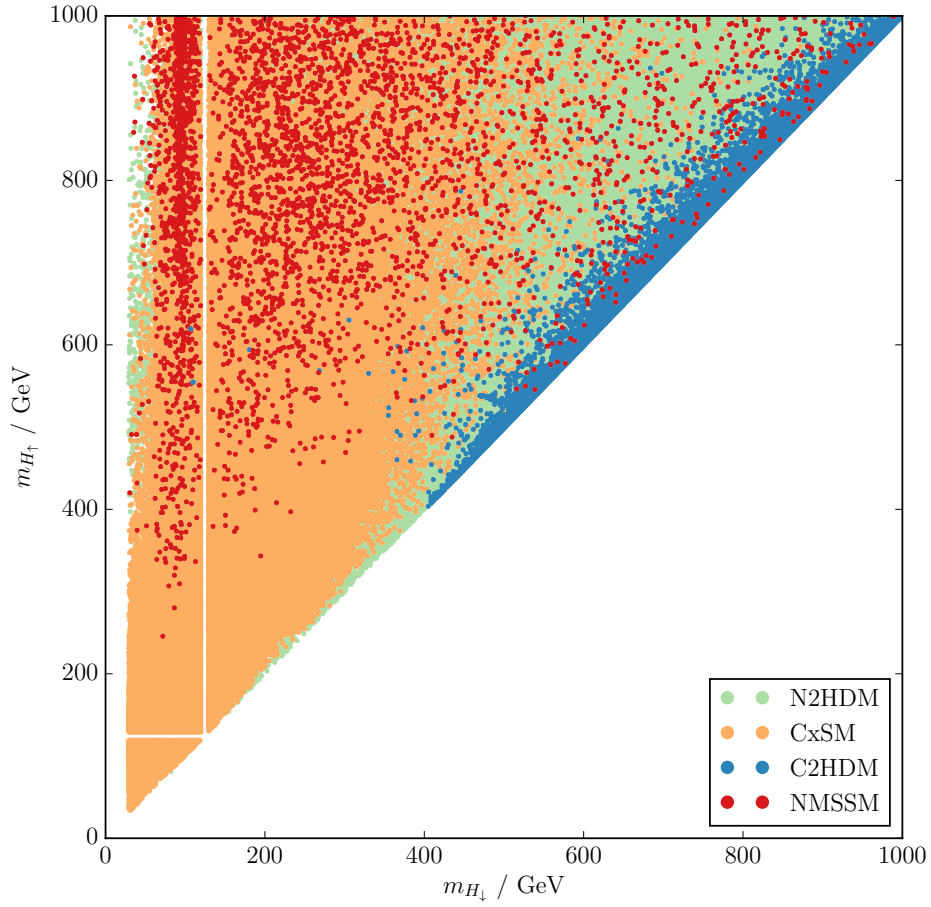


Figure 4.1.: Masses of the two non- h_{125} neutral scalars in our four models. Note that by definition $m_{H_\downarrow} \leq m_{H_\uparrow}$. The gaps at 125 GeV are the windows around h_{125} to avoid degenerate Higgs signals (see e.g. section 4.1).

this section, we study the mass distributions of the two non- h_{125} particles out of these three. We call the lighter of the two H_{\downarrow} and the heavier H_{\uparrow} .

Figure 4.1 shows the distribution of the masses of these two particles in our models. A first observation is that all of our models can produce points with $m_{H_{\downarrow}} < m_{h_{125}}$. In the C2HDM our sample only contains two points in this region (here shown in front of the NMSSM points to be visible at all). This is insufficient to conclude anything about the C2HDM behavior in this region. We will continue to show these points in the plots but will not comment on them any further. Only the N2HDM and the CxSM contain parameter points where $m_{H_{\uparrow}} < m_{h_{125}}$. The N2HDM points cover this whole region but are almost completely hidden behind CxSM points. We note that the light NMSSM pseudoscalar A_1 as well as an R2HDM pseudoscalar A may also be located in this mass range.

Apart from the differences in this region the CxSM, N2HDM and NMSSM can cover most of the parameter space. The C2HDM, however, behaves very differently and always has H_{\uparrow} heavier than about 400 GeV. This is the behavior mentioned in section 4.2.1 and can be understood as follows. The T parameter strongly constrains the allowed mass difference between $m_{H^{\pm}}$ and the nearest neutral Higgs boson masses. Since there is no charged Higgs boson in the CxSM the T parameter does not constrain this model. In the C2HDM, N2HDM and NMSSM it forces at least one and usually two neutral Higgs bosons to be close in mass to the charged Higgs boson. The contributions of these neutral Higgs bosons can then cancel the contribution of the charged Higgs boson to the T parameter. The N2HDM and NMSSM, however, have additional pseudoscalar Higgs bosons which can help to fulfill this constraint, greatly reducing its influence on the mass distributions of the CP-even Higgs bosons. In the C2HDM there are only three neutral Higgs bosons, one of which is identified with h_{125} . This forces at least one of the remaining two neutral Higgs bosons to be close in mass to $m_{H^{\pm}}$ which is heavier than 480 GeV due to the constraints from $\text{BR}(B \rightarrow X_s \gamma)$ [106]. This leads to additional light Higgs bosons being extremely rare in the C2HDM, which could allow us to distinguish it from the other models.

4.6. The effect of new constraints on the C2HDM parameter space

In this section, we compare the results of our parameter scan in the C2HDM type II to the results from [39]. To do so we recreate figures 1 to 3 from [39] using both our sample of physical parameter points as described in section 4.2 (sample I) and a sample with the constraints from `HiggsBounds` and the electron electric dipole moment (eEDM) turned off (sample II). The constraints applied on sample II are roughly equivalent to the ones used in [39].

To properly compare with [38] we explicitly use the parametrization (2.9) for the C2HDM mixing matrix R . For simplicity we only include points where h_{125} is the lightest neutral Higgs boson H_1 . The h_{125} state is then given by

$$h_{125} = R_{11}\rho_1 + R_{12}\rho_2 + R_{13}\rho_3 = [c_{\alpha_1}c_{\alpha_2}]\rho_1 + [c_{\alpha_2}s_{\alpha_1}]\rho_2 + s_{\alpha_2}\rho_3 \quad (4.25)$$

as a linear combination of the states $\rho_{1,2,3}$ from section 2.2.

Figure 4.2 shows the two mixing angles that enter in the admixtures of h_{125} . The angle α_1 mixes the two CP-even parts of the Higgs-doublets while α_2 parametrizes the CP-violating pseudoscalar admixture. We see that in sample I α_2 is constrained to be very small, while it can take much bigger values with the eEDM constraint turned off. The shape of sample II approximately agrees with [39].

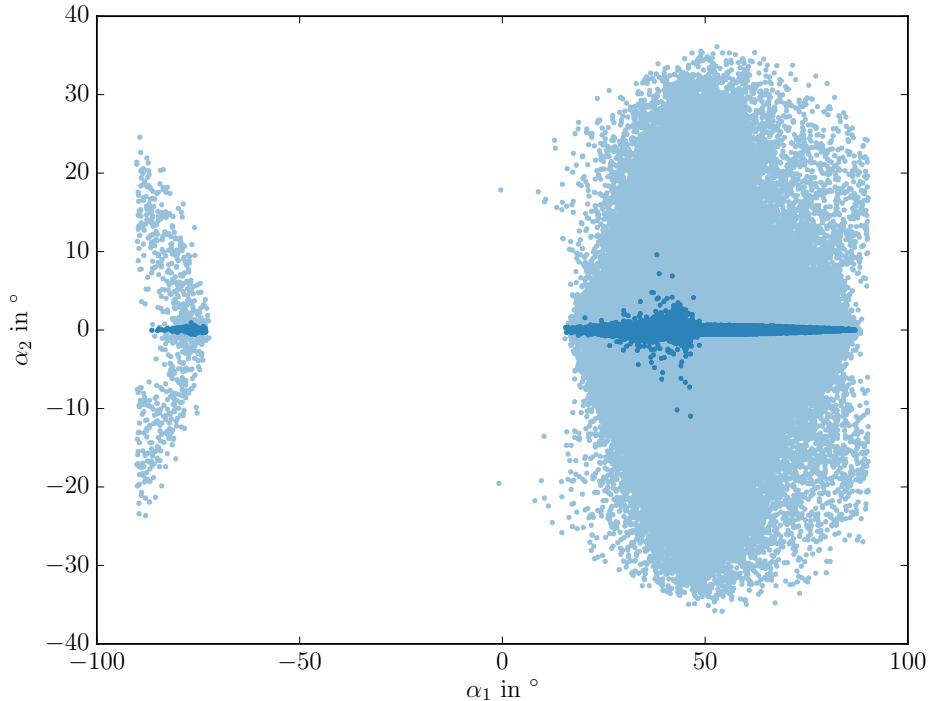


Figure 4.2.: Mixing angles α_1 and α_2 of the C2HDM mixing matrix R (see e.g. eq. (2.9)) in degree. The dark blue points are sample I and the light blue points sample II, respectively. To be compared to fig. 1 from [39].

The mixing matrix elements R_{11} and R_{13} are shown in fig. 4.3. We do not show the plot for the matrix element R_{12} as there are no significant differences between the samples I and II and [39]. The sample II points behave very similarly to [39] in both figs. 4.3a and 4.3b. The main difference between the samples I and II in fig. 4.3a is the exclusion of $R_{11} \approx 0$ points by the stronger constraints applied in sample I. The phenomenology of these points, where the couplings of h_{125} to d -type quarks and leptons are purely CP-odd, was studied in detail in [39]. In fig. 4.3b we see that in sample I the CP-violating R_{13} is constrained to be smaller than 0.01 except for points of small $\tan\beta$.

Figure 4.4 shows $\tan\beta$ over

$$\text{sgn}(c(h_{125}VV)) \cdot \sin(\alpha_1 - \pi/2) , \quad (4.26)$$

with $c(h_{125}VV)$ given by eq. (2.27). In the R2HDM a plot of $\tan\beta$ over $x := \text{sgn}(c(h_{125}VV)) \cdot \sin(\alpha)$ splits the parameter space into the correct-sign-regime (where $x < 0$) and the wrong-sign-regime [129] (where $x > 0$). In [39] it is shown that letting $R_{13} \rightarrow 0 \Leftrightarrow \alpha_2 \rightarrow 0$ (and $(\alpha_1 - \pi/2) \rightarrow \alpha$ to match the R2HDM conventions) leads h_{125} into the R2HDM limit of the C2HDM. Since employing the eEDM and HiggsBounds constraints enforces $|R_{13}| < 0.01$ for most of our sample I points h_{125} is usually in the R2HDM limit. This is the case for all points with eq. (4.26) larger than zero. We can, therefore, use the condition

$$\text{sgn}(c(h_{125}VV)) \cdot \sin(\alpha_1 - \frac{\pi}{2}) > 0 \quad (4.27)$$

for the wrong-sign-limit. The phenomenology of the wrong-sign-limit points is very different from the other C2HDM points. We will frequently comment on their behavior in chapter 5.

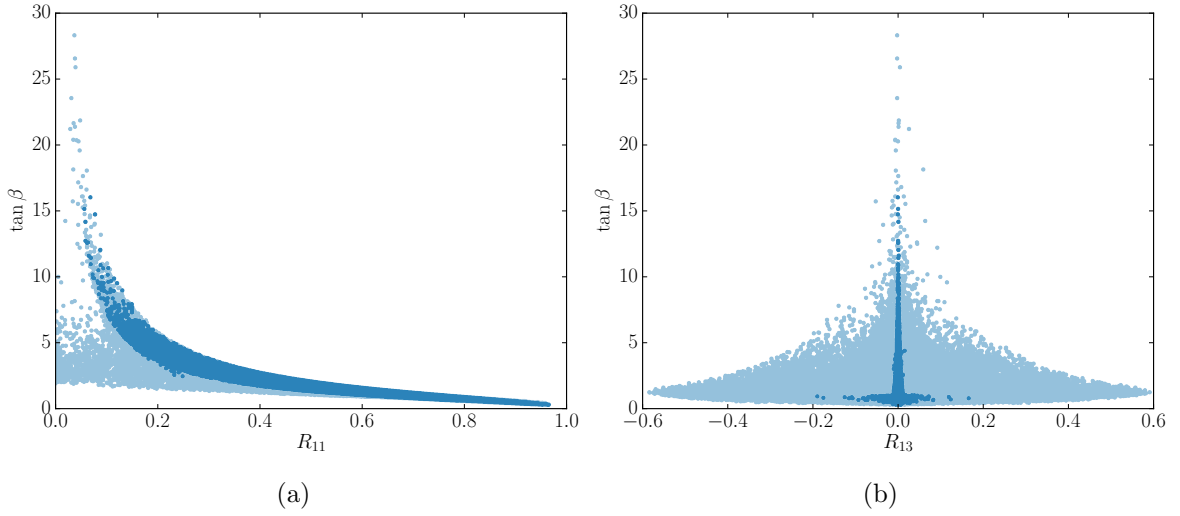


Figure 4.3.: The parameter $\tan \beta$ as a function of the mixing matrix elements R_{11} in (a) and R_{13} in (b), which contribute to h_{125} . The dark blue points are sample I and the light blue points sample II, respectively. To be compared to fig. 1 from [39].

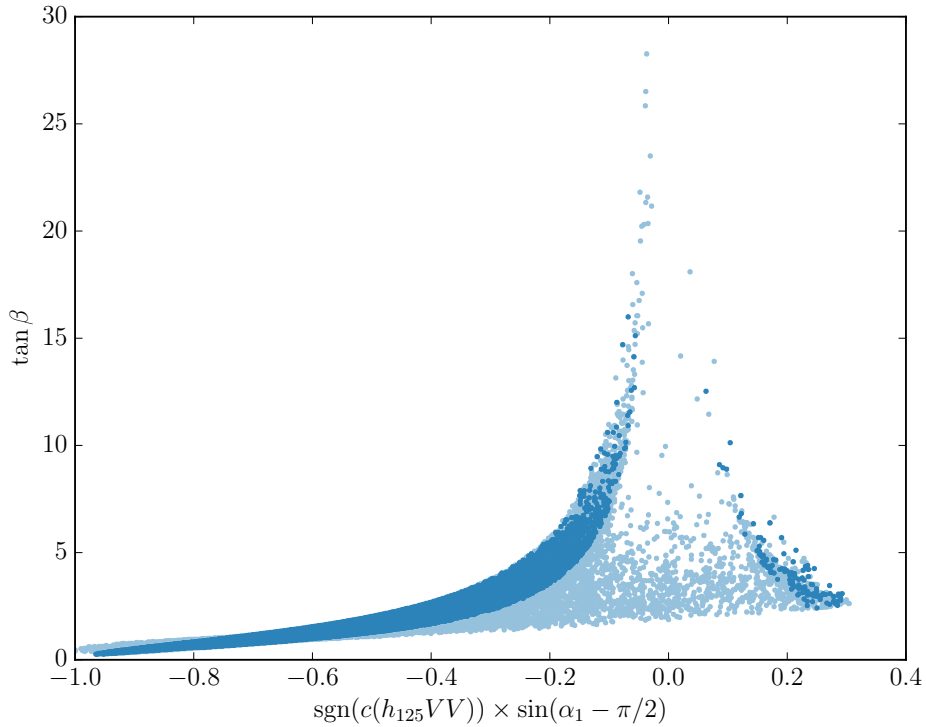


Figure 4.4.: The parameter $\tan \beta$ as a function of $\text{sgn}(c(h_{125}VV)) \cdot \sin(\alpha_1 - \pi/2)$. The dark blue points are sample I and the light blue points sample II, respectively. To be compared to fig. 3 from [39].

Phenomenological results

In this chapter, we present the results of the parameter scans described in chapter 4. In section 5.1 we study the properties of the h_{125} in our four models. We discuss how the physical parameter points of our models can deviate from the SM expectation. We focus on the possibility of singlet (or pseudoscalar) admixture to h_{125} and how points with high admixture are kept in agreement with current experimental data. Section 5.2 shows ways to distinguish between our four models. In section 5.2.1 we study the properties of a second neutral Higgs boson. We explain the model predictions for signal rates in the LHC Higgs search channels and point out how the observation of a second Higgs boson could help distinguish among our models. In section 5.2.2 we present an analysis of coupling sums, relying on sum-rules fulfilled by the models. This analysis is a promising way to differentiate between models and can allow the exclusion of a model using the coupling measurements of only two scalar particles.

In the models with a \mathbb{Z}_2 -symmetric Yukawa sector (the N2HDM and the C2HDM), we only study the type II in detail. However, we comment on the behavior of the other types in the sum-rule analysis.

5.1. Properties of the h_{125}

In this section we study the properties of the h_{125} in our models by looking at its admixtures. The singlet admixture Σ_i in the N2HDM has already been defined in eq. (3.16) as

$$\Sigma_i^{\text{N2HDM}} := (R_{i3})^2 . \quad (5.1)$$

The definition in the NMSSM is the same using the NLO mixing matrix calculated by `NMSSM-tools`. In the CxSM the singlet admixture is the sum of the real and complex singlet parts

$$\Sigma_i^{\text{CxSM}} := (R_{i2})^2 + (R_{i3})^2 . \quad (5.2)$$

In the C2HDM we define the pseudoscalar admixture

$$\Psi_i^{\text{C2HDM}} := (R_{i3})^2 . \quad (5.3)$$

Since we will only study the h_{125} we denote its admixtures simply by Σ for singlet admixtures and Ψ for the pseudoscalar admixture.

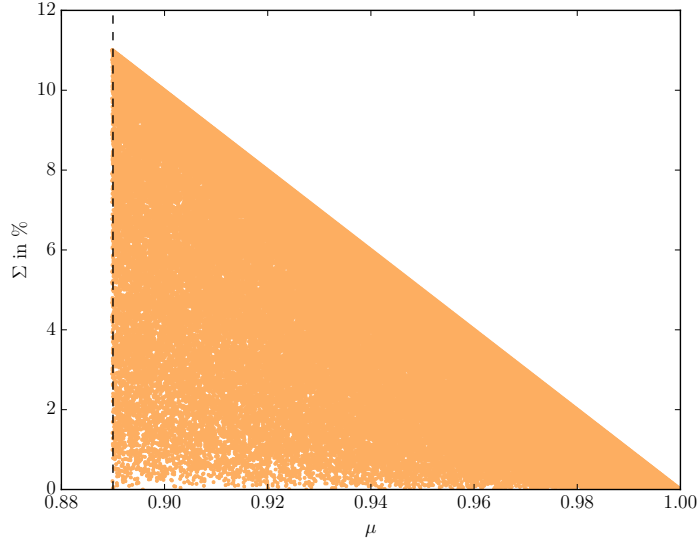


Figure 5.1.: Singlet admixture Σ of h_{125} as a function of the global signal strength μ in the CxSM. The dashed line denotes the experimental lower limit on μ from [9].

We use the individual signal strengths (4.9) as a parametrization for the observable properties of h_{125} . In the CxSM we instead use the global signal strength μ (see eq. (4.2)) due to its simple coupling structure. We observe that the measurement of $\mu_{b\bar{b}}$ is not sufficiently precise to constrain our models and thus do not show it. We further note that

$$\mu_{ZZ} = \mu_{WW} =: \mu_{VV} \quad (5.4)$$

holds in our models since they all preserve custodial symmetry. We, therefore, combine the lower $2 \times 1\sigma$ bound from μ_{ZZ} with the upper bound on μ_{WW} [9] and use

$$0.79 < \mu_{VV} < 1.48 . \quad (5.5)$$

5.1.1. Phenomenology of the h_{125} singlet admixture

We start the discussion with the CxSM, where all couplings to the SM particles are rescaled by a common factor. Due to this simple behavior, it is not possible to keep large singlet admixtures in agreement with the experimental data. This is shown in fig. 5.1. The maximum allowed singlet admixture in the CxSM is given through the lower bound on the global signal strength μ by

$$\Sigma_{\max}^{\text{CxSM}} = 1 - \mu_{\min} \approx 11\% . \quad (5.6)$$

The large number of free parameters in the N2HDM allows for more non-standard properties of h_{125} . Figure 5.2 shows the distribution of the parameter points in the space of signal strengths with the color code indicating the amount of singlet admixture Σ . We observe that the N2HDM parameter space is constrained by both upper and lower limits in μ_{VV} and $\mu_{\gamma\gamma}$ as well as the lower bounds from $\mu_{\tau\tau}$ and μ_V/μ_F . Figure 5.3 shows correlations between the effective couplings of the theory and the influence of singlet admixture on the couplings.

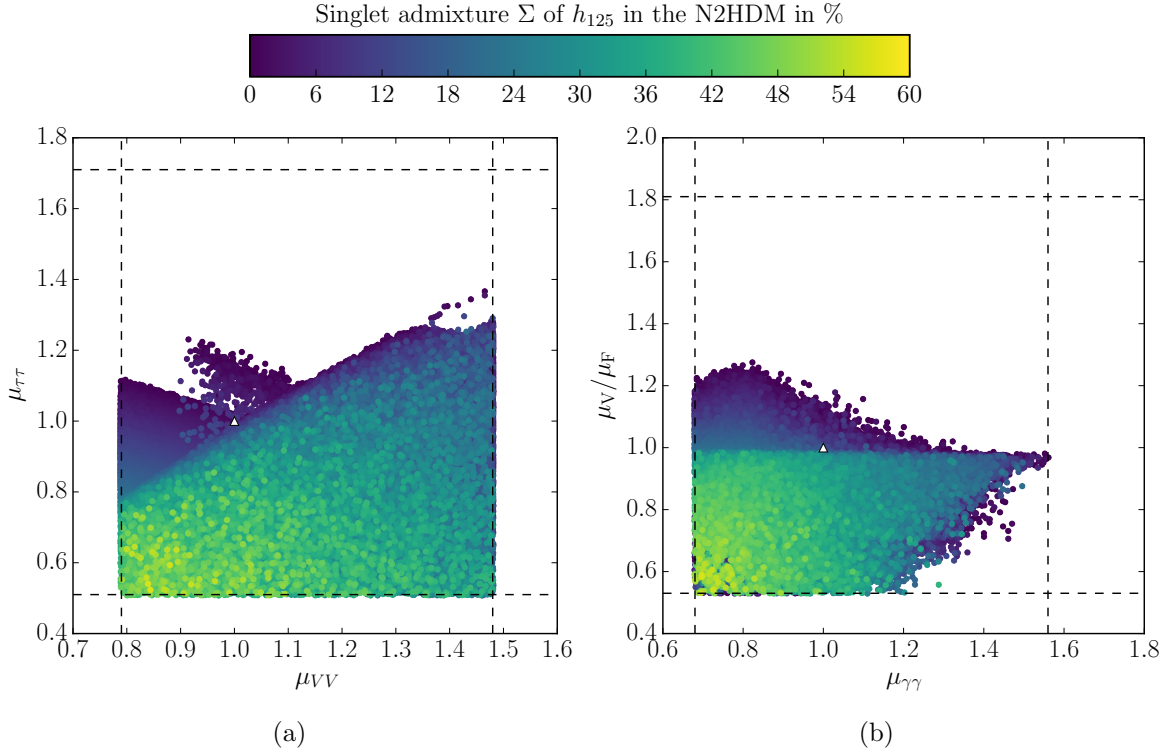


Figure 5.2.: Singlet admixture Σ in the N2HDM as a function of the most constraining measured signal strengths from eq. (4.9). The dashed lines show the experimental limits from [9] (and eq. (5.5)) and the white triangle denotes the SM value.

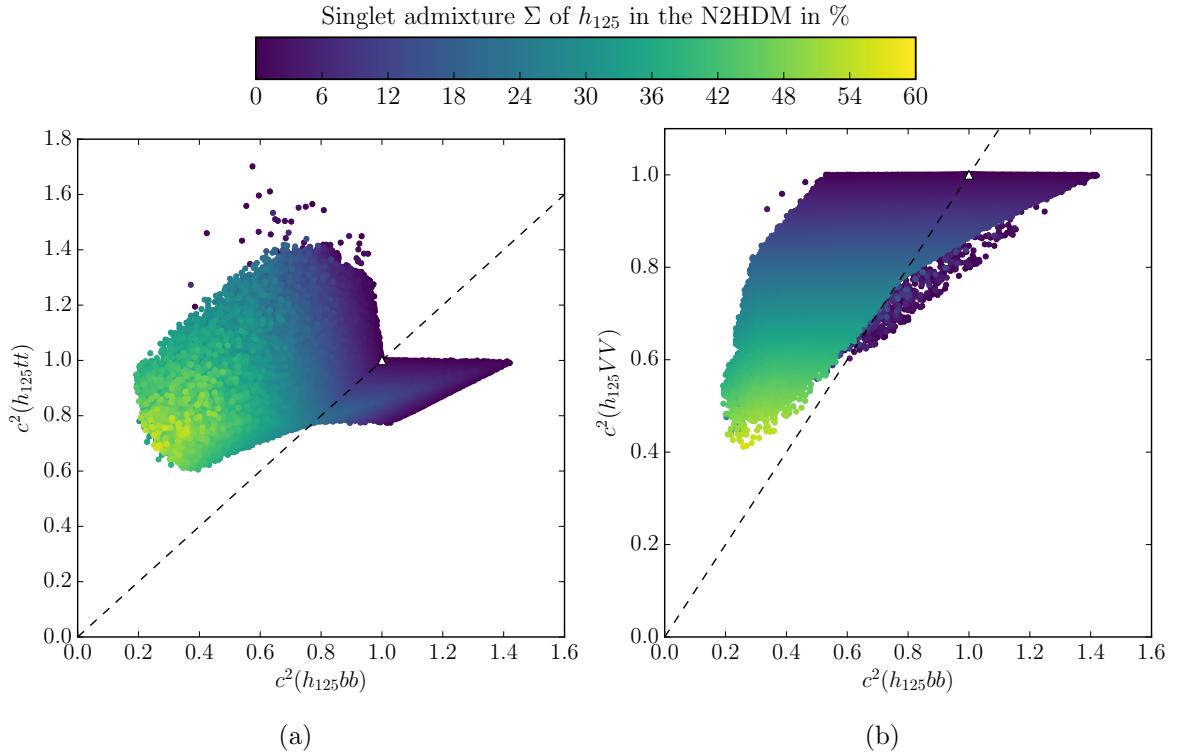


Figure 5.3.: Singlet admixture Σ of the N2HDM h_{125} as a function of its effective couplings squared. The white triangle denotes the SM value. The dashed line is the line of equal scaling of both couplings.

We first study the possibility of an enhanced $\mu_{\tau\tau}$. The largest enhancements compared to the SM are reached in the R2HDM limit of vanishing singlet admixture. There are three distinct regions with different ways of enhancing $\mu_{\tau\tau}$. The largest enhancement of up to 40% can happen if μ_{VV} is simultaneously enhanced. These are the points with an enhanced coupling to t quarks in fig. 5.3a. This enhancement increases ggF production while the decay properties stay SM-like. The points with an enhanced $\mu_{\tau\tau}$ and $\mu_{VV} \approx 1$ are (wrong-sign-limit) points where the coupling to gauge bosons is reduced. In fig. 5.3b they are located below the dashed line and isolated from the bulk of the points. The resulting reduction of the decay width $\Gamma(h_{125} \rightarrow VV)$ leads to an increased BR into $\tau\bar{\tau}$. The final $\mathcal{O}(10\%)$ enhancements of $\mu_{\tau\tau}$ near the lower bound from μ_{VV} are points where the coupling to τ leptons and b quarks is enhanced (the spikes to the right in fig. 5.3). This increases the decay widths into $\tau\bar{\tau}$ and the dominating decay width into $b\bar{b}$. The decay width $\Gamma(h_{125} \rightarrow VV)$, which in the SM is comparable to $\Gamma(h_{125} \rightarrow \tau\tau)$, is not enhanced. This leads to a reduction of BR($h_{125} \rightarrow VV$) in favor of BR($h_{125} \rightarrow \tau\tau$). We stress again that these enhancements are possible in the R2HDM limit without any singlet admixture to h_{125} .

Looking at the singlet admixture we observe that a Σ of up to 55% can still be compatible with current measurements. It is especially interesting that μ_{VV} and $\mu_{\gamma\gamma}$, which have the best experimental sensitivity, do not put the strongest limits on the singlet admixture as even a measurement of $\mu_{VV} = 1$ would still allow for a sizable $\Sigma \approx 45\%$. A measurement of $\mu_{\tau\tau} = 1$ would, on the other hand, enforce $\Sigma \lesssim 25\%$. We will now explain this behavior by studying how points with high singlet admixture stay in agreement with observations.

In fig. 5.3a we see, that a high singlet admixture reduces the effective coupling to b quarks, which scales the dominant decay width into $b\bar{b}$, more strongly than the coupling to t quarks, which is the dominant loop contribution in ggF production. Figure 5.3b shows that the b quark coupling also decreases faster with rising singlet admixture than the effective coupling to gauge bosons. This means that a high-singlet-admixture point has a reduced $\Gamma(h_{125})_{\text{tot}}$ due to the strongly reduced $\Gamma(h_{125} \rightarrow b\bar{b})$ which dominates the SM reference. This reduction of the total width enhances the BR in the VV and $\gamma\gamma$ channels sufficiently to compensate for both the reduced ggF production cross section and the reduced partial decay widths in these channels. The decay width $\Gamma(h_{125} \rightarrow \tau\tau)$, however, gets rescaled by the same coupling as the $b\bar{b}$ channel (since we are in the type II). A high singlet admixture therefore always reduces $\mu_{\tau\tau}$. Values of $\mu_{\tau\tau} \gtrsim 1$ are only possible in the presence of singlet admixture if $\mu_{\tau\tau}$ is enhanced by one of the effects in the R2HDM limit described above. On the other hand, $\mu_{VV} \approx 1$ can be reached through a sufficient reduction of $\Gamma(h_{125} \rightarrow b\bar{b})$ even for strongly reduced gauge couplings. We conclude that a more precise measurement of $\mu_{\tau\tau}$ is the best way to constrain the amount of singlet admixture in the N2HDM.

In fig. 5.3a we further see that in the case of small Σ the effective coupling to top quarks in the N2HDM can be considerably enhanced. This allows the model to contain an enhancement of the $t\bar{t}H$ production process which is very well compatible with current measurements [9]. Finally, we observe that the maximum possible enhancement of the $b\bar{b}$ coupling in the N2HDM is not high enough for bbF to play a relevant role in the production of h_{125} .

Figure 5.4 shows the same plots as fig. 5.2 for the NMSSM parameter points. The parameter space of the NMSSM is clearly more constrained as compared to the N2HDM. This is due to the correlations enforced upon the Higgs sector by supersymmetry. We observe that in the NMSSM $\mu_{\tau\bar{\tau}}$ cannot be enhanced by more than a few percent. We will now explain the absence of the tree regions of enhancement we observed in the N2HDM. The region of enhanced ggF production does not exist as fig. 5.5a shows that in the NMSSM

$$c^2(h_{125}t\bar{t}) \leq 1. \quad (5.7)$$

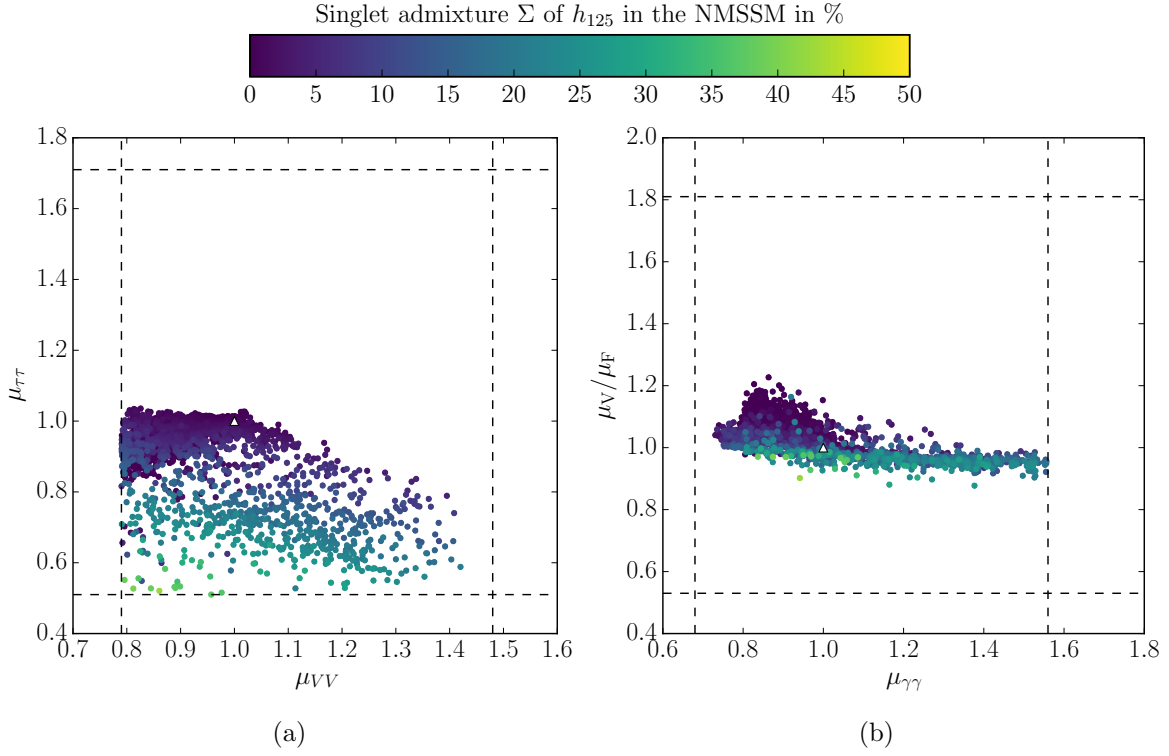


Figure 5.4.: Singlet admixture Σ of h_{125} in the NMSSM as a function of the most constraining measured signal strengths from eq. (4.9). The dashed lines show the experimental limits from [9] (and eq. (5.5)) and the white triangle denotes the SM value.

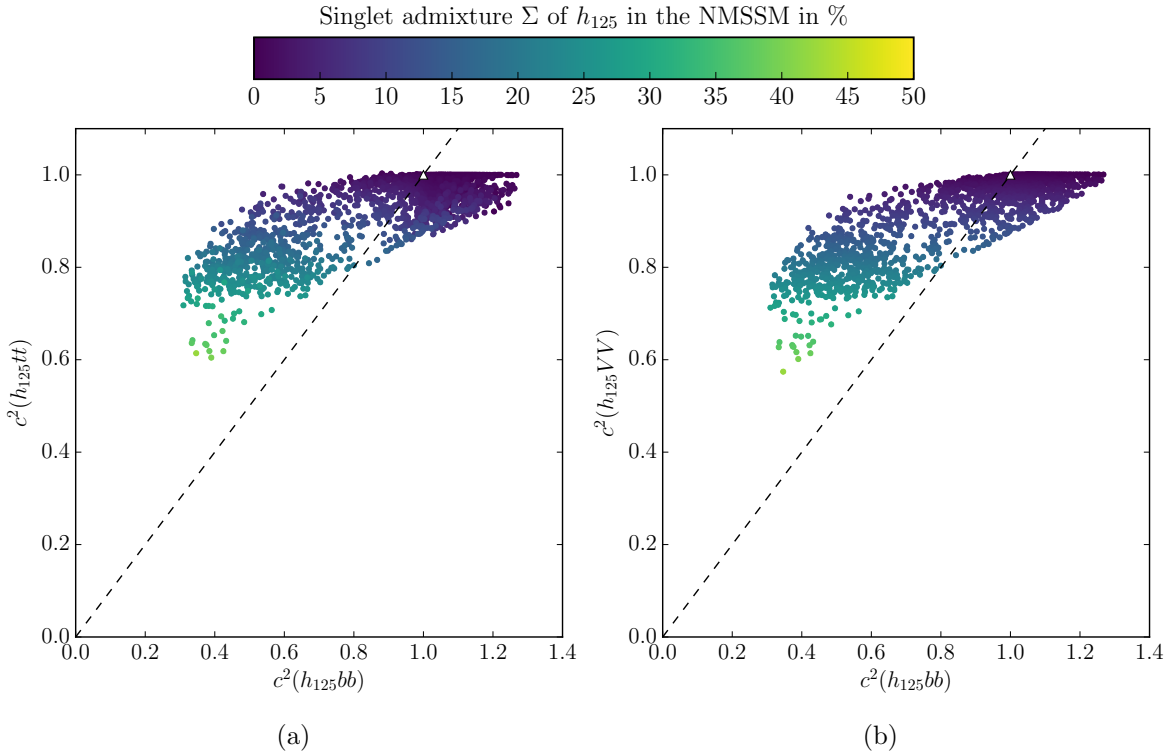


Figure 5.5.: Singlet admixture Σ of the NMSSM h_{125} as a function of its effective couplings squared. The white triangle denotes the SM value. The dashed line is the line of equal scaling of both couplings.

A region with $\mu_{\tau\tau} > 1$ and $\mu_{VV} \approx 1$ does not exist as these are wrong-sign-limit points in the N2DHM and the wrong-sign-limit is excluded in the NMSSM. The enhancement of $\mu_{\tau\tau}$ with simultaneously reduced μ_{VV} relied on increased couplings of h_{125} to b quarks and leptons. Comparing fig. 5.5 to fig. 5.3 we observe that the allowed enhancement of this coupling is only about 20% in the NMSSM compared to 40% in the N2HDM. The possible enhancement of $\mu_{\tau\tau}$ in this region is therefore way lower than in the N2HDM.

We further observe that the ratio of production signal strengths in fig. 5.4b is constrained to be close to one. The correlation that is apparent between fig. 5.5a and fig. 5.5b shows that

$$c^2(h_{125}t\bar{t}) \approx c^2(h_{125}VV) . \quad (5.8)$$

The t quark couplings dominates ggF production and thus μ_F while $c^2(h_{125}VV) \approx \mu_V$. This leads to $\mu_V \approx \mu_F$ and explains why $\mu_V/\mu_F \approx 1$. This is a consequence of SUSY relations.

Despite these constraints, the NMSSM can still accommodate a considerable singlet admixture of up to $\Sigma \approx 45\%$. These points stay in agreement with the observations in the same way as described for the N2HDM. The effective couplings in fig. 5.5 show the required scaling behavior of $c^2(h_{125}b\bar{b})$ being reduced by singlet admixture more strongly than $c^2(h_{125}VV)$ and $c^2(h_{125}t\bar{t})$. Since the NMSSM cannot enhance $\mu_{\tau\tau}$ to compensate for a singlet admixture, the lower bound of $\mu_{\tau\tau}$ constrains the allowed Σ even more strongly than in the N2HDM. A measurement of $\mu_{\tau\tau} = 1$ would exclude any relevant singlet admixture to h_{125} .

5.1.2. Pseudoscalar admixture in the C2HDM

The CP-violation present in the C2HDM leads to a very different phenomenology compared to the CP-conserving models. The pseudoscalar admixture Ψ of h_{125} cannot exceed a few percent, as can be inferred from fig. 5.6. It is clear that the bounds on Ψ do not stem from measurements of the h_{125} properties. They instead originate mainly from the bound on the electron EDM as discussed in section 4.6.

Since the allowed amount of pseudoscalar admixture is small the possible properties of h_{125} in the C2HDM are well approximated by the R2HDM. In the previous section, we have already discussed some of the phenomenology of the R2HDM limit in the N2HDM. Comparing fig. 5.6 to fig. 5.2 we indeed observe a similar behavior of the low admixture points in both models. We specifically observe the same three regions of enhanced $\mu_{\tau\tau}$ in fig. 5.6a and fig. 5.2a which we discussed for the N2HDM. We have verified that the mechanisms of enhancement in these regions are the same in the C2HDM and N2HDM. The sharp edges in fig. 5.6a are reproduced in the N2HDM if we only include points with negligible singlet admixture. In the limit of vanishing admixture there are only two non-zero mixing matrix elements which contribute to h_{125} . The orthogonality of the mixing matrix then leads to these sharp edges in the R2HDM limit of both the C2HDM and N2HDM.

The points deviating from the bulk (towards the top left in fig. 5.6a and the bottom left in fig. 5.6b) are the wrong-sign-limit points from section 4.6. In the C2HDM it is instructive to look at the signal strengths μ_V and μ_F individually. They are shown in fig. 5.7 with the color code indicating

$$c(h_{125}VV) \times c(h_{125}b\bar{b}) . \quad (5.9)$$

The sign of this product specifies the correct-sign-limit (> 0) or the wrong-sign-limit (< 0). We approximate the coupling to b quarks by its CP-even part a from table 2.2 since Ψ is always small. In fig. 5.7 we see that the wrong sign limit points are the only points in the C2HDM where $c^2(h_{125}VV) = \mu_V$ can deviate from one. This leads to the reduced μ_{VV} and enhanced $\mu_{\tau\tau}$ behavior in fig. 5.6a. The reduced μ_V also leads to the reduced μ_V/μ_F we observe for the wrong-sign-limit points in fig. 5.6b.

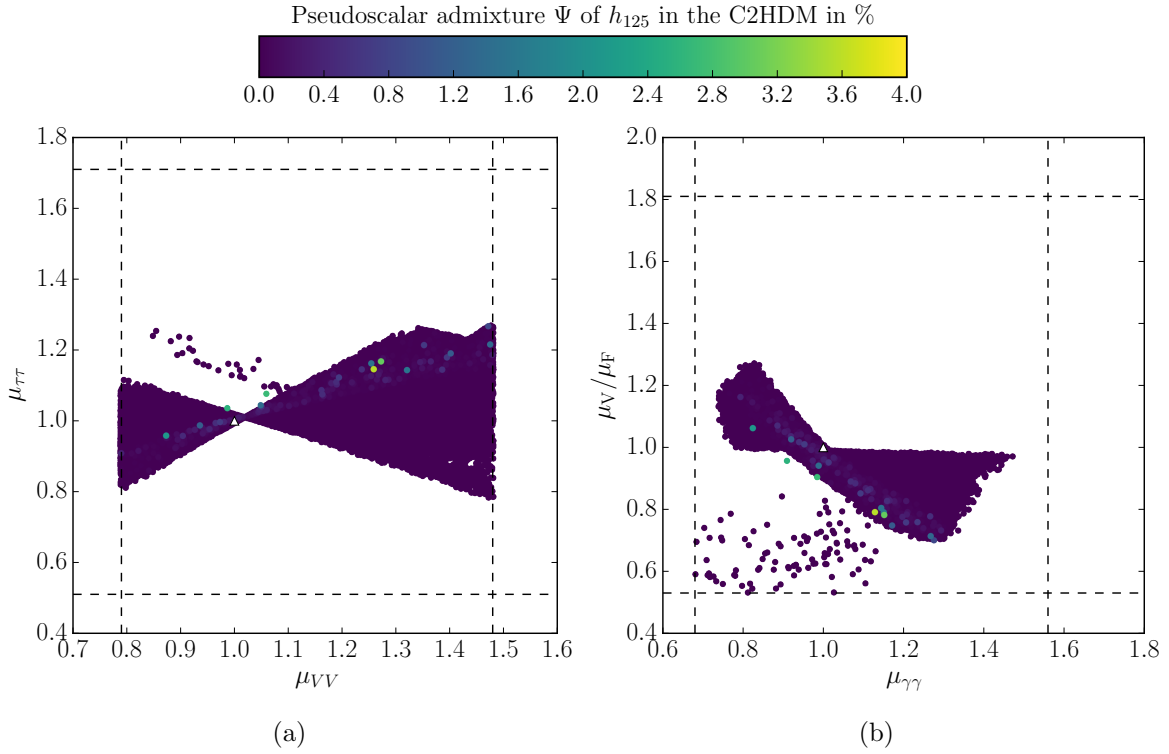


Figure 5.6.: Pseudoscalar admixture Ψ of h_{125} in the C2HDM as a function of the most constraining measured signal strengths from eq. (4.9). The dashed lines show the experimental limits from [9] (and eq. (5.5)) and the white triangle denotes the SM value.

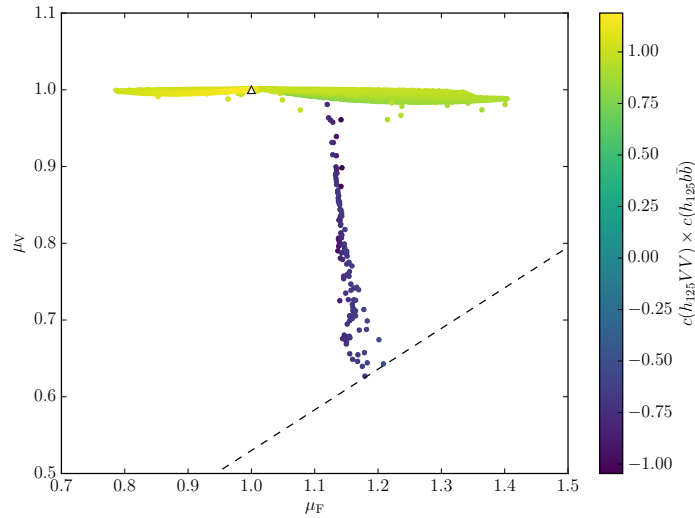


Figure 5.7.: Signal strengths of gauge-boson-mediated (μ_V) and fermion-mediated (μ_F) production processes in the C2HDM. The color axis shows the product of the effective couplings to gauge bosons and to d -type quarks and leptons. If this product is negative the parameter point is in the wrong-sign-limit. The dashed line denotes the lower bound on μ_V/μ_F , the upper bound is outside the plot range.

5.2. Distinguishing Higgs sector extensions through the properties of two Higgs bosons

In the following sections, we discuss the properties of the non- h_{125} Higgs bosons of the theory. The focus will be on distinguishing the four different models assuming that only one additional Higgs boson will be discovered.

We adopt the notation from section 4.5 and denote by H_{\downarrow} the lighter of the two non- h_{125} neutral (CP-even in the CxSM, N2HDM, and NMSSM) Higgs bosons and the heavier one by H_{\uparrow} .

5.2.1. Decays into SM particles

We first study the inclusive rates of producing a H_{\downarrow} which decays into various SM particles. We compare the predictions of our models and discuss which observations could allow us to distinguish between them. The main point of interest is what kind of observations a given model could not explain. To this end, we also comment on the behavior of H_{\uparrow} whenever appropriate.

In the first stage of discovery, it will be challenging to measure the CP nature of the discovered particle. Analyses testing the pure CP-odd against the pure CP-even hypothesis will, however, likely be performed in this early stage. Such an analysis is possible even if no couplings to gauge bosons are observed [130]. We, therefore, assume that the possibility of the new particle being a pure pseudoscalar state can be excluded. Distinguishing a C2HDM Higgs boson of mixed CP from a pure CP-even Higgs boson will be considerably more challenging. Under these assumptions, we can consistently compare the behavior of H_{\downarrow} in all of our models.

In the following, we plot signal rates obtained by multiplying the production cross section with the corresponding branching ratio obtained from HDECAY. The production cross section

$$\sigma_H(pp) = \sigma_H(\text{ggF}) + \sigma_H(\text{bbF}) \quad (5.10)$$

at a 13 TeV LHC was calculated with SusHi at NNLO QCD using the effective t and b couplings of the theory. We include bbF to account for possible large b quark couplings. Since none of our models can enhance the coupling to gauge bosons, we neglect the subleading production through vector boson fusion. We also neglect all associated and Higgs-strahlung production channels since their cross sections are negligible compared to ggF and bbF. In all plots we impose a lower limit of 0.1 fb for the signal rate and cut off any points below.

In fig. 5.8 the signal rates in the ZZ channel are shown. The branching ratio calculation in HDECAY allows for the Z to be off-shell and interpolates around the on-shell resonance such that both $m_H < 2m_Z$ and $m_H > 2m_Z$ are accurately described. In none of our models, the coupling to gauge bosons can be enhanced above the SM value. Furthermore the gauge boson sum-rule

$$\sum_{i=1}^3 c^2(H_i VV) = 1, \quad (5.11)$$

which stems from unitarity of the mixing matrix, is realized in all our models (this will be discussed in detail in section 5.2.2.1). This forces the gauge coupling of H_{\downarrow} to be considerably below the SM value as h_{125} needs substantial gauge couplings to agree with the observations in the ZZ and W^+W^- final states. The room for deviations in the gauge couplings of the non- h_{125} Higgs bosons mainly depends on the number of free parameters of the model and therefore on the ability to accommodate independent coupling variations. A reduction of the

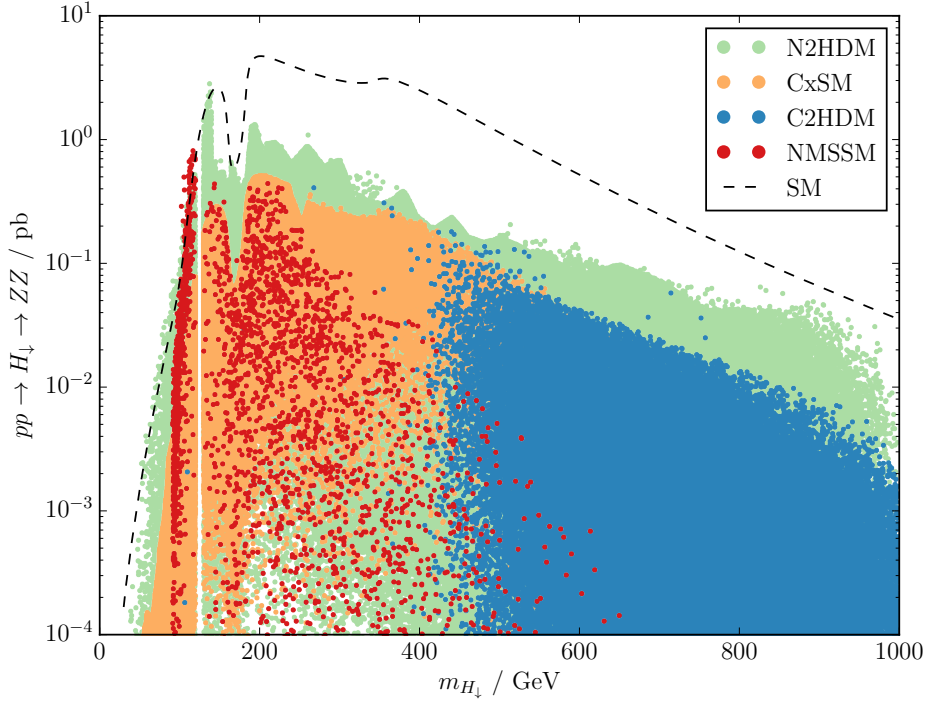


Figure 5.8.: Signal rate of the production of a H_{\downarrow} decaying into a pair of Z bosons at the 13 TeV LHC as a function of the H_{\downarrow} mass. The dashed black line denotes the signal rate of a SM Higgs boson of the same mass. The gap at 125 GeV is the window we require around $m_{h_{125}}$ (see e.g. section 4.1).

decay width into gauge bosons can be compensated by either a reduction of the total decay width or an increased production cross section.

We first look at the CxSM, where the common scaling of all couplings together with eq. (5.11) and fig. 5.1 enforces

$$c_{\text{CxSM}}^2(H_{\downarrow}VV) \lesssim 0.1 . \quad (5.12)$$

It is furthermore impossible to enhance the production cross sections in the CxSM. This keeps all CxSM rates below the SM reference at all masses $m_{H_{\downarrow}}$ as can be seen in fig. 5.8. This behavior is the same for all decay channels and for H_{\uparrow} , which makes the discovery of additional Higgs bosons in the CxSM most likely through Higgs-to-Higgs decays [11].

In fig. 5.7 we saw that in the C2HDM $c^2(h_{125}VV) \approx 1$ for all parameter points except for the wrong-sign-limit ones. This severely constrains the gauge coupling available for H_{\downarrow} and leads to the clear upper bound of the bulk of the C2HDM points in fig. 5.8. The few outliers that can match the rates of the N2HDM are the wrong-sign-limit points where eq. (5.11) allows for a larger gauge coupling of H_{\downarrow} .

In the N2HDM the gauge couplings of h_{125} can be reduced up to $c^2(h_{125}VV) = 0.4$ (see fig. 5.3b). The sumrule eq. (5.11) therefore allows H_{\downarrow} to have sizable gauge couplings of up to $c^2(H_{\downarrow}VV) \approx 0.6$. A reduced total width (compared to the SM reference) through a reduced $c(H_{\downarrow}b\bar{b})$ or an increased ggF cross section through an increased $c(H_{\downarrow}t\bar{t})$ can compensate $c^2(H_{\downarrow}VV) < 1$. We specifically found that $c(H_{\downarrow}t\bar{t})$ can be enhanced by up to a factor of 2.5. This allows the N2HDM to reach the SM reference in the $m_{H_{\downarrow}} < 200$ GeV mass region of fig. 5.8. In the high mass region the N2HDM can no longer reach the SM reference as both the dominating ggF production and the dominating $t\bar{t}$ decay width depend on the same

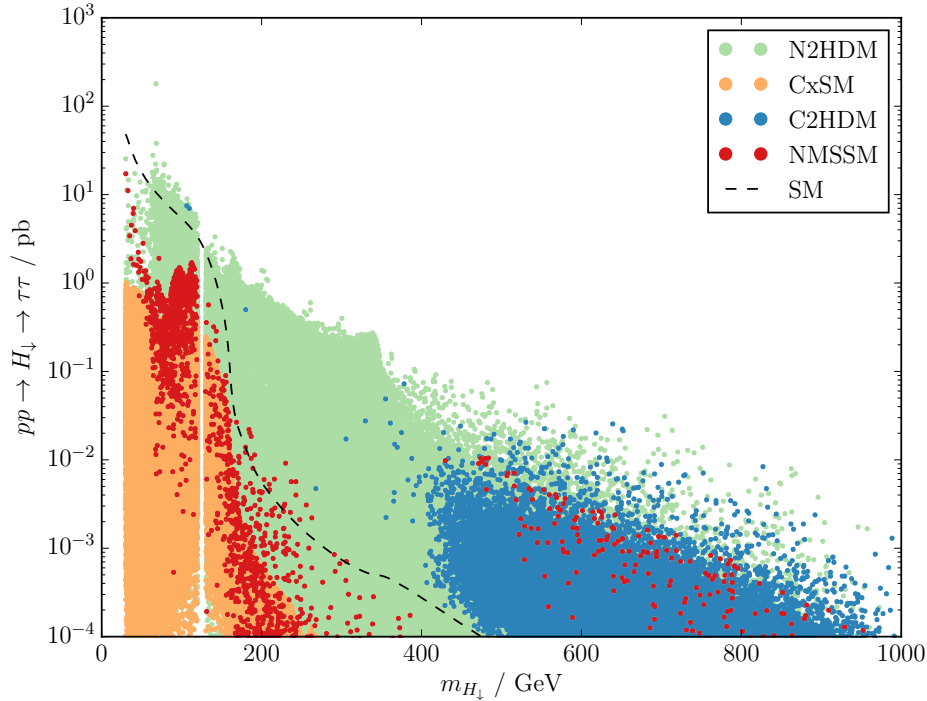


Figure 5.9.: Signal rate of the production of a H_{\downarrow} decaying into a pair of τ leptons at the 13 TeV LHC as a function of the H_{\downarrow} mass. The dashed black line denotes the signal rate of a SM Higgs boson of the same mass. The gap at 125 GeV is the window we require around $m_{h_{125}}$ (see e.g. section 4.1).

coupling. However, it is still possible to obtain larger rates in the N2HDM than in any of our other models with the exception of the C2HDM wrong-sign-limit points.

In the NMSSM the sum rule (5.11) and fig. 5.5b enforce $c^2(H_{\downarrow}VV) < 0.45$. Furthermore SUSY relations force $c^2(H_{\downarrow}t\bar{t}) < 1$ just as we observed for h_{125} . This makes an enhancement of the ggF cross section impossible. However, sufficient reduction of the total decay width can still enhance the rate in the ZZ channel. Such a reduction of the dominant $b\bar{b}$ decay width allows the NMSSM to have a few points above the SM reference at $m_{H_{\downarrow}} \approx 100$ GeV in fig. 5.8. A combination of sum-rules and SUSY relations strongly suppress the rate in the ZZ channel for high $m_{H_{\downarrow}}$. We observe the same behavior for H_{\uparrow} . An observation of a neutral scalar with an $\mathcal{O}(100 \text{ fb})$ rate in the ZZ channel and a mass of at least 500 GeV might be sufficient to exclude the NMSSM.

Figure 5.9 shows the signal rates in the $\tau\bar{\tau}$ channel as an example of the fermionic decay channels. In all models except for the CxSM, it is possible to enhance the couplings of H_{\downarrow} to d -type quarks and leptons with respect to their SM values. Enhancements of the signal rates above the SM reference are therefore possible provided the production cross section is not too strongly suppressed.

All physical C2HDM points predict H_{\downarrow} signal rates above the SM reference in fig. 5.9 (this statement remains valid for the points below the 0.1 fb cutoff). This is a result of the incoherent addition of scalar and pseudoscalar contributions to both ggF production and the $\tau\bar{\tau}$ decay width, which allows for large enhancements. We further saw in fig. 5.8 that the decay rate into gauge bosons is suppressed by about an order of magnitude. Since the gauge boson decay widths of the SM reference are sizable in this mass range this leads to a reduction of the total width and a further enhancement of the $\tau\bar{\tau}$ rate. The observation that the C2HDM

rates are always above the SM reference is true for H_\downarrow and H_\uparrow in both the $b\bar{b}$ and $\tau\bar{\tau}$ channel. In the $t\bar{t}$ channel, however, rates below SM reference are possible for points with high $\tan\beta$ as this suppresses both the scalar and pseudoscalar parts of the t quark coupling (see table 2.2).

The N2HDM shows a rich phenomenology in the $\tau\bar{\tau}$ channel of fig. 5.9. It can, on the one hand, match the high rates of the C2HDM through enhanced t quark couplings leading to a high production cross section. In contrast to the C2HDM, it can also predict rates far below the SM reference. This is because singlet admixture reduces all couplings to SM particles, while pseudoscalar admixture usually (depending on $\tan\beta$, see table 2.2) enhances fermionic couplings. A notable feature is the mass range between 200 and 400 GeV where the N2HDM can predict rates higher than the other models. The exception is again the wrong-sign-limit C2HDM which has several points that can match the N2HDM rates in this region.

The only NMSSM points that exceed the SM reference in fig. 5.9 are points with high $\tan\beta$. The increased b quark coupling ($\propto 1/\cos\beta$) enhances the production cross section through bbF which compensates for the reduction in ggF (due to the t quark coupling being $\propto 1/\sin\beta$). These reduced t quark couplings together with small gauge couplings [66] make $b\bar{b}$ and $\tau\bar{\tau}$ the dominant SM decay modes even above the $t\bar{t}$ -threshold. In fig. 5.9 we observe a gap between the NMSSM points above the SM reference with $m_{H_\downarrow} > 400$ GeV and the points near the SM reference and $m_{H_\downarrow} \approx 200$ GeV. This gap can be understood from figure 5 in [66]. This shows that it is exceedingly rare for an NMSSM parameter point to have both a high $\tan\beta$, which is a requirement for the point to produce rates above the SM reference and $125 \text{ GeV} < m_{H_\downarrow} \lesssim 400 \text{ GeV}$. This is a result of the NMSSM Higgs mass calculation purely due to the supersymmetric structure of the NMSSM Higgs sector regardless of experimental constraints. We note that H_\uparrow can be located inside this gap, though with lower maximum rates than the N2HDM.

An observation of a Higgs boson H with $200 \text{ GeV} < m_H < 400 \text{ GeV}$ and a rate in the $\tau\tau$ channel $\gtrsim 0.1 \text{ pb}$ would, therefore, leave the N2HDM as the natural model candidate. The C2HDM wrong-sign-limit can produce comparable rates in this mass region, it is however strongly constrained by the measurements of h_{125} and could be excluded that way [129]. This is only true if the new particle is not a pure pseudoscalar, as we have verified in our samples that the NMSSM A_1 can produce similar rates, as can the N2HDM pseudoscalar A .

We conclude this part of the analysis by studying the $\gamma\gamma$ channel in fig. 5.10. The C2HDM predicts $\gamma\gamma$ rates above the SM reference for most of its parameter points. The rate is enhanced by large t contributions to the ggF production. In the mass region above the $t\bar{t}$ threshold, where most of the C2HDM points are located, this enhancement is partially compensated by an increase in the dominating $\Gamma(H_\downarrow \rightarrow t\bar{t})$.

In the N2HDM the $\gamma\gamma$ rate of fig. 5.10 is also enhanced by a large ggF production cross section due to large t quark couplings. Especially in the mass range between 200 and 400 GeV below the $t\bar{t}$ threshold the $\gamma\gamma$ rates can be enhanced by two orders of magnitude compared to the SM reference. As in the $\tau\tau$ channel, the N2HDM is the only model that could explain $\gamma\gamma$ rates far above the SM reference in this mass range. The N2HDM can also exceed the SM reference if $m_{H_\downarrow} < 125 \text{ GeV}$. In addition to an enhanced ggF production cross section, these points have low b quark couplings thus reducing the total width and enhancing $\text{BR}(H_\downarrow \rightarrow \gamma\gamma)$.

In fig. 5.10, the NMSSM can also produce rates above the SM reference in the $m_{H_\downarrow} < 125 \text{ GeV}$ region even though no enhancement of the t quark coupling is possible. This behavior has been studied in [131]. It can be explained by loop contributions from light SUSY particles like staus or charginos and a suppression of the dominant $\Gamma(H_\downarrow \rightarrow b\bar{b})$.

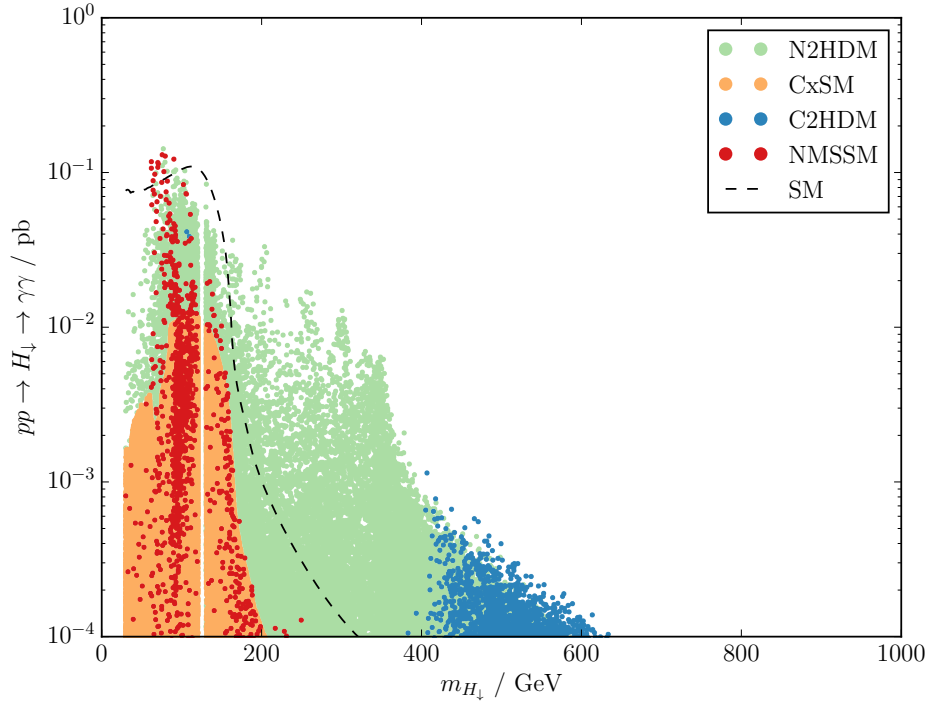


Figure 5.10.: Signal rate of the production of a H_\downarrow decaying into a pair of photons at the 13 TeV LHC as a function of the H_\downarrow mass. The dashed black line denotes the signal rate of a SM Higgs boson of the same mass. The gap at 125 GeV is the window we require around $m_{h_{125}}$ (see e.g. section 4.1).

We conclude that the distinction between models based on inclusive rates alone is very challenging. However, we have still identified a number of discriminating properties. The CxSM could be excluded by any measurement of a signal rate enhanced above the SM reference. A discovery of an $m_H > 500$ GeV Higgs boson with a rate of about 100 fb in the ZZ channel would put considerable strain on the NMSSM. Furthermore, a discovery in the 200 to 400 GeV mass range with $\gamma\gamma$ and/or $\tau\bar{\tau}$ rates enhanced compared to the SM reference could only be easily explained by the N2HDM.

5.2.2. Yukawa and gauge boson sum-rules

In this section, we present a comparison of the models based on the sums of the couplings of the h_{125} and H_\downarrow from their spectrum. We will study the gauge boson sum

$$\Pi_{VV}^i = \sum_{j=1}^i |c(H_i VV)|^2 \quad (5.13)$$

and the Yukawa sum

$$\Pi_{\text{Yuk}}^i = \frac{1}{\sum_{j=1}^i |c(H_i \tau\bar{\tau})|^2} + \frac{1}{\sum_{j=1}^i |c(H_i t\bar{t})|^2}. \quad (5.14)$$

We sum all CP-even Higgs bosons in the CxSM, N2HDM and NMSSM, respectively, and the three neutral Higgs bosons in the C2HDM. Note that

$$\Pi_{VV}^i \leq \Pi_{VV}^{i+1} \quad (5.15)$$

and

$$\Pi_{\text{Yuk}}^i \geq \Pi_{\text{Yuk}}^{i+1}. \quad (5.16)$$

In type II models the coupling to b quarks could be used instead of the coupling to τ -leptons if it was known more precisely. While this could also be done in models with a different Yukawa structure it would no longer result in a sum-rule independent of $\tan\beta$ (see section 5.2.2.2 below). In the following, we study the quantities Π_{VV}^2 and Π_{Yuk}^2 , which include h_{125} and H_\downarrow in the sum. This assumes that H_\downarrow is the only additional neutral Higgs boson with gauge couplings (see below) discovered. Points where h_{125} is the heaviest neutral CP-even (since this is only possible in the CxSM and N2HDM) Higgs boson are not included in this analysis.

At the LHC the Higgs couplings are not directly observable and can only be extracted with model assumptions. In [79–81] a precision of about 10% for the h_{125} couplings to gauge bosons, t quarks, and τ leptons is expected from a 3000 fb^{-1} High-Luminosity-LHC (HL-LHC) dataset. The precision of the b quark coupling will be closer to 20% which is why we use the lepton coupling in eq. (5.14). The couplings of H_\downarrow will, presumably, be known less precisely than for h_{125} due to lower statistics. At a linear collider (LC) the measurement of the Higgs couplings is possible in a model-independent way. A 500 GeV linear collider with a 500 fb^{-1} dataset could extract the required h_{125} couplings with a precision of a few percent [80, 81]. Combining the LHC and LC analysis may further improve this precision. This analysis will, therefore, become relevant only toward the end of the HL-LHC run. At this point, statistics should be sufficient to test the CP-nature of H_\downarrow . It could, however, still be very challenging to differentiate a state of mixed CP from a pure CP-even Higgs boson. For this reason, we include the C2HDM in this analysis.

The sum-rule analysis only works if H_\downarrow mixes with h_{125} . In the C2HDM and CxSM, this requirement is fulfilled for any additional neutral particle. In the N2HDM and NMSSM, however, we have to make sure that we are able to distinguish H_\downarrow from the pseudoscalar Higgs bosons of the models. The easiest way to exclude the observed particle from being a pure CP-odd state is to observe the ZZ decay channel [130]. For this reason, we require the rate

$$ggF \rightarrow H_\downarrow \rightarrow ZZ > 10 \text{ fb}. \quad (5.17)$$

This should be observable at the HL-LHC if the particle has previously been discovered in another decay mode so that we already know its mass. This condition still allows H_\downarrow to be a state of mixed CP, as it is in the C2HDM, with interesting phenomenological consequences.

It has been shown in [132] that the R2HDM contains points with considerable rates in the loop-induced $A \rightarrow ZZ$ channel. If a similar behavior is possible in the N2HDM the observation of the ZZ decay channel might not be sufficient to distinguish H_\downarrow from the pseudoscalar A . In this case measurements of the angular distributions in $H_\downarrow \rightarrow ZZ \rightarrow 4l$, $ggF \rightarrow H_\downarrow \rightarrow \gamma\gamma$ or the fermionic decay modes could be used to verify the CP nature of the discovered particle [130].

5.2.2.1. The gauge boson sum-rule

All our models fulfill the gauge boson sum-rule

$$\Pi_{\text{VV}}^3 = 1. \quad (5.18)$$

Therefore

$$\Pi_{\text{VV}}^2 \leq 1 \quad (5.19)$$

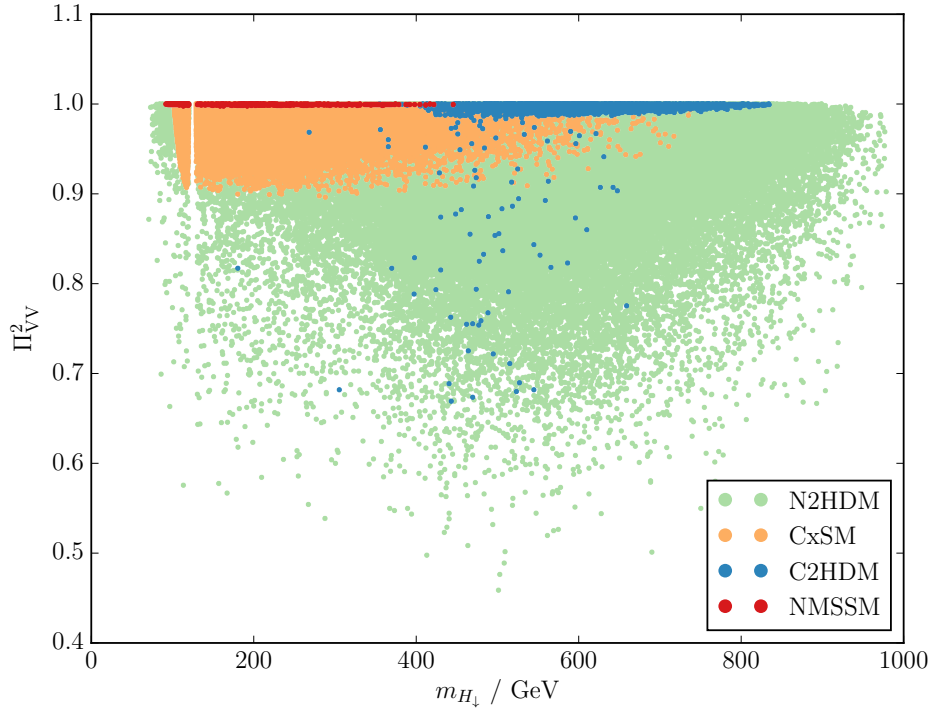


Figure 5.11.: The partial gauge boson sum Π_{VV}^2 as a function of m_{H_\downarrow} . All four models fulfill the sum-rule (5.18) for Π_{VV}^3 , as well as $\Pi_{VV}^2 \leq \Pi_{VV}^3$.

holds for all points. For models with smaller Higgs sectors like the R2HDM and CP-conserving MSSM, which only contain two CP-even neutral scalars, we have

$$\Pi_{VV}^2 = 1 . \quad (5.20)$$

Figure 5.11 shows the partial gauge boson sum Π_{VV}^2 in the four models that we study in this thesis. In the CxSM Π_{VV}^2 cannot be smaller than about 0.9. This is a result of the simple coupling structure and the bound from the global signal strength. This bound enforces $c^2(h_{125}VV) \gtrsim 0.9$ which is equivalent to $\Pi_{VV}^2 \gtrsim 0.9$, even if H_\downarrow does not couple to gauge bosons at all. This provides a handle on excluding the CxSM. It is, however, likely for the CxSM to be excluded by deviations from the common scaling, before an analysis like this one can be performed.

Most of the C2HDM points in fig. 5.11 have Π_{VV}^2 close to one. This is mostly due to $c(h_{125}VV) \approx 1$ which we observed in fig. 5.7. The only points where H_\downarrow can have a considerable gauge coupling are the wrong-sign-limit points in fig. 5.7 where the gauge coupling of h_{125} is reduced. The C2HDM points where Π_{VV}^2 deviates more considerably from one are, therefore, wrong sign limit points with rather small $c(H_\downarrow VV)$ (but eq. (5.17) still satisfied). In these points H_\uparrow has considerable couplings to gauge bosons.

In the N2HDM the possibility of having large singlet admixtures in h_{125} together with a gauge-phobic H_\downarrow leads to large deviations from $\Pi_{VV}^2 = 1$ in agreement with the applied constraints. The C2HDM wrong-sign-limit points are the only ones that can produce a range of Π_{VV}^2 values comparable to the N2HDM.

Despite the NMSSM having the largest Higgs sector, it is clearly the most constrained model in fig. 5.11. We observe deviations from one by a few percent at most. As we saw in fig. 5.5b

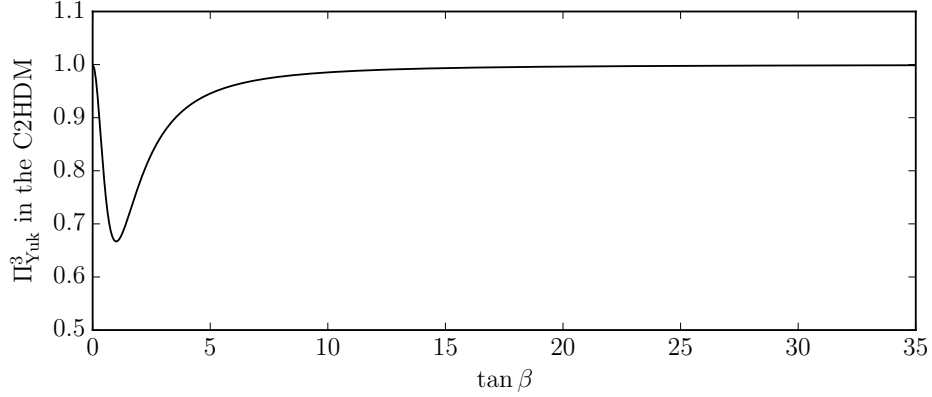


Figure 5.12.: The Yukawa sum eq. (5.24) as a function of $\tan \beta$ in the C2HDM.

this is not due to h_{125} always having a gauge coupling of one. We instead observe the (approximate) sum rule

$$\Pi_{VV}^2 = 1 , \quad (5.21)$$

or equivalently $c(H_{\uparrow}VV) \approx 0$, which is enforced by SUSY relations. This makes the NMSSM very hard to distinguish from the R2HDM or the MSSM, where this sum-rule is exact at tree-level. The CxSM and the C2HDM points in the correct-sign-limit would require a coupling resolution of a few percent be distinguished from models with smaller Higgs sectors. Conversely, this sum-rule allows the exclusion of the CxSM and NMSSM if Π_{VV}^2 deviates significantly from one. In the C2HDM an observation of $\Pi_{VV}^2 < 1$ would force the wrong-sign-limit to be realized.

5.2.2.2. The Yukawa sum-rule

The CxSM fulfills the Yukawa sum-rule

$$\Pi_{\text{Yuk}}^3 = 2 , \quad (5.22)$$

while the NMSSM as well as the type II (and lepton-specific) N2HDM fulfill

$$\Pi_{\text{Yuk}}^3 = 1 . \quad (5.23)$$

In the C2HDM we use $|c(Hf\bar{f})|^2 = a^2 + b^2$, with a and b as in eq. (2.28), for the effective coupling to fermions. This is the value that rescales inclusive cross sections and thus would be extracted from data if no direct hints of CP-violation should have been discovered. It leads to the C2HDM type II sum-rule

$$\Pi_{\text{Yuk}}^3 = 2 \left(\frac{24}{17 - \cos(4\beta)} - 1 \right) . \quad (5.24)$$

The behavior of eq. (5.24) is plotted in fig. 5.12. The function has a minimum of $\Pi_{\text{Yuk}}^3 = 2/3$ at $\tan \beta = 1$ and quickly approaches one for other values of $\tan \beta$.

For completeness, in the flipped N2HDM a

$$\Pi_{\text{Yuk}}^3 = 1 \quad (5.25)$$

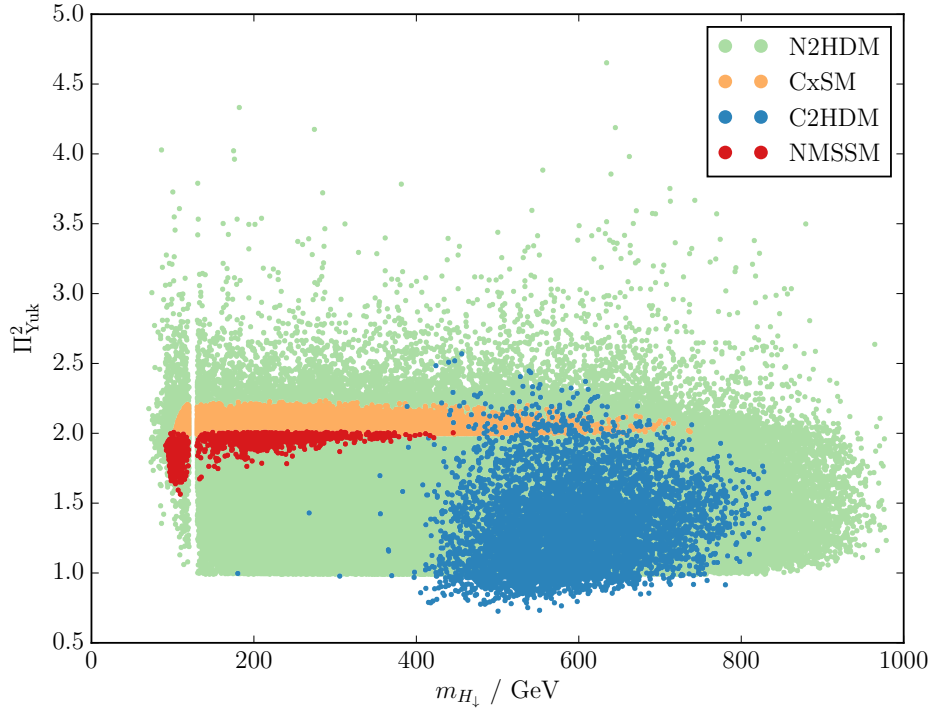


Figure 5.13.: The partial Yukawa sum Π_{Yuk}^2 as a function of m_{H_\downarrow} . The NMSSM and N2HDM (type II) fulfill $\Pi_{\text{Yuk}}^3 = 1$, while in the CxSM $\Pi_{\text{Yuk}}^3 = 2$ and the C2HDM fulfills eq. (5.24). In all models $\Pi_{\text{Yuk}}^2 \geq \Pi_{\text{Yuk}}^3$ holds.

sum-rule can be constructed by using the b quark instead of the τ coupling. The type I N2HDM fulfills

$$\Pi_{\text{Yuk}}^3 = 2 \sin^2 \beta \approx 2, \quad (5.26)$$

as $\tan \beta > 2$ is enforced by flavor constraints [104, 105].

The Yukawa types of the R2HDM fulfill the same sum rules as the N2HDM with Π_{Yuk}^2 instead of Π_{Yuk}^3 and the CP-conserving MSSM fulfills

$$\Pi_{\text{Yuk}}^2 = 1. \quad (5.27)$$

The Yukawa sum Π_{Yuk}^2 , depicted in fig. 5.13, provides another clear handle on excluding the CxSM. If $\Pi_{\text{Yuk}}^2 < 2$ is measured the CxSM is excluded. The maximum reachable value in the CxSM again depends on the bound of the global signal strength.

A measurement of $\Pi_{\text{Yuk}}^2 < 1$ would be very interesting. In the C2HDM this is possible due to the pseudoscalar admixture with CP-odd Yukawa couplings. According to eq. (5.24) this would fix $\tan \beta \approx 1$ while excluding all of our CP-conserving models. A dedicated analysis of the C2HDM could additionally extract the CP-even and CP-odd Yukawa couplings separately and verify that $\Pi_{\text{Yuk}}^2 > 1$ if only the CP-even part a of the Yukawa couplings is included.

Figure 5.13 shows that the N2HDM could explain any value in the range $1 < \Pi_{\text{Yuk}}^2 \lesssim 5$. A dedicated parameter scan in the region of large Yukawa couplings would presumably yield points with even higher values of Π_{Yuk}^2 . This agrees with section 5.2.1 where the flexibility of this model regarding the Higgs couplings to fermions became evident. In the region $200 \text{ GeV} < m_{H_\downarrow} < 400 \text{ GeV}$ and $\Pi_{\text{Yuk}}^2 < 1.5$ the N2HDM is the only model with a lot of parameter points.

While the C2HDM might be able to reproduce such a value it would again require the wrong-sign-limit.

In the NMSSM we observe that $\Pi_{\text{Yuk}}^2 \leq 2$ is fulfilled by all points. This is linked to a number of correlations between couplings enforced by supersymmetry. In fig. 5.5 we saw that

$$c(h_{125}VV) \approx c(h_{125}tt) . \quad (5.28)$$

We have verified that this also holds for H_\downarrow (but not for H_\uparrow). If we combine this with eq. (5.21) we obtain

$$c^2(h_{125}tt) + c^2(H_\downarrow tt) \approx 1 . \quad (5.29)$$

We also observe that

$$c^2(h_{125}b\bar{b}) + c^2(H_\downarrow b\bar{b}) \geq 1 , \quad (5.30)$$

while no relation between the b coupling and t quark or gauge coupling is evident. Inserting eqs. (5.29) and (5.30) into Π_{Yuk}^2 immediately yields $\Pi_{\text{Yuk}}^2 \leq 2$. Note that none of these relations come from the orthogonality of the mixing matrix. If this were the case they would also be realized in the N2HDM. The NMSSM could thus be excluded by an observation of $\Pi_{\text{Yuk}}^2 > 2$ or an observed deviation from eqs. (5.29) and (5.30). Note that all of these relations only hold for the two lightest CP-even scalars of the NMSSM. If H_\uparrow would be discovered instead of H_\downarrow the behavior could be very different. We also observe in fig. 5.13 that the NMSSM points never saturate $\Pi_{\text{Yuk}}^2 = 1$. This behavior is due to the cut on the $H_\downarrow \rightarrow ZZ$ rate (see eq. (5.17)) which cuts off all NMSSM points where $\Pi_{\text{Yuk}}^2 \approx 1$. These are points with high $\tan\beta$ where the b quark and τ couplings of H_\downarrow are very large [66]. They could be reincluded in the analysis if the CP-nature of H_\downarrow was verified without observing $H_\downarrow \rightarrow ZZ$.

We finally note that an observation of $\Pi_{\text{Yuk}}^2 < 2/3$ (which is the minimum value reachable in the C2HDM) cannot be explained by any of our models and would hint at a more complex Higgs sector.

5.2.2.3. Correlations between the sum-rules

Correlations between the coupling sums allow for a further improvement of this analysis if both the values of Π_{V}^2 and Π_{Yuk}^2 are known. Figure 5.14 shows the predictions of the four models in these two parameters. The CxSM shows the simplest behavior. Due to the common scaling factor of all SM couplings, all CxSM parameter points lie exactly on a line starting at $\Pi_{\text{V}}^2 = 1$ and $\Pi_{\text{Yuk}}^2 = 2$.

The C2HDM shows the possibility of $\Pi_{\text{Yuk}}^2 < 1$ as described in the previous section. The bulk of the C2HDM parameter points is located at $\Pi_{\text{V}}^2 \approx 1$. The exceptions are the wrong-sign-limit points which behave completely different. They not only deviate substantially from $\Pi_{\text{V}}^2 = 1$ but for large deviations they tend strongly towards $\Pi_{\text{Yuk}}^2 = 1$.

The N2HDM is by far the least constrained of our models. One notable feature is the sharp lower boundary. This is a result of the orthogonality of the mixing matrix without any physical constraints involved. An observation of $\Pi_{\text{V}}^2 < 1$ and $\Pi_{\text{Yuk}}^2 \approx 1$ could therefore exclude all models with a 3×3 mixing of CP-even scalars.

The coupling sums of the NMSSM are severely constrained by SUSY relations. All points have $\Pi_{\text{V}}^2 \approx 1$ and $1.5 \leq \Pi_{\text{Yuk}}^2 \leq 2$. The minimum of the NMSSM predictions for Π_{Yuk}^2 depends strongly on the cut imposed in eq. (5.17). If this condition were removed the NMSSM would cover the range $1 \leq \Pi_{\text{Yuk}}^2 \leq 2$.

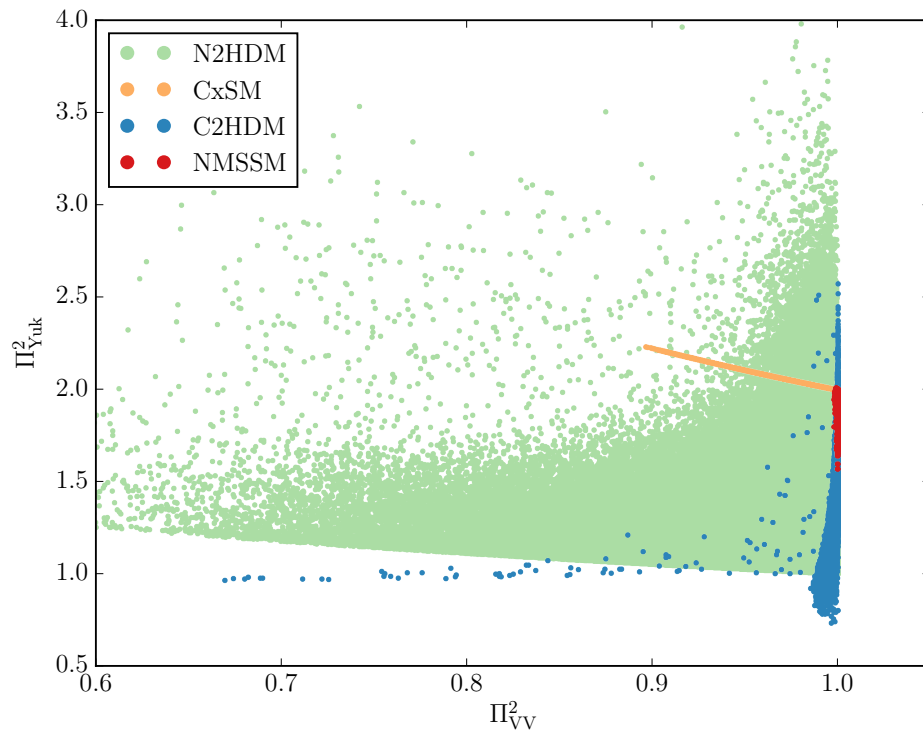


Figure 5.14.: The partial Yukawa sum Π_{Yuk}^2 as a function of the partial gauge boson sum Π_{VV}^2 . Note that a few outlying N2HDM points have been cut off.

CHAPTER 6

Conclusions

In this thesis, we have analyzed and compared the phenomenology of the CxSM, C2HDM, N2HDM, and NMSSM. We have investigated what kind of deviations from the SM expectations for h_{125} are possible and in agreement with current observations. We have compared the signal rates predicted for a second neutral (CP-even in the CxSM, N2HDM, and NMSSM) Higgs boson H_\downarrow and shown which observations could allow us to differentiate between the four models. We have finally introduced a sum-rule analysis using the couplings of h_{125} and H_\downarrow , which can allow for a clear distinction between the four models.

We started by reviewing the CxSM, C2HDM, and NMSSM models. Afterward we introduced the N2HDM in detail and derived all tree-level couplings and theoretical constraints required to study the phenomenology of the model. This work contains the first study of the N2HDM without any approximations employed on the mixing among the scalars.

We subsequently described the parameter scans performed in our models. We began with a short introduction of the **ScannerS** framework we used for the parameter scans in the non-supersymmetric models. We then gave an overview of the constraints applied on the CxSM using the publicly available implementation of the model in **ScannerS**. Our new implementation of the C2HDM in **ScannerS** contains a more complete set of constraints than previous parameter scans in the model. We are the first to check all exclusion bounds from Higgs searches at colliders using the **HiggsBounds** code. This is possible because of an in-house implementation of the C2HDM in **HDECAY** to calculate the decay properties of all Higgs bosons. We furthermore are the first to include the constraints on the electric dipole moment of the electron (eEDM) in a full parameter scan. The **ScannerS** implementation of the C2HDM will be included in a future release as soon as the **HDECAY** implementation of the C2HDM is officially published. Thereafter, we presented our implementation of the N2HDM in **ScannerS**. It relies on the **N2HDECAY** code, which implements the model in **HDECAY**, to calculate the Higgs boson decay properties including QCD corrections. Our N2HDM parameter scan checks the theoretical constraints we have derived as well as all experimental constraints applicable to the model. The implementation of the N2HDM is included in the latest public release of the **ScannerS** program and the **N2HDECAY** code will be made publicly available as well. We finally discussed the parameter scan in the NMSSM using the **NMSSMtools** package and described all constraints applied to the model.

Through these parameter scans, we generated samples of physical parameter points in our four models for the subsequent numerical analysis. We started this analysis with a discussion of the mass distributions of the non- h_{125} neutral (CP-even in the CxSM, N2HDM, and NMSSM) scalars. We especially discussed why the neutral Higgs bosons of the C2HDM are usually both heavy, while very light CP-even Higgs bosons are still possible in the other models. Afterward, we compared the parameter space of the physical C2HDM points in our scan to a previous work in the literature. We found that the constraints from the eEDM severely limit the allowed amount of CP violation in the h_{125} . We used our scan results to generalize the R2HDM wrong-sign-limit to the C2HDM.

We then discussed properties of h_{125} in the CP-conserving models. We compared the phenomenology predicted by the models and studied the influence of singlet admixture to the h_{125} . We showed that measurements in the $\tau\tau$ channel can best constrain the amount of singlet admixture to h_{125} and we demonstrated in which ways the NMSSM is constrained by supersymmetry. We also studied the amount of pseudoscalar admixture to h_{125} allowed in the C2HDM. We saw that the pseudoscalar admixture is most strongly constrained by the eEDM bound and not by the measurements of the h_{125} properties. The allowed pseudoscalar admixture to h_{125} cannot exceed a few percent and h_{125} is therefore always close to the R2HDM limit. We further showed that the wrong-sign-limit of the C2HDM results in a phenomenology very different from the correct-sign-regime.

Subsequently, the inclusive signal rates of H_{\downarrow} were discussed. We pointed out several observations that could exclude one of our models. We especially found a mass range of $200 \text{ GeV} < m_{H_{\downarrow}} < 400 \text{ GeV}$ where enhanced rates (with respect to the SM reference) in the $\gamma\gamma$ and $\tau\bar{\tau}$ channels could easily be explained only in the N2HDM.

We finally described an analysis based on sum-rules which allows for a better distinction between our models. For this analysis, it is essential that a CP-odd Higgs boson (present in the N2HDM and NMSSM) is not misidentified as H_{\downarrow} . We therefore only included parameter points with a rate in the $ggF \rightarrow H_{\downarrow} \rightarrow ZZ$ channel of at least 10 fb. For the remaining points we constructed a partial gauge boson and Yukawa coupling sum using the couplings of h_{125} and H_{\downarrow} . These partial coupling sums are constructed such that the inclusion of the third neutral (CP-even in the CxSM, N2HDM, and NMSSM) Higgs boson H_{\uparrow} in the sum would lead to a sum-rule being satisfied. These sum rules follow from the unitarity of the mixing matrix in the neutral (CP-even) sector. We showed how the CxSM, the correct-sign-limit C2HDM, and the NMSSM could be excluded using this analysis. In the C2HDM we again observed a very different behavior of the wrong-sign-limit points which are better constrained by measurements of h_{125} than by the sum-rule analysis. We further discuss how a measurement of the Yukawa sum could indicate the presence of CP-violation and simultaneously fix $\tan\beta$ to one in the C2HDM. The N2HDM showed a great flexibility in the sum-rule analysis and is the only model to saturate the constraints from orthogonality of the mixing matrix. We observed several additional sum-rules enforced by SUSY relations in the NMSSM. These lead to a very distinct behavior of the NMSSM in this analysis and can allow for a clear exclusion of the model. We propose this analysis as a promising way to distinguish between Higgs sector extensions if only an H_{\downarrow} is discovered.

Explicit parameter transformations and triple-Higgs couplings

In this chapter, the formulas for the explicit transformation between the basis of the Lagrangian and the physical basis defined in section 3.1.3 are shown. The second part contains the formulas for the simplified triple Higgs couplings.

A.1. Explicit parameter transformation

The λ_i parameters of the N2HDM scalar potential can be written as a function of the physical parameters (3.18) as shown below. The transformation is given as a function of the elements R_{ij} of the mixing matrix

$$R = \begin{pmatrix} c_{\alpha_1} c_{\alpha_2} & c_{\alpha_2} s_{\alpha_1} & s_{\alpha_2} \\ -c_{\alpha_3} s_{\alpha_1} - c_{\alpha_1} s_{\alpha_2} s_{\alpha_3} & c_{\alpha_1} c_{\alpha_3} - s_{\alpha_1} s_{\alpha_2} s_{\alpha_3} & c_{\alpha_2} s_{\alpha_3} \\ -c_{\alpha_1} c_{\alpha_3} s_{\alpha_2} + s_{\alpha_1} s_{\alpha_3} & -c_{\alpha_3} s_{\alpha_1} s_{\alpha_2} - c_{\alpha_1} s_{\alpha_3} & c_{\alpha_2} c_{\alpha_3} \end{pmatrix} \quad (\text{A.1})$$

from eq. (3.12). The parameter

$$\tilde{\mu}^2 = \frac{m_{12}^2}{s_{\beta} c_{\beta}} \quad (\text{A.2})$$

is introduced to further simplify the following expressions.

With these conventions, the λ_i are given by

$$v^2 c_{\beta}^2 \cdot \lambda_1 = -\tilde{\mu}^2 s_{\beta}^2 + \sum_{i=1}^3 m_{H_i}^2 R_{i1}^2, \quad (\text{A.3})$$

$$v^2 s_{\beta}^2 \cdot \lambda_2 = -\tilde{\mu}^2 c_{\beta}^2 + \sum_{i=1}^3 m_{H_i}^2 R_{i2}^2, \quad (\text{A.4})$$

$$v^2 \cdot \lambda_3 = -\tilde{\mu}^2 + \frac{1}{c_{\beta} s_{\beta}} \sum_{i=1}^3 m_{H_i}^2 R_{i1} R_{i2} + 2m_{H^{\pm}}^2, \quad (\text{A.5})$$

$$v^2 \cdot \lambda_4 = \tilde{\mu}^2 + m_A^2 - 2m_{H^{\pm}}^2, \quad (\text{A.6})$$

$$v^2 \cdot \lambda_5 = \tilde{\mu}^2 - m_A^2, \quad (\text{A.7})$$

$$v_s^2 \cdot \lambda_6 = \sum_{i=1}^3 m_{H_i}^2 R_{i3}^2, \quad (\text{A.8})$$

$$v v_s c_\beta \cdot \lambda_7 = \sum_{i=1}^3 m_{H_i}^2 R_{i1} R_{i3}, \quad (\text{A.9})$$

$$2v v_s s_\beta \cdot \lambda_8 = \sum_{i=1}^3 m_{H_i}^2 R_{i2} R_{i3}. \quad (\text{A.10})$$

A.2. Triple-Higgs couplings

The triple Higgs couplings g_{abc} can be simplified using the relations above. They are given here as functions of only the physical parameters. A coupling g_{abc} is defined as

$$g_{abc} = \frac{\partial^3 \mathcal{L}}{\partial H_a \partial H_b \partial H_c}, \quad (\text{A.11})$$

where the Lagrangian is taken to be in the physical basis and a , b and c can denote any of the physical charged or neutral Higgs bosons. These triple-Higgs couplings are used in the N2HDECAY code.

The indices i , j , k can in the following take unique values from $\{1, 2, 3\}$ and denote the three CP-even Higgs bosons $H_{1,2,3}$. We define the three dimensional Levi-Civita-Tensor as

$$\epsilon_{ijk} = \begin{cases} 1 & \text{if } (i, j, k) \text{ is an even permutation of } (1, 2, 3), \\ -1 & \text{if } (i, j, k) \text{ is an odd permutation of } (1, 2, 3), \\ 0 & \text{otherwise.} \end{cases} \quad (\text{A.12})$$

In the following formulas there is no summation implied by repeated indices.

$$v \cdot g_{iAA} = -\tilde{\mu}^2 \left[R_{i1} \frac{1}{c_\beta} + R_{i2} \frac{1}{s_\beta} \right] + m_{H_i}^2 \left[R_{i1} \frac{s_\beta^2}{c_\beta} + R_{i2} \frac{c_\beta^2}{s_\beta} \right] + 2m_A^2 [R_{i1} c_\beta + R_{i2} s_\beta] \quad (\text{A.13})$$

$$v \cdot g_{i\pm\pm} = -\tilde{\mu}^2 \left[R_{i1} \frac{1}{c_\beta} + R_{i2} \frac{1}{s_\beta} \right] + m_{H_i}^2 \left[R_{i2} \frac{c_\beta^2}{s_\beta} + R_{i1} \frac{s_\beta^2}{c_\beta} \right] + 2m_{H^\pm}^2 [R_{i1} c_\beta + R_{i2} s_\beta] \quad (\text{A.14})$$

$$\begin{aligned} \frac{1}{3} v \cdot g_{iii} &= -\tilde{\mu}^2 \left[R_{i2}^2 c_\beta \left(\frac{R_{i2} c_\beta}{s_\beta} - R_{i1} \right) + R_{i1}^2 s_\beta \left(\frac{R_{i1} s_\beta}{c_\beta} - R_{i2} \right) \right] \\ &+ \frac{m_{H_i}^2}{v_s} \left[R_{i3}^2 v + R_{i2}^3 \frac{v_s}{s_\beta} + R_{i1}^3 \frac{v_s}{c_\beta} \right] \end{aligned} \quad (\text{A.15})$$

$$\begin{aligned} v \cdot g_{iij} &= -\frac{1}{2} \tilde{\mu}^2 \left[\left(R_{i2} \frac{1}{s_\beta} + R_{i1} \frac{1}{c_\beta} \right) \left(6R_{i2} R_{j2} + 6R_{i3} R_{j3} s_\beta^2 + \sum_k \epsilon_{ijk} R_{k3} s_{2\beta} \right) \right] \\ &+ \frac{2m_{H_i}^2 + m_{H_j}^2}{v_s} \left[R_{i3}^2 R_{j3} v + R_{i2}^2 R_{j2} \frac{v_s}{s_\beta} + R_{i1}^2 R_{j1} \frac{v_s}{c_\beta} \right] \end{aligned} \quad (\text{A.16})$$

$$\begin{aligned}
v \cdot g_{123} = & -\tilde{\mu}^2 \left[(2R_{12}R_{13} + R_{32}R_{33}) c_\beta + (R_{31}R_{33} - 3R_{12}R_{23}R_{33} - R_{21}R_{23}) s_\beta \right. \\
& \left. + 3R_{12}R_{22} \left(R_{31} \frac{1}{c_\beta} - R_{32} \frac{1}{s_\beta} \right) + 3R_{13}R_{23}R_{31} \frac{s_\beta^2}{c_\beta} \right] \\
& + \frac{m_{H1}^2 + m_{H2}^2 + m_{H3}^2}{v_s} \left[R_{13}R_{23}R_{33}v + R_{12}R_{22}R_{32} \frac{v_s}{s_\beta} \right. \\
& \left. - R_{11} (R_{22}R_{32} + R_{23}R_{33}) \frac{v_s}{c_\beta} \right]
\end{aligned} \tag{A.17}$$

The sums of different powers of mixing matrix elements arise from simplifications due to the orthogonality of the mixing matrix. The formula employed is

$$R_{mn} = (-1)^{m+n} \det(\mathcal{R}_{mn}) , \tag{A.18}$$

which follows from the properties of the adjugate of an orthogonal matrix. The matrix \mathcal{R}_{mn} is the submatrix formed by deleting the m -th row and n -th columns from R . The indices m and n take any values in $\{1, 2, 3\}$.

APPENDIX B

N2HDM parameter points with global charge and CP-breaking minima

Here we give examples of N2HDM parameter points that contain both a charge and CP-conserving (normal) local minimum with $v_1^2 + v_2^2 \approx 246 \text{ GeV}$ and a deeper charge or CP-breaking minimum. The existence of such configurations has been disproven in the 2HDM [95]. These examples serve as counterexamples to a naive generalization of this proof to the N2HDM.

The charge-breaking parameter point in table B.1 has a normal minimum at

$$v_1 = 192.715 \text{ GeV} , \quad v_2 = 152.887 \text{ GeV} , \quad v_s = 626.334 \text{ GeV} . \quad (\text{B.1})$$

The value of the potential at this minimum is

$$V_{\text{normal}} = -2.26 \times 10^{10} \text{ GeV} . \quad (\text{B.2})$$

The global minimum is

$$v_1 = 496.073 \text{ GeV} , \quad v_2 = 101.843 \text{ GeV} , \quad v_{\text{cb}} = 529.567 \text{ GeV} , \quad v_s = v_{\text{cp}} = 0 \text{ GeV} , \quad (\text{B.3})$$

with a value of

$$V_{\text{charge}} = -4.01 \times 10^{10} \text{ GeV} . \quad (\text{B.4})$$

The normal minimum in the CP-breaking parameter point in table B.1 is

$$v_1 = 102.66 \text{ GeV} , \quad v_2 = 223.553 \text{ GeV} , \quad v_s = -491.912 \text{ GeV} , \quad (\text{B.5})$$

with

$$V_{\text{normal}} = -7.29 \times 10^9 \text{ GeV} . \quad (\text{B.6})$$

The CP-breaking global minimum is at

$$v_1 = 778.838 \text{ GeV} , \quad v_2 = 69.9478 \text{ GeV} , \quad v_{\text{cp}} = 999.254 \text{ GeV} , \quad v_s = v_{\text{cb}} = 0 \text{ GeV} , \quad (\text{B.7})$$

with

$$V_{\text{CP}} = -1.87 \times 10^{10} \text{ GeV} . \quad (\text{B.8})$$

Table B.1.: Parameter values of exemplary N2HDM points with both a normal minimum and a global charge or CP-breaking minimum, respectively.

	charge	CP
m_{11}^2 / GeV^2	$-2.836\,82 \times 10^5$	$3.271\,66 \times 10^4$
m_{22}^2 / GeV^2	$-1.989\,90 \times 10^5$	$-9.223\,17 \times 10^4$
m_{12}^2 / GeV^2	$-1.409\,96 \times 10^5$	$-9.874\,25 \times 10^4$
m_s^2 / GeV^2	$3.389\,65 \times 10^5$	$2.200\,53 \times 10^4$
λ_1	7.788 11	7.359 30
λ_2	5.294 42	2.912 79
λ_3	-4.639 41	7.089 98
λ_4	$1.281\,59 \times 10^1$	$-1.120\,02 \times 10^1$
λ_5	$6.027\,84 \times 10^{-1}$	$4.039\,30 \times 10^{-1}$
λ_6	$4.495\,21 \times 10^{-1}$	$7.074\,93 \times 10^{-1}$
λ_7	1.556 82	$5.705\,95 \times 10^{-1}$
λ_8	2.046 19	$4.056\,77 \times 10^{-1}$

APPENDIX C

Global minimum conditions

Using the procedure described in section 3.3.2 we obtain all stationary points of the scalar potential. To ensure that the physical minimum is the global one we check that none of the other stationary points has a smaller value of the scalar potential V . Table C.1 which characterizes the possible stationary points is identical to table 3.5 and shown again for ease of reference.

In the following, we use shorthands for combinations of the λ_i ,

$$\lambda_{345} := \lambda_3 + \lambda_4 + \lambda_5, \quad (\text{C.1})$$

$$\lambda_{34-5} := \lambda_3 + \lambda_4 - \lambda_5, \quad (\text{C.2})$$

$$\Lambda_{kl}^{ij} := \lambda_i \lambda_j - \lambda_k \lambda_l. \quad (\text{C.3})$$

Note that λ_{345} and λ_{34-5} can appear in Λ_{kl}^{ij} .

We have defined the field configuration eq. (3.26) such that the VEVs v_1 , v_2 , v_{cp} , and v_{cb} are real parameters. Any solution of the stationarity conditions has to satisfy this assumption. We are, therefore, only interested in solutions where all VEVs squared are positive. These are the positivity conditions we state together with the corresponding stationary values. If any of these conditions are not satisfied the corresponding stationary point of the scalar potential does not exist. We remind that the \mathbb{Z}_2 -symmetries of the N2HDM potential allow us to choose all VEVs except v_2 to be positive without loss of generality.

Table C.1.: Shows and names all possible cases of VEVs being zero (0) or non-zero (1). The cases, that are only allowed when certain parameter conditions are satisfied, are not shown.

Case	I	IIa	IIb	IIIa	IIIb	IIIc	sI	sIIa	sIIb	sIIIa	sIIIb	sIIIc	sIV
v_1	1	1	1	0	0	0	1	1	1	0	0	0	0
v_2	1	1	1	0	0	0	1	1	1	0	0	0	0
v_{cp}	0	1	0	1	1	0	0	1	0	1	1	0	0
v_{cb}	0	0	1	1	0	1	0	0	1	1	0	1	0
v_s	0	0	0	0	0	0	1	1	1	1	1	1	1

C.1. 2HDM-like stationary points

The six cases of 2HDM-like stationary points with $v_s = 0$ are the stationary points of an R2HDM potential with the same parameters $m_{11}^2, m_{22}^2, m_{12}^2$ and λ_{1-5} . The resulting condition in the R2HDM has been checked numerically against the discriminant condition [94].

C.1.1. Case I

The CP and charge conserving case is the most complicated one. We rewrite the system of minimum conditions in terms of

$$v_1 = v \cos \delta , \quad (\text{C.4})$$

$$v_2 = v \sin \delta . \quad (\text{C.5})$$

The convention $v_1 > 0$ leads to

$$-\frac{\pi}{2} < \delta < \frac{\pi}{2} . \quad (\text{C.6})$$

We can eliminate v from the resulting system of equations and obtain a single quartic equation for $\sin^2 \delta$

$$\begin{aligned} 0 = & (m_{12}^2)^2 \lambda_1^2 \\ & + \sin^2 \delta \left[-(m_{11}^2 \lambda_{345} - m_{22}^2 \lambda_1)^2 - 4(m_{12}^2)^2 \lambda_1^2 \right] \\ & + (\sin^2 \delta)^2 \left[3(m_{11}^2 \lambda_{345} - m_{22}^2 \lambda_1)^2 + 2(m_{11}^2 \lambda_{345} - m_{22}^2 \lambda_1)(m_{22}^2 \lambda_{345} - m_{11}^2 \lambda_2) \right. \\ & \quad \left. + 2(m_{12}^2)^2 (3\lambda_1^2 - \lambda_1 \lambda_2) \right] \\ & + (\sin^2 \delta)^3 \left[-3(m_{11}^2 \lambda_{345} - m_{22}^2 \lambda_1)^2 + 4(m_{12}^2)^2 \lambda_1 (\lambda_2 - \lambda_1) \right. \\ & \quad \left. - (m_{22}^2 \lambda_{345} - m_{11}^2 \lambda_2)((4m_{11}^2 + m_{22}^2)\lambda_{345} - 4m_{22}^2 \lambda_1 - m_{11}^2 \lambda_2) \right] \\ & + (\sin^2 \delta)^4 \left[(m_{11}^2 \lambda_{345} - m_{22}^2 \lambda_1)^2 + (m_{12}^2)^2 (\lambda_1 - \lambda_2)^2 \right. \\ & \quad \left. + (m_{22}^2 \lambda_{345} - m_{11}^2 \lambda_2)((2m_{11}^2 + m_{22}^2)\lambda_{345} - 2m_{22}^2 \lambda_1 - m_{11}^2 \lambda_2) \right] . \end{aligned} \quad (\text{C.7})$$

This equation can be solved numerically. Out of the four solutions of eq. (C.7) only real solutions in the open interval $(0, 1)$ are valid solutions for $\sin^2 \delta$. Reality of $\sin^2 \delta$ is required for v_1 and v_2 to be real.

Each of these solutions yields two possible values for

$$v^2 = \frac{2 \left(m_{22}^2 - m_{12}^2 \left(\pm \sqrt{\frac{1}{\sin^2 \delta} - 1} \right) \right)}{\lambda_{345} (\sin^2 \delta - 1) - \lambda_2 \sin^2 \delta} . \quad (\text{C.8})$$

The \pm corresponds to the two possible signs of $\sin \delta$ in the region (C.6). Valid solutions for v^2 have to be positive. We then use eqs. (C.4) and (C.5) to compute v_1 and v_2 where both possible signs for v_2 need to be considered.

We finally compute the values of the scalar potential for these up to 16 solutions for v_1 and v_2 (up to four solutions for $\sin^2 \delta$ times two for the sign of $\sin \delta$ times two for the sign of v_2). These values are compared to the value of the physical minimum to ensure the physical minimum is the global one.

C.1.2. Case II

In the cases IIa and IIb, the system of the minimum conditions can be solved analytically. There are two quadratic equations to be solved in the process leading to two discriminants that have to be positive for the solution to exist. This is equivalent to requiring that all VEVs squared are positive. We have obtained analytic formulae for the value of the potential at these points.

The value and positivity conditions are

$$V(\text{II}) = \frac{(m_{11}^2)^2 \lambda_2 - 2m_{11}^2 m_{22}^2 x + (m_{22}^2)^2 \lambda_1}{2\Lambda_{12}^{xx}} - \frac{(m_{12}^2)^2}{\lambda_{345} - x}, \quad (\text{C.9})$$

$$0 < v_{\text{cb}}^2 + v_{\text{cp}}^2 = \frac{(m_{12}^2)^2 \Lambda_{12}^{xx}}{(\lambda_{345} - x)^2 (m_{22}^2 x - m_{11}^2 \lambda_2)} - \frac{2xm_{11}^2 - 2m_{22}^2 \lambda_1}{\Lambda_{12}^{xx}}, \quad (\text{C.10})$$

$$0 < v_1^2 = -\frac{2m_{22}^2 x - 2m_{11}^2 \lambda_2}{\Lambda_{12}^{xx}}. \quad (\text{C.11})$$

Positivity of v_2^2 is guaranteed if v_1^2 is positive. Setting

$$x = \begin{cases} \lambda_{34-5} & \text{in case IIa} \\ \lambda_3 & \text{in case IIb} \end{cases} \quad (\text{C.12})$$

we obtain the results of the two sub-cases.

C.1.3. Case III

In the cases III, the minimum conditions simplify to a linear system for the VEVs squared. All three cases lead to the same value stationary value

$$V(\text{IIIabc}) = -\frac{(m_{22}^2)^2}{2\lambda_2}. \quad (\text{C.13})$$

This solution only exists if

$$m_{22}^2 < 0 \quad (\text{C.14})$$

which follows by simplifying the positivity conditions of the squared VEVs with eqs. (3.24) and (3.25).

C.2. Stationary points with a singlet VEV

The procedure for the stationary points with $v_s \neq 0$ is the same as for the 2HDM-like cases.

C.2.1. Case sI

The quartic equation in $\sin^2 \delta$ reads

$$\begin{aligned}
0 = & (m_{12}^2)^2 (\Lambda_{16}^{77})^2 \\
& + \sin^2 \delta \left[- \left\{ (m_{11}^2 \lambda_6 - m_s^2 \lambda_7) \lambda_{345} + m_{22}^2 \Lambda_{16}^{77} + (m_s^2 \lambda_1 - m_{11}^2 \lambda_7) \lambda_8 \right\}^2 \right. \\
& \quad \left. - 4(m_{12}^2)^2 (\Lambda_{16}^{77})^2 \right] \\
& + (\sin^2 \delta)^2 \left[\left\{ (m_{11}^2 \lambda_6 - m_s^2 \lambda_7) \lambda_{345} - m_{11}^2 (\lambda_7 \lambda_8) + m_{22}^2 \Lambda_{16}^{77} + m_s^2 (\lambda_1 \lambda_8) \right\} \right. \\
& \quad \times \left\{ (3m_{11}^2 \lambda_6 + 2m_{22}^2 \lambda_6 - m_s^2 (3\lambda_7 + 2\lambda_8)) \lambda_{345} + m_{11}^2 (2\Lambda_{26}^{88} - 3\lambda_7 \lambda_8) \right. \\
& \quad \left. \left. + m_{22}^2 (3\Lambda_{16}^{77} - 2\lambda_7 \lambda_8) + m_s^2 (2\lambda_2 \lambda_7 + 3\lambda_1 \lambda_8) \right\} \right. \\
& \quad \left. + 2(m_{12}^2)^2 \Lambda_{16}^{77} (3\Lambda_{16}^{77} - \Lambda_{26}^{88}) \right] \\
& + (\sin^2 \delta)^3 \left[\left\{ (m_s^2 (3\lambda_7 + \lambda_8) - (3m_{11}^2 + m_{22}^2) \lambda_6) \lambda_{345} + m_{11}^2 (3\lambda_7 \lambda_8 - \Lambda_{26}^{88}) \right. \right. \\
& \quad \left. \left. + m_{22}^2 (\lambda_7 \lambda_8 - 3\Lambda_{16}^{77}) - m_s^2 (\lambda_2 \lambda_7 + 3\lambda_1 \lambda_8) \right\} \right. \\
& \quad \times \left\{ ((m_{11}^2 + m_{22}^2) \lambda_6 - m_s^2 (\lambda_7 + \lambda_8)) \lambda_{345} + m_{11}^2 (\Lambda_{26}^{88} - \lambda_7 \lambda_8) \right. \\
& \quad \left. \left. + m_{22}^2 (\Lambda_{16}^{77} - \lambda_7 \lambda_8) + m_s^2 (\lambda_2 \lambda_7 + \lambda_1 \lambda_8) \right\} \right. \\
& \quad \left. + 4(m_{12}^2)^2 \Lambda_{16}^{77} (\Lambda_{26}^{88} - \Lambda_{16}^{77}) \right] \\
& + (\sin^2 \delta)^4 \left[\left\{ ((m_{11}^2 + m_{22}^2) \lambda_6 - m_s^2 (\lambda_7 + \lambda_8)) \lambda_{345} + m_{11}^2 (\Lambda_{26}^{88} - \lambda_7 \lambda_8) \right. \right. \\
& \quad \left. \left. + m_{22}^2 (\Lambda_{16}^{77} - \lambda_8 \lambda_7) + m_s^2 (\lambda_2 \lambda_7 + \lambda_1 \lambda_8) \right\}^2 \right. \\
& \quad \left. + (m_{12}^2)^2 (\Lambda_{26}^{88} - \Lambda_{16}^{77})^2 \right]
\end{aligned} \tag{C.15}$$

The corresponding values for v^2 and v_s^2 are obtained through

$$v^2 = \frac{2\lambda_6 \left(m_{22}^2 - m_{12}^2 \left(\pm \sqrt{\frac{1}{\sin^2 \delta} - 1} \right) \right) - 2m_s^2 \lambda_8}{(\sin^2 \delta - 1)(\lambda_6 \lambda_{345} - \lambda_7 \lambda_8) + \Lambda_{26}^{88} \sin^2 \delta}, \tag{C.16}$$

$$v_s^2 = \frac{-\lambda_7 v_1^2 - \lambda_8 v_2^2 - 2m_s^2}{\lambda_6}. \tag{C.17}$$

The requirements on a solution are as in case I with the addition of $v_s^2 > 0$. The sign of v_s is irrelevant leading again to a maximum of 16 solutions.

C.2.2. Case sII

The stationary values and positivity conditions in case sII are given by

$$\begin{aligned}
V(\text{sII}) = & -\frac{(m_{12}^2)^2}{\lambda_{345} - x} - \frac{-(m_{11}^2)^2 \Lambda_{26}^{88} - (m_{22}^2)^2 \Lambda_{16}^{77} - (m_s^2)^2 \Lambda_{12}^{xx}}{2(\lambda_7 \Lambda_{27}^{x8} + x \Lambda_{x6}^{78} - \lambda_1 \Lambda_{26}^{88})} \\
& - \frac{m_{11}^2 m_{22}^2 \Lambda_{x6}^{78} + m_{11}^2 m_s^2 \Lambda_{27}^{x8} + m_{22}^2 m_s^2 \Lambda_{18}^{x7}}{\lambda_7 \Lambda_{27}^{x8} + x \Lambda_{x6}^{78} - \lambda_1 \Lambda_{26}^{88}},
\end{aligned} \tag{C.18}$$

$$0 < v_{\text{cb}}^2 + v_{\text{cp}}^2 = \frac{2(m_{12}^2)^2(\lambda_7\Lambda_{27}^{x8} + x\Lambda_{x6}^{78} - \lambda_1\Lambda_{26}^{88})}{(\lambda_{345} - x)^2(m_s^2\Lambda_{27}^{x8} + m_{22}^2\Lambda_{x6}^{78} - m_{11}^2\Lambda_{26}^{88})} + \frac{2m_{22}^2\Lambda_{16}^{77} - 2m_s^2\Lambda_{18}^{x7} - 2m_{11}^2\Lambda_{x6}^{78}}{\lambda_7\Lambda_{27}^{x8} + x\Lambda_{x6}^{78} - \lambda_1\Lambda_{26}^{88}}, \quad (\text{C.19})$$

$$0 < v_s^2 = \frac{2m_s^2\Lambda_{12}^{xx} - 2m_{11}^2\Lambda_{27}^{x8} - 2m_{22}^2\Lambda_{18}^{x7}}{\lambda_7\Lambda_{27}^{x8} + x\Lambda_{x6}^{78} - \lambda_1\Lambda_{26}^{88}}, \quad (\text{C.20})$$

$$0 < v_1^2 = \frac{-2m_s^2\Lambda_{27}^{x8} - 2m_{22}^2\Lambda_{x6}^{78} + 2m_{11}^2\Lambda_{26}^{88}}{\lambda_7\Lambda_{27}^{x8} + x\Lambda_{x6}^{78} - \lambda_1\Lambda_{26}^{88}}. \quad (\text{C.21})$$

Positivity of v_2^2 is ensured if v_1^2 is positive.

Setting

$$x = \begin{cases} \lambda_{34-5} & \text{in case sIIa} \\ \lambda_3 & \text{in case sIIb} \end{cases} \quad (\text{C.22})$$

again yields the two sub-cases.

C.2.3. Case sIII

The cases sIII all yield the same result. The stationary value of the scalar potential is given by

$$V(\text{sIII}) = \frac{(m_{22}^2)^2\lambda_6 - 2m_{22}^2m_s^2\lambda_8 + (m_s^2)^2\lambda_2}{2\Lambda_{26}^{88}}. \quad (\text{C.23})$$

The two conditions that need to be satisfied are

$$0 < \frac{2m_{22}^2\lambda_6 - 2m_s^2\lambda_8}{\Lambda_{26}^{88}}, \quad (\text{C.24})$$

$$0 < \frac{2m_s^2\lambda_2 - 2m_{22}^2\lambda_8}{\Lambda_{26}^{88}}. \quad (\text{C.25})$$

C.2.4. Case sIV

The case sIV stationary point has a value of

$$V(\text{sIV}) = -\frac{(m_s^2)^2}{2\lambda_6}, \quad (\text{C.26})$$

which is only a valid solution if

$$m_s^2 < 0. \quad (\text{C.27})$$

C.3. Special case $\lambda_4 = \lambda_5$

If $\lambda_4 = \lambda_5$ all VEVs can be simultaneously non-zero. This special case yields a scalar potential value of

$$V(\lambda_4 = \lambda_5) = -\frac{(m_{12}^2)^2}{2\lambda_4} + \frac{(m_{11}^2)^2\Lambda_{26}^{88} + (m_s^2)^2\Lambda_{12}^{33} + (m_{22}^2)^2\Lambda_{16}^{77}}{2(\lambda_7\Lambda_{27}^{38} + \lambda_3\Lambda_{36}^{78} - \lambda_1\Lambda_{26}^{88})} - \frac{m_{11}^2m_s^2\Lambda_{27}^{38} + m_{11}^2m_{22}^2\Lambda_{36}^{78} + m_{22}^2m_s^2\Lambda_{18}^{37}}{\lambda_7\Lambda_{27}^{38} + \lambda_3\Lambda_{36}^{78} - \lambda_1\Lambda_{26}^{88}}. \quad (\text{C.28})$$

The positivity conditions are

$$0 < v_{\text{cb}}^2 + v_{\text{cp}}^2 = \frac{(m_{12}^2)^2 (\lambda_7 \Lambda_{27}^{38} + \lambda_3 \Lambda_{36}^{78} - \lambda_1 \Lambda_{26}^{88})}{2\lambda_4^2 (m_s^2 \Lambda_{27}^{38} + m_{22}^2 \Lambda_{36}^{78} - m_{11}^2 \Lambda_{26}^{88})} + \frac{2m_{22}^2 \Lambda_{16}^{77} - 2m_s^2 \Lambda_{18}^{x7} - 2m_{11}^2 \Lambda_{36}^{78}}{\lambda_7 \Lambda_{27}^{38} + \lambda_3 \Lambda_{36}^{78} - \lambda_1 \Lambda_{26}^{88}}, \quad (\text{C.29})$$

$$0 < v_s^2 = \frac{2m_s^2 \Lambda_{12}^{33} - 2m_{11}^2 \Lambda_{27}^{38} - 2m_{22}^2 \Lambda_{18}^{37}}{\lambda_7 \Lambda_{27}^{38} + \lambda_3 \Lambda_{36}^{78} - \lambda_1 \Lambda_{26}^{88}}, \quad (\text{C.30})$$

$$0 < v_1^2 = \frac{2m_s^2 \Lambda_{27}^{38} + 2m_{22}^2 \Lambda_{36}^{78} - 2m_{11}^2 \Lambda_{26}^{88}}{-\lambda_7 \Lambda_{27}^{38} - \lambda_3 \Lambda_{36}^{78} + \lambda_1 \Lambda_{26}^{88}}. \quad (\text{C.31})$$

APPENDIX D

The code N2HDECAY

N2HDECAY¹ is an HDECAY implementation of the N2HDM written in FORTRAN. It is based on HDECAY v6.51 [76, 77] and builds largely on the implementation of the 2HDM [77]. The code is completely self-contained. Compiling it with the supplied `makefile` creates a portable executable called `run` which reads a file called `n2hdecay.in` in the same directory as input.

Part of an example input file is shown below. All parameters not shown are set to their default values. The lines colored gray contain parameters unused in the N2HDM and can be set to any value. The input flag called N2HDM near the top of the input file (not shown) turns on the model if set to 1. The flag PARAM has to be set to 1 for the code to work.

```
***** 2 Higgs Doublet Model *****
TYPE: 1 (I), 2 (II), 3 (lepton-specific), 4 (flipped)
PARAM: 1 (masses), 2 (lambda_i)

PARAM    = 1
TYPE     = 2
*****
TGBET2HDM= 1.17639226D0
M_12^2   = 3.28390121D5
***** PARAM=1:
ALPHA_H  = 10.D0
MHL      = 10.D0
MHH      = 10.D0
MHA      = 9.02919728D2
MH+-     = 8.59398112D2
***** PARAM=2:
LAMBDA1  = 0D0
LAMBDA2  = 0D0
LAMBDA3  = 0D0
LAMBDA4  = 0D0
LAMBDA5  = 0D0
***** N2HDM *****
*** needs TYPE, TGBET2HDM, M12^2, MHA and MH+- from the 2HDM block ***
MH1      = 1.25090000D2
MH2      = 8.17422761D2
MH3      = 9.76339405D2
alpha1   = 0.79503834
alpha2   = 0.13549279
alpha3   = 1.46729273
V_SING   = 1.49629673D3
*****
```

¹available at <https://www.itp.kit.edu/~maggie/N2HDECAY/>

Running with this input file produces output files containing the branching ratios and total widths for the Higgs bosons $H_{1,2,3}$ (`br.H1_N2HDM_a`, `br.H1_N2HDM_b`, ...), A (`br.A_N2HDM_a`, ...), H^\pm (`br.H+_N2HDM_a`, ...) and the top-quark (`br.top`). The total width and branching ratio of the t quark are calculated to account for the decay

$$t \rightarrow H^+ b \quad (\text{D.1})$$

if the charged Higgs boson is sufficiently light.

As an example, the output for the heaviest Higgs boson (`br.H3_N2HDM_a`, `br.H3_N2HDM_b`, `br.H3_N2HDM_c`, `br.H3_N2HDM_d`) for this parameter point is given below. Each line of values corresponds to one of the output files.

MH3	BB	TAU TAU	MU MU	SS	CC	TT
976.339	0.3458E-03	0.5450E-04	0.1927E-06	0.1259E-06	0.1267E-04	0.8026
MH3	GG	GAM GAM	Z GAM	WW	ZZ	
976.339	0.1326E-02	0.3417E-05	0.6717E-06	0.4762E-01	0.2350E-01	
MH3	H1H1	H1H2	H2H2	AA	Z A	
976.339	0.6375E-01	0.2923E-03	0.000	0.9115E-13	0.7821E-04	
MH3	W+- H-+	H+ H-	WIDTH			
976.339	0.6038E-01	0.000	43.40			

Acknowledgement / Danksagung

Ich bedanke mich herzlichst bei Frau Prof. Dr. M. Margarete Mühlleiter für die spannende Themenstellung der Arbeit und die ausgezeichnete Atmosphäre in ihrer Arbeitsgruppe am Institut für Theoretische Physik. Besonders bedanke ich mich für die vielen spannenden und lehrreichen Diskussionen, die mich immer wieder von einem überraschend aussehenden Plot zu einem tieferen physikalischen Verständnis geführt haben. Weiterhin möchte ich mich bei ihr für die Teilnahme am DAAD-Programm bedanken, wodurch ein hochinteressanter Forschungsaufenthalt in Portugal ermöglicht wurde.

Ich bedanke mich bei P.D. Dr. Michael Spira, der sich bereiterklärte Koreferent dieser Arbeit zu sein.

A very special thanks goes out to Dr. Marco Sampaio for the **ScannerS** code and helping me use it. Apart from the numerous programming-related discussions I am also extremely grateful for his input regarding the N2HDM global minimum analysis. Discussing with Marco is always a pleasure, especially due to his extremely helpful and exhaustive replies to questions via email.

Vielen Dank an Philipp Basler, der mich besonders in der Anfangszeit meiner Masterarbeit viel unterstützt hat und mir sein Scanprogramm zur Verfügung gestellt hat bis ich auf **ScannerS** umgestiegen bin. Diskussionen über seine Arbeit waren immer eine willkommene Ablenkung wenn ich mal wieder vor Programmierproblemen saß. Insbesondere lieferte Philipp die Idee doch mal kurz das C2HDM in ScannerS zu implementieren und hat mich bei der Implementierung der eEDM Formeln unterstützt.

Thanks to Dr. David Lopez-Val with whom I had several great discussions about the N2HDM and who offered to proof-read my thesis before I even had really started writing.

I also thank Prof. Dr. Rui Santos for his hospitality during our stay in Portugal and for answering several questions on the couplings of the C2HDM.

I am grateful to David Lopez-Val, Alexander Wlotzka and Marco Sampaio for proof-reading my thesis and all the helpful feedback they provided.

Zum Abschluss danke ich allen meinen Freunden, die mich gegen Ende der Arbeit von meinem Stress abgelenkt haben. Im Besonderen vielen Dank an meine Freundin für die gute Gesellschaft beim Schreiben in der Freiburger UB und für alles andere.

Bibliography

- [1] Georges Aad et al. “Observation of a new particle in the search for the Standard Model Higgs boson with the ATLAS detector at the LHC”. In: *Phys. Lett.* B716 (2012), pp. 1–29. DOI: 10.1016/j.physletb.2012.08.020. arXiv: 1207.7214 [hep-ex].
- [2] Serguei Chatrchyan et al. “Observation of a new boson at a mass of 125 GeV with the CMS experiment at the LHC”. In: *Phys. Lett.* B716 (2012), pp. 30–61. DOI: 10.1016/j.physletb.2012.08.021. arXiv: 1207.7235 [hep-ex].
- [3] S. L. Glashow. “Partial Symmetries of Weak Interactions”. In: *Nucl. Phys.* 22 (1961), pp. 579–588. DOI: 10.1016/0029-5582(61)90469-2.
- [4] Abdus Salam. “Weak and Electromagnetic Interactions”. In: *Conf. Proc.* C680519 (1968), pp. 367–377.
- [5] Steven Weinberg. “A Model of Leptons”. In: *Phys. Rev. Lett.* 19 (1967), pp. 1264–1266. DOI: 10.1103/PhysRevLett.19.1264.
- [6] F. Englert and R. Brout. “Broken Symmetry and the Mass of Gauge Vector Mesons”. In: *Phys. Rev. Lett.* 13 (1964), pp. 321–323. DOI: 10.1103/PhysRevLett.13.321.
- [7] Peter W. Higgs. “Broken Symmetries and the Masses of Gauge Bosons”. In: *Phys. Rev. Lett.* 13 (1964), pp. 508–509. DOI: 10.1103/PhysRevLett.13.508.
- [8] Georges Aad et al. “Combined Measurement of the Higgs Boson Mass in pp Collisions at $\sqrt{s} = 7$ and 8 TeV with the ATLAS and CMS Experiments”. In: *Phys. Rev. Lett.* 114 (2015), p. 191803. DOI: 10.1103/PhysRevLett.114.191803. arXiv: 1503.07589 [hep-ex].
- [9] Georges Aad et al. “Measurements of the Higgs boson production and decay rates and constraints on its couplings from a combined ATLAS and CMS analysis of the LHC pp collision data at $\sqrt{s} = 7$ and 8 TeV”. In: *JHEP* 08 (2016), p. 045. DOI: 10.1007/JHEP08(2016)045. arXiv: 1606.02266 [hep-ex].
- [10] Rita Coimbra, Marco O. P. Sampaio, and Rui Santos. “ScannerS: Constraining the phase diagram of a complex scalar singlet at the LHC”. In: *Eur. Phys. J.* C73 (2013), p. 2428. DOI: 10.1140/epjc/s10052-013-2428-4. arXiv: 1301.2599 [hep-ph].
- [11] Raul Costa et al. “Singlet Extensions of the Standard Model at LHC Run 2: Benchmarks and Comparison with the NMSSM”. In: *JHEP* 06 (2016), p. 034. DOI: 10.1007/JHEP06(2016)034. arXiv: 1512.05355 [hep-ph].
- [12] Vanda Silveira and A. Zee. “Scalar Phantoms”. In: *Phys. Lett.* B161 (1985), pp. 136–140. DOI: 10.1016/0370-2693(85)90624-0.
- [13] John McDonald. “Gauge singlet scalars as cold dark matter”. In: *Phys. Rev.* D50 (1994), pp. 3637–3649. DOI: 10.1103/PhysRevD.50.3637. arXiv: hep-ph/0702143 [HEP-PH].

- [14] M. C. Bento et al. “Selfinteracting dark matter and invisibly decaying Higgs”. In: *Phys. Rev. D* 62 (2000), p. 041302. DOI: 10.1103/PhysRevD.62.041302. arXiv: astro-ph/0003350 [astro-ph].
- [15] C. P. Burgess, Maxim Pospelov, and Tonnis ter Veldhuis. “The Minimal model of nonbaryonic dark matter: A Singlet scalar”. In: *Nucl. Phys.* B619 (2001), pp. 709–728. DOI: 10.1016/S0550-3213(01)00513-2. arXiv: hep-ph/0011335 [hep-ph].
- [16] Hooman Davoudiasl et al. “The New minimal standard model”. In: *Phys. Lett.* B609 (2005), pp. 117–123. DOI: 10.1016/j.physletb.2005.01.026. arXiv: hep-ph/0405097 [hep-ph].
- [17] Alexander Kusenko. “Sterile neutrinos, dark matter, and the pulsar velocities in models with a Higgs singlet”. In: *Phys. Rev. Lett.* 97 (2006), p. 241301. DOI: 10.1103/PhysRevLett.97.241301. arXiv: hep-ph/0609081 [hep-ph].
- [18] J. J. van der Bij. “The Minimal non-minimal standard model”. In: *Phys. Lett.* B636 (2006), pp. 56–59. DOI: 10.1016/j.physletb.2006.03.018. arXiv: hep-ph/0603082 [hep-ph].
- [19] Xiao-Gang He et al. “Constraints on Scalar Dark Matter from Direct Experimental Searches”. In: *Phys. Rev. D* 79 (2009), p. 023521. DOI: 10.1103/PhysRevD.79.023521. arXiv: 0811.0658 [hep-ph].
- [20] Matthew Gonderinger et al. “Vacuum Stability, Perturbativity, and Scalar Singlet Dark Matter”. In: *JHEP* 01 (2010), p. 053. DOI: 10.1007/JHEP01(2010)053. arXiv: 0910.3167 [hep-ph].
- [21] Y. Mambrini. “Higgs searches and singlet scalar dark matter: Combined constraints from XENON 100 and the LHC”. In: *Phys. Rev. D* 84 (2011), p. 115017. DOI: 10.1103/PhysRevD.84.115017. arXiv: 1108.0671 [hep-ph].
- [22] Matthew Gonderinger, Hyungjun Lim, and Michael J. Ramsey-Musolf. “Complex Scalar Singlet Dark Matter: Vacuum Stability and Phenomenology”. In: *Phys. Rev. D* 86 (2012), p. 043511. DOI: 10.1103/PhysRevD.86.043511. arXiv: 1202.1316 [hep-ph].
- [23] Xiao-Gang He, Bo Ren, and Jusak Tandean. “Hints of Standard Model Higgs Boson at the LHC and Light Dark Matter Searches”. In: *Phys. Rev. D* 85 (2012), p. 093019. DOI: 10.1103/PhysRevD.85.093019, 10.1103/PhysRevD.85.119902, 10.1103/PhysRevD.85.119906. arXiv: 1112.6364 [hep-ph].
- [24] James M. Cline et al. “Update on scalar singlet dark matter”. In: *Phys. Rev. D* 88 (2013). [Erratum: *Phys. Rev. D* 92, no. 3, 039906 (2015)], p. 055025. DOI: 10.1103/PhysRevD.92.039906, 10.1103/PhysRevD.88.055025. arXiv: 1306.4710 [hep-ph].
- [25] Emidio Gabrielli et al. “Towards Completing the Standard Model: Vacuum Stability, EWSB and Dark Matter”. In: *Phys. Rev. D* 89.1 (2014), p. 015017. DOI: 10.1103/PhysRevD.89.015017. arXiv: 1309.6632 [hep-ph].
- [26] Stefano Profumo et al. “Singlet-catalyzed electroweak phase transitions and precision Higgs boson studies”. In: *Phys. Rev. D* 91.3 (2015), p. 035018. DOI: 10.1103/PhysRevD.91.035018. arXiv: 1407.5342 [hep-ph].
- [27] T. D. Lee. “A Theory of Spontaneous T Violation”. In: *Phys. Rev. D* 8 (1973). [516(1973)], pp. 1226–1239. DOI: 10.1103/PhysRevD.8.1226.
- [28] John F. Gunion et al. *The Higgs Hunter’s Guide*. Vol. 80. Frontiers in Physics. New York City, NY: Addison-Wesley, 2000. URL: <http://alice.cern.ch/format/showfull?sysnb=0245390>.

- [29] G. C. Branco et al. “Theory and phenomenology of two-Higgs-doublet models”. In: (June 2011). eprint: 1106.0034. URL: <http://arxiv.org/abs/1106.0034>.
- [30] Ilya F. Ginzburg, Maria Krawczyk, and Per Osland. “Two Higgs doublet models with CP violation”. In: *Linear colliders. Proceedings, International Workshop on physics and experiments with future electron-positron linear colliders, LCWS 2002, Seogwipo, Jeju Island, Korea, August 26-30, 2002*. [703(2002)]. 2002, pp. 703–706. arXiv: hep-ph/0211371 [hep-ph]. URL: <http://weplib.cern.ch/abstract?CERN-TH-2002-330>.
- [31] Wafaa Khater and Per Osland. “CP violation in top quark production at the LHC and two Higgs doublet models”. In: *Nucl. Phys.* B661 (2003), pp. 209–234. DOI: 10.1016/S0550-3213(03)00300-6. arXiv: hep-ph/0302004 [hep-ph].
- [32] Abdul Wahab El Kaffas et al. “Consistency of the two Higgs doublet model and CP violation in top production at the LHC”. In: *Nucl. Phys.* B775 (2007), pp. 45–77. DOI: 10.1016/j.nuclphysb.2007.03.041. arXiv: hep-ph/0605142 [hep-ph].
- [33] Abdul Wahab El Kaffas, Per Osland, and Odd Magne OGREID. “CP violation, stability and unitarity of the two Higgs doublet model”. In: *Nonlin. Phenom. Complex Syst.* 10 (2007), pp. 347–357. arXiv: hep-ph/0702097 [HEP-PH].
- [34] B. Grzadkowski and P. Osland. “Tempered Two-Higgs-Doublet Model”. In: *Phys. Rev.* D82 (2010), p. 125026. DOI: 10.1103/PhysRevD.82.125026. arXiv: 0910.4068 [hep-ph].
- [35] A. Arhrib et al. “CP violation in charged Higgs production and decays in the Complex Two Higgs Doublet Model”. In: *JHEP* 04 (2011), p. 089. DOI: 10.1007/JHEP04(2011)089. arXiv: 1011.6560 [hep-ph].
- [36] A. Barroso et al. “Probing the scalar-pseudoscalar mixing in the 125 GeV Higgs particle with current data”. In: *Phys. Rev.* D86 (2012), p. 015022. DOI: 10.1103/PhysRevD.86.015022. arXiv: 1205.4247 [hep-ph].
- [37] Duarte Fontes, J. C. Romão, and João P. Silva. “ $h \rightarrow Z\gamma$ in the complex two Higgs doublet model”. In: *JHEP* 12 (2014), p. 043. DOI: 10.1007/JHEP12(2014)043. arXiv: 1408.2534 [hep-ph].
- [38] Duarte Fontes et al. “Large pseudo-scalar components in the C2HDM”. In: *2nd Toyama International Workshop on Higgs as a Probe of New Physics (HPNP2015) Toyama, Japan, February 11-15, 2015*. 2015. arXiv: 1506.00860 [hep-ph]. URL: <http://inspirehep.net/record/1374236/files/arXiv:1506.00860.pdf>.
- [39] Duarte Fontes et al. “Large pseudoscalar Yukawa couplings in the complex 2HDM”. In: *JHEP* 06 (2015), p. 060. DOI: 10.1007/JHEP06(2015)060. arXiv: 1502.01720 [hep-ph].
- [40] Chien-Yi Chen, Michael Freid, and Marc Sher. “The Next-to-Minimal Two Higgs Doublet Model”. In: (Dec. 2013). eprint: 1312.3949. URL: <http://arxiv.org/abs/1312.3949>.
- [41] Aleksandra Drozd et al. “Extending two-Higgs-doublet models by a singlet scalar field - the Case for Dark Matter”. In: (Aug. 2014). eprint: 1408.2106. URL: <http://arxiv.org/abs/1408.2106>.
- [42] Yun Jiang, Lingfeng Li, and Rui Zheng. “Boosted scalar confronting 750 GeV di-photon excess”. In: (2016). arXiv: 1605.01898 [hep-ph].
- [43] Nilendra G. Deshpande and Ernest Ma. “Pattern of Symmetry Breaking with Two Higgs Doublets”. In: *Phys. Rev.* D18 (1978), p. 2574. DOI: 10.1103/PhysRevD.18.2574.

- [44] Riccardo Barbieri, Lawrence J. Hall, and Vyacheslav S. Rychkov. “Improved naturalness with a heavy Higgs: An Alternative road to LHC physics”. In: *Phys. Rev.* D74 (2006), p. 015007. DOI: 10.1103/PhysRevD.74.015007. arXiv: hep-ph/0603188 [hep-ph].
- [45] Qing-Hong Cao, Ernest Ma, and G. Rajasekaran. “Observing the Dark Scalar Doublet and its Impact on the Standard-Model Higgs Boson at Colliders”. In: *Phys. Rev.* D76 (2007), p. 095011. DOI: 10.1103/PhysRevD.76.095011. arXiv: 0708.2939 [hep-ph].
- [46] Laura Lopez Honorez et al. “The Inert Doublet Model: An Archetype for Dark Matter”. In: *JCAP* 0702 (2007), p. 028. DOI: 10.1088/1475-7516/2007/02/028. arXiv: hep-ph/0612275 [hep-ph].
- [47] Ethan M. Dolle and Shufang Su. “The Inert Dark Matter”. In: *Phys. Rev.* D80 (2009), p. 055012. DOI: 10.1103/PhysRevD.80.055012. arXiv: 0906.1609 [hep-ph].
- [48] Laura Lopez Honorez and Carlos E. Yaguna. “The inert doublet model of dark matter revisited”. In: *JHEP* 09 (2010), p. 046. DOI: 10.1007/JHEP09(2010)046. arXiv: 1003.3125 [hep-ph].
- [49] Dorota Sokolowska. “Dark Matter Data and Constraints on Quartic Couplings in IDM”. In: (2011). arXiv: 1107.1991 [hep-ph].
- [50] Pierre Fayet. “Supergauge Invariant Extension of the Higgs Mechanism and a Model for the electron and Its Neutrino”. In: *Nucl. Phys.* B90 (1975), pp. 104–124. DOI: 10.1016/0550-3213(75)90636-7.
- [51] Michael Dine, Willy Fischler, and Mark Srednicki. “A Simple Solution to the Strong CP Problem with a Harmless Axion”. In: *Phys. Lett.* B104 (1981), pp. 199–202. DOI: 10.1016/0370-2693(81)90590-6.
- [52] Riccardo Barbieri, S. Ferrara, and Carlos A. Savoy. “Gauge Models with Spontaneously Broken Local Supersymmetry”. In: *Phys. Lett.* B119 (1982), p. 343. DOI: 10.1016/0370-2693(82)90685-2.
- [53] J. M. Frere, D. R. T. Jones, and S. Raby. “Fermion Masses and Induction of the Weak Scale by Supergravity”. In: *Nucl. Phys.* B222 (1983), pp. 11–19. DOI: 10.1016/0550-3213(83)90606-5.
- [54] Hans Peter Nilles, M. Srednicki, and D. Wyler. “Weak Interaction Breakdown Induced by Supergravity”. In: *Phys. Lett.* B120 (1983), p. 346. DOI: 10.1016/0370-2693(83)90460-4.
- [55] J. P. Derendinger and Carlos A. Savoy. “Quantum Effects and $SU(2) \times U(1)$ Breaking in Supergravity Gauge Theories”. In: *Nucl. Phys.* B237 (1984), pp. 307–328. DOI: 10.1016/0550-3213(84)90162-7.
- [56] John R. Ellis et al. “Higgs Bosons in a Nonminimal Supersymmetric Model”. In: *Phys. Rev.* D39 (1989), p. 844. DOI: 10.1103/PhysRevD.39.844.
- [57] Manuel Drees. “Supersymmetric Models with Extended Higgs Sector”. In: *Int. J. Mod. Phys.* A4 (1989), p. 3635. DOI: 10.1142/S0217751X89001448.
- [58] Ulrich Ellwanger, Michel Rausch de Traubenberg, and Carlos A. Savoy. “Particle spectrum in supersymmetric models with a gauge singlet”. In: *Phys. Lett.* B315 (1993), pp. 331–337. DOI: 10.1016/0370-2693(93)91621-S. arXiv: hep-ph/9307322 [hep-ph].
- [59] Ulrich Ellwanger, Michel Rausch de Traubenberg, and Carlos A. Savoy. “Higgs phenomenology of the supersymmetric model with a gauge singlet”. In: *Z. Phys.* C67 (1995), pp. 665–670. DOI: 10.1007/BF01553993. arXiv: hep-ph/9502206 [hep-ph].

- [60] S. F. King and P. L. White. “Resolving the constrained minimal and next-to-minimal supersymmetric standard models”. In: *Phys. Rev. D* 52 (1995), pp. 4183–4216. DOI: 10.1103/PhysRevD.52.4183. arXiv: hep-ph/9505326 [hep-ph].
- [61] T. Elliott, S. F. King, and P. L. White. “Unification constraints in the next-to-minimal supersymmetric standard model”. In: *Phys. Lett. B* 351 (1995), pp. 213–219. DOI: 10.1016/0370-2693(95)00381-T. arXiv: hep-ph/9406303 [hep-ph].
- [62] F. Franke and H. Fraas. “Neutralinos and Higgs bosons in the next-to-minimal supersymmetric standard model”. In: *Int. J. Mod. Phys. A* 12 (1997), pp. 479–534. DOI: 10.1142/S0217751X97000529. arXiv: hep-ph/9512366 [hep-ph].
- [63] U. Ellwanger, Michel Rausch de Traubenberg, and Carlos A. Savoy. “Phenomenology of supersymmetric models with a singlet”. In: *Nucl. Phys. B* 492 (1997), pp. 21–50. DOI: 10.1016/S0550-3213(97)80026-0, 10.1016/S0550-3213(97)00128-4. arXiv: hep-ph/9611251 [hep-ph].
- [64] Ulrich Ellwanger, Cyril Hugonie, and Ana M. Teixeira. “The Next-to-Minimal Supersymmetric Standard Model”. In: *Phys. Rept.* 496 (2010), pp. 1–77. DOI: 10.1016/j.physrep.2010.07.001. arXiv: 0910.1785 [hep-ph].
- [65] M. Maniatis. “The Next-to-Minimal Supersymmetric extension of the Standard Model reviewed”. In: *Int. J. Mod. Phys. A* 25 (2010), pp. 3505–3602. DOI: 10.1142/S0217751X10049827. arXiv: 0906.0777 [hep-ph].
- [66] S. F. King et al. “Discovery Prospects for NMSSM Higgs Bosons at the High-Energy Large Hadron Collider”. In: *Phys. Rev. D* 90.9 (2014), p. 095014. DOI: 10.1103/PhysRevD.90.095014. arXiv: 1408.1120 [hep-ph].
- [67] Jihn E. Kim and Hans Peter Nilles. “The mu Problem and the Strong CP Problem”. In: *Phys. Lett. B* 138 (1984), pp. 150–154. DOI: 10.1016/0370-2693(84)91890-2.
- [68] P. M. Ferreira et al. “Wrong sign and symmetric limits and non-decoupling in 2HDMs”. In: *JHEP* 12 (2014), p. 067. DOI: 10.1007/JHEP12(2014)067. arXiv: 1409.6723 [hep-ph].
- [69] G. Belanger et al. “Relic density of dark matter in the NMSSM”. In: *JCAP* 0509 (2005), p. 001. DOI: 10.1088/1475-7516/2005/09/001. arXiv: hep-ph/0505142 [hep-ph].
- [70] Debottam Das, Ulrich Ellwanger, and Ana M. Teixeira. “NMSDECAY: A Fortran Code for Supersymmetric Particle Decays in the Next-to-Minimal Supersymmetric Standard Model”. In: *Comput. Phys. Commun.* 183 (2012), pp. 774–779. DOI: 10.1016/j.cpc.2011.11.021. arXiv: 1106.5633 [hep-ph].
- [71] U. Ellwanger, C. -C. Jean-Louis, and A. M. Teixeira. “Phenomenology of the General NMSSM with Gauge Mediated Supersymmetry Breaking”. In: *JHEP* 05 (2008), p. 044. DOI: 10.1088/1126-6708/2008/05/044. arXiv: 0803.2962 [hep-ph].
- [72] Ulrich Ellwanger and Cyril Hugonie. “NMSPEC: A Fortran code for the sparticle and Higgs masses in the NMSSM with GUT scale boundary conditions”. In: *Comput. Phys. Commun.* 177 (2007), pp. 399–407. DOI: 10.1016/j.cpc.2007.05.001. arXiv: hep-ph/0612134 [hep-ph].
- [73] Ulrich Ellwanger, John F. Gunion, and Cyril Hugonie. “NMHDECAY: A Fortran code for the Higgs masses, couplings and decay widths in the NMSSM”. In: *JHEP* 02 (2005), p. 066. DOI: 10.1088/1126-6708/2005/02/066. arXiv: hep-ph/0406215 [hep-ph].
- [74] M. Muhlleitner, A. Djouadi, and Y. Mambrini. “SDECAY: A Fortran code for the decays of the supersymmetric particles in the MSSM”. In: *Comput. Phys. Commun.* 168 (2005), pp. 46–70. DOI: 10.1016/j.cpc.2005.01.012. arXiv: hep-ph/0311167 [hep-ph].

- [75] The ACME Collaboration. “Order of Magnitude Smaller Limit on the Electric Dipole Moment of the Electron”. In: *Science* 343 (2014), pp. 269–272. DOI: 10.1126/science.1248213. arXiv: 1310.7534 [physics.atom-ph].
- [76] A. Djouadi, J. Kalinowski, and M. Spira. “HDECAY: A Program for Higgs boson decays in the standard model and its supersymmetric extension”. In: *Comput. Phys. Commun.* 108 (1998), pp. 56–74. DOI: 10.1016/S0010-4655(97)00123-9. arXiv: hep-ph/9704448 [hep-ph].
- [77] J. M. Butterworth et al. “THE TOOLS AND MONTE CARLO WORKING GROUP Summary Report from the Les Houches 2009 Workshop on TeV Colliders”. In: *Physics at TeV colliders. Proceedings, 6th Workshop, dedicated to Thomas Binoth, Les Houches, France, June 8-26, 2009*. 2010. arXiv: 1003.1643 [hep-ph]. URL: <http://inspirehep.net/record/848006/files/arXiv:1003.1643.pdf>.
- [78] Philip Bechtle et al. “HiggsBounds – 4: Improved Tests of Extended Higgs Sectors against Exclusion Bounds from LEP, the Tevatron and the LHC”. In: *Eur. Phys. J. C* 74.3 (2014), p. 2693. DOI: 10.1140/epjc/s10052-013-2693-2. arXiv: 1311.0055 [hep-ph].
- [79] Markus Klute et al. “Measuring Higgs Couplings from LHC Data”. In: *Phys. Rev. Lett.* 109 (2012), p. 101801. DOI: 10.1103/PhysRevLett.109.101801. arXiv: 1205.2699 [hep-ph].
- [80] Markus Klute et al. “Measuring Higgs Couplings at a Linear Collider”. In: *Europhys. Lett.* 101 (2013), p. 51001. DOI: 10.1209/0295-5075/101/51001. arXiv: 1301.1322 [hep-ph].
- [81] C. Englert et al. “Precision Measurements of Higgs Couplings: Implications for New Physics Scales”. In: *J. Phys.* G41 (2014), p. 113001. DOI: 10.1088/0954-3899/41/11/113001. arXiv: 1403.7191 [hep-ph].
- [82] F. J. Botella and Joao P. Silva. “Jarlskog - like invariants for theories with scalars and fermions”. In: *Phys. Rev.* D51 (1995), pp. 3870–3875. DOI: 10.1103/PhysRevD.51.3870. arXiv: hep-ph/9411288 [hep-ph].
- [83] L. Lavoura and Joao P. Silva. “Fundamental CP violating quantities in a SU(2) x U(1) model with many Higgs doublets”. In: *Phys. Rev.* D50 (1994), pp. 4619–4624. DOI: 10.1103/PhysRevD.50.4619. arXiv: hep-ph/9404276 [hep-ph].
- [84] G. D’Ambrosio et al. “Minimal flavor violation: An Effective field theory approach”. In: *Nucl. Phys.* B645 (2002), pp. 155–187. DOI: 10.1016/S0550-3213(02)00836-2. arXiv: hep-ph/0207036 [hep-ph].
- [85] E. A. Paschos. “Diagonal Neutral Currents”. In: *Phys. Rev.* D15 (1977), p. 1966. DOI: 10.1103/PhysRevD.15.1966.
- [86] Sheldon L. Glashow and Steven Weinberg. “Natural Conservation Laws for Neutral Currents”. In: *Phys. Rev.* D15 (1977), p. 1958. DOI: 10.1103/PhysRevD.15.1958.
- [87] Vardan Khachatryan et al. “Search for Resonant Production of High-Mass Photon Pairs in Proton-Proton Collisions at $\sqrt{s} = 8$ and 13 TeV”. In: *Phys. Rev. Lett.* 117.5 (2016), p. 051802. DOI: 10.1103/PhysRevLett.117.051802. arXiv: 1606.04093 [hep-ex].
- [88] Morad Aaboud et al. “Search for resonances in diphoton events at $\sqrt{s}=13$ TeV with the ATLAS detector”. In: *JHEP* 09 (2016), p. 001. DOI: 10.1007/JHEP09(2016)001. arXiv: 1606.03833 [hep-ex].
- [89] The ATLAS collaboration. “Search for scalar diphoton resonances with 15.4 fb⁻¹ of data collected at $\sqrt{s}=13$ TeV in 2015 and 2016 with the ATLAS detector”. In: (2016).

- [90] CMS Collaboration. “Search for resonant production of high mass photon pairs using 12.9 fb^{-1} of proton-proton collisions at $\sqrt{s} = 13 \text{ TeV}$ and combined interpretation of searches at 8 and 13 TeV”. In: (2016).
- [91] K. G. Klimenko. “On Necessary and Sufficient Conditions for Some Higgs Potentials to Be Bounded From Below”. In: *Theor. Math. Phys.* 62 (1985). [Teor. Mat. Fiz.62,87(1985)], pp. 58–65. DOI: 10.1007/BF01034825.
- [92] Sidney R. Coleman. “The Fate of the False Vacuum. 1. Semiclassical Theory”. In: *Phys. Rev. D* 15 (1977). [Erratum: *Phys. Rev. D* 16,1248(1977)], pp. 2929–2936. DOI: 10.1103/PhysRevD.15.2929, 10.1103/PhysRevD.16.1248.
- [93] Curtis G. Callan Jr. and Sidney R. Coleman. “The Fate of the False Vacuum. 2. First Quantum Corrections”. In: *Phys. Rev. D* 16 (1977), pp. 1762–1768. DOI: 10.1103/PhysRevD.16.1762.
- [94] A. Barroso et al. “Metastability bounds on the two Higgs doublet model”. In: *JHEP* 06 (2013), p. 045. DOI: 10.1007/JHEP06(2013)045. arXiv: 1303.5098 [hep-ph].
- [95] P. M. Ferreira, R. Santos, and A. Barroso. “Stability of the tree-level vacuum in two Higgs doublet models against charge or CP spontaneous violation”. In: *Phys. Lett. B* 603 (2004). [Erratum: *Phys. Lett. B* 629,114(2005)], pp. 219–229. DOI: 10.1016/j.physletb.2004.10.022. arXiv: hep-ph/0406231 [hep-ph].
- [96] J. Horejsi and M. Kladiva. “Tree-unitarity bounds for THDM Higgs masses revisited”. In: *Eur. Phys. J. C* 46 (2006), pp. 81–91. DOI: 10.1140/epjc/s2006-02472-3. arXiv: hep-ph/0510154 [hep-ph].
- [97] William H. Press et al. *Numerical Recipes in C (2Nd Ed.): The Art of Scientific Computing*. New York, NY, USA: Cambridge University Press, 1992. ISBN: 0-521-43108-5.
- [98] Michael E. Peskin and Tatsu Takeuchi. “Estimation of oblique electroweak corrections”. In: *Phys. Rev. D* 46 (1992), pp. 381–409. DOI: 10.1103/PhysRevD.46.381.
- [99] M. Baak et al. “The global electroweak fit at NNLO and prospects for the LHC and ILC”. In: *Eur. Phys. J. C* 74 (2014), p. 3046. DOI: 10.1140/epjc/s10052-014-3046-5. arXiv: 1407.3792 [hep-ph].
- [100] Philip Bechtel et al. “*HiggsSignals*: Confronting arbitrary Higgs sectors with measurements at the Tevatron and the LHC”. In: *Eur. Phys. J. C* 74.2 (2014), p. 2711. DOI: 10.1140/epjc/s10052-013-2711-4. arXiv: 1305.1933 [hep-ph].
- [101] I. P. Ivanov and Joao P. Silva. “Tree-level metastability bounds for the most general two Higgs doublet model”. In: *Phys. Rev. D* 92.5 (2015), p. 055017. DOI: 10.1103/PhysRevD.92.055017. arXiv: 1507.05100 [hep-ph].
- [102] Howard E. Haber and Heather E. Logan. “Radiative corrections to the Z b anti-b vertex and constraints on extended Higgs sectors”. In: *Phys. Rev. D* 62 (2000), p. 015011. DOI: 10.1103/PhysRevD.62.015011. arXiv: hep-ph/9909335 [hep-ph].
- [103] O. Deschamps et al. “The Two Higgs Doublet of Type II facing flavour physics data”. In: *Phys. Rev. D* 82 (2010), p. 073012. DOI: 10.1103/PhysRevD.82.073012. arXiv: 0907.5135 [hep-ph].
- [104] Farvah Mahmoudi and Oscar Stal. “Flavor constraints on the two-Higgs-doublet model with general Yukawa couplings”. In: *Phys. Rev. D* 81 (2010), p. 035016. DOI: 10.1103/PhysRevD.81.035016. arXiv: 0907.1791 [hep-ph].
- [105] Thomas Hermann, Mikolaj Misiak, and Matthias Steinhauser. “ $\bar{B} \rightarrow X_s \gamma$ in the Two Higgs Doublet Model up to Next-to-Next-to-Leading Order in QCD”. In: *JHEP* 11 (2012), p. 036. DOI: 10.1007/JHEP11(2012)036. arXiv: 1208.2788 [hep-ph].

- [106] M. Misiak et al. “Updated NNLO QCD predictions for the weak radiative B-meson decays”. In: *Phys. Rev. Lett.* 114.22 (2015), p. 221801. DOI: 10.1103/PhysRevLett.114.221801. arXiv: 1503.01789 [hep-ph].
- [107] Robert V. Harlander, Stefan Liebler, and Hendrik Mantler. “SusHi Bento: Beyond NNLO and the heavy-top limit”. In: (May 2016). eprint: 1605.03190. URL: <http://arxiv.org/abs/1605.03190>.
- [108] Satoru Inoue, Michael J. Ramsey-Musolf, and Yue Zhang. “CP-violating phenomenology of flavor conserving two Higgs doublet models”. In: *Phys. Rev.* D89.11 (2014), p. 115023. DOI: 10.1103/PhysRevD.89.115023. arXiv: 1403.4257 [hep-ph].
- [109] Tomohiro Abe et al. “Gauge invariant Barr-Zee type contributions to fermionic EDMs in the two-Higgs doublet models”. In: *JHEP* 01 (2014). [Erratum: JHEP04,161(2016)], p. 106. DOI: 10.1007/JHEP01(2014)106, 10.1007/JHEP04(2016)161. arXiv: 1311.4704 [hep-ph].
- [110] W. Grimus et al. “A Precision constraint on multi-Higgs-doublet models”. In: *J. Phys.* G35 (2008), p. 075001. DOI: 10.1088/0954-3899/35/7/075001. arXiv: 0711.4022 [hep-ph].
- [111] W. Grimus et al. “The Oblique parameters in multi-Higgs-doublet models”. In: *Nucl. Phys.* B801 (2008), pp. 81–96. DOI: 10.1016/j.nuclphysb.2008.04.019. arXiv: 0802.4353 [hep-ph].
- [112] Aug. 2016. URL: <http://www.th.u-psud.fr/NMHDECAY/nmssmtools.html>.
- [113] Georges Aad et al. “Search for direct pair production of the top squark in all-hadronic final states in proton-proton collisions at $\sqrt{s} = 8$ TeV with the ATLAS detector”. In: *JHEP* 09 (2014), p. 015. DOI: 10.1007/JHEP09(2014)015. arXiv: 1406.1122 [hep-ex].
- [114] Georges Aad et al. “Search for direct third-generation squark pair production in final states with missing transverse momentum and two b -jets in $\sqrt{s} = 8$ TeV pp collisions with the ATLAS detector”. In: *JHEP* 10 (2013), p. 189. DOI: 10.1007/JHEP10(2013)189. arXiv: 1308.2631 [hep-ex].
- [115] Georges Aad et al. “Search for direct top-squark pair production in final states with two leptons in pp collisions at $\sqrt{s} = 8$ TeV with the ATLAS detector”. In: *JHEP* 06 (2014), p. 124. DOI: 10.1007/JHEP06(2014)124. arXiv: 1403.4853 [hep-ex].
- [116] Georges Aad et al. “Search for light scalar top quark pair production in final states with two leptons with the ATLAS detector in $\sqrt{s} = 7$ TeV proton-proton collisions”. In: *Eur. Phys. J.* C72 (2012), p. 2237. DOI: 10.1140/epjc/s10052-012-2237-1. arXiv: 1208.4305 [hep-ex].
- [117] Georges Aad et al. “Search for light top squark pair production in final states with leptons and b^- jets with the ATLAS detector in $\sqrt{s} = 7$ TeV proton-proton collisions”. In: *Phys. Lett.* B720 (2013), pp. 13–31. DOI: 10.1016/j.physletb.2013.01.049. arXiv: 1209.2102 [hep-ex].
- [118] Serguei Chatrchyan et al. “Search for new physics in events with same-sign dileptons and jets in pp collisions at $\sqrt{s} = 8$ TeV”. In: *JHEP* 01 (2014). [Erratum: JHEP01,014(2015)], p. 163. DOI: 10.1007/JHEP01(2015)014, 10.1007/JHEP01(2014)163. arXiv: 1311.6736.
- [119] Georges Aad et al. “Search for pair-produced third-generation squarks decaying via charm quarks or in compressed supersymmetric scenarios in pp collisions at $\sqrt{s} = 8$ TeV with the ATLAS detector”. In: *Phys. Rev.* D90.5 (2014), p. 052008. DOI: 10.1103/PhysRevD.90.052008. arXiv: 1407.0608 [hep-ex].

- [120] Georges Aad et al. “Search for squarks and gluinos with the ATLAS detector in final states with jets and missing transverse momentum using $\sqrt{s} = 8$ TeV proton–proton collision data”. In: *JHEP* 09 (2014), p. 176. DOI: 10.1007/JHEP09(2014)176. arXiv: 1405.7875 [hep-ex].
- [121] Vardan Khachatryan et al. “Search for supersymmetry using razor variables in events with b -tagged jets in pp collisions at $\sqrt{s} = 8$ TeV”. In: *Phys. Rev. D* 91 (2015), p. 052018. DOI: 10.1103/PhysRevD.91.052018. arXiv: 1502.00300 [hep-ex].
- [122] Serguei Chatrchyan et al. “Search for top squark and higgsino production using diphoton Higgs boson decays”. In: *Phys. Rev. Lett.* 112 (2014), p. 161802. DOI: 10.1103/PhysRevLett.112.161802. arXiv: 1312.3310 [hep-ex].
- [123] Georges Aad et al. “Search for top squark pair production in final states with one isolated lepton, jets, and missing transverse momentum in $\sqrt{s} = 8$ TeV pp collisions with the ATLAS detector”. In: *JHEP* 11 (2014), p. 118. DOI: 10.1007/JHEP11(2014)118. arXiv: 1407.0583 [hep-ex].
- [124] Serguei Chatrchyan et al. “Search for top-squark pair production in the single-lepton final state in pp collisions at $\sqrt{s} = 8$ TeV”. In: *Eur. Phys. J. C* 73.12 (2013), p. 2677. DOI: 10.1140/epjc/s10052-013-2677-2. arXiv: 1308.1586 [hep-ex].
- [125] Vardan Khachatryan et al. “Search for top-squark pairs decaying into Higgs or Z bosons in pp collisions at $\sqrt{s} = 8$ TeV”. In: *Phys. Lett. B* 736 (2014), pp. 371–397. DOI: 10.1016/j.physletb.2014.07.053. arXiv: 1405.3886 [hep-ex].
- [126] Vardan Khachatryan et al. “Searches for supersymmetry using the M_{T2} variable in hadronic events produced in pp collisions at 8 TeV”. In: *JHEP* 05 (2015), p. 078. DOI: 10.1007/JHEP05(2015)078. arXiv: 1502.04358 [hep-ex].
- [127] G. Bélanger et al. “micrOMEGAs4.1: two dark matter candidates”. In: *Comput. Phys. Commun.* 192 (2015), pp. 322–329. DOI: 10.1016/j.cpc.2015.03.003. arXiv: 1407.6129 [hep-ph].
- [128] P. A. R. Ade et al. “Planck 2013 results. XVI. Cosmological parameters”. In: *Astron. Astrophys.* 571 (2014), A16. DOI: 10.1051/0004-6361/201321591. arXiv: 1303.5076 [astro-ph.CO].
- [129] P. M. Ferreira et al. “Probing wrong-sign Yukawa couplings at the LHC and a future linear collider”. In: *Phys. Rev. D* 89.11 (2014), p. 115003. DOI: 10.1103/PhysRevD.89.115003. arXiv: 1403.4736 [hep-ph].
- [130] J R Andersen et al. “Handbook of LHC Higgs Cross Sections: 3. Higgs Properties”. In: (2013). Ed. by S Heinemeyer et al. DOI: 10.5170/CERN-2013-004. arXiv: 1307.1347 [hep-ph].
- [131] S. F. King, M. Muhlleitner, and R. Nevzorov. “NMSSM Higgs Benchmarks Near 125 GeV”. In: *Nucl. Phys. B* 860 (2012), pp. 207–244. DOI: 10.1016/j.nuclphysb.2012.02.010. arXiv: 1201.2671 [hep-ph].
- [132] Werner Bernreuther, Patrick Gonzalez, and Martin Wiebusch. “Pseudoscalar Higgs Bosons at the LHC: Production and Decays into Electroweak Gauge Bosons Revisited”. In: *Eur. Phys. J. C* 69 (2010), pp. 31–43. DOI: 10.1140/epjc/s10052-010-1335-1. arXiv: 1003.5585 [hep-ph].